
Comparison of mobilities of peptides and proteins by capillary electrophoresis and ion mobility coupled to mass spectrometry

Auteur : p222893

Promoteur(s) : Eppe, Gauthier

Faculté : Faculté des Sciences

Diplôme : Master en sciences chimiques, à finalité approfondie

Année académique : 2023-2024

URI/URL : <http://hdl.handle.net/2268.2/19973>

Avertissement à l'attention des usagers :

Tous les documents placés en accès ouvert sur le site le site MatheO sont protégés par le droit d'auteur. Conformément aux principes énoncés par la "Budapest Open Access Initiative"(BOAI, 2002), l'utilisateur du site peut lire, télécharger, copier, transmettre, imprimer, chercher ou faire un lien vers le texte intégral de ces documents, les disséquer pour les indexer, s'en servir de données pour un logiciel, ou s'en servir à toute autre fin légale (ou prévue par la réglementation relative au droit d'auteur). Toute utilisation du document à des fins commerciales est strictement interdite.

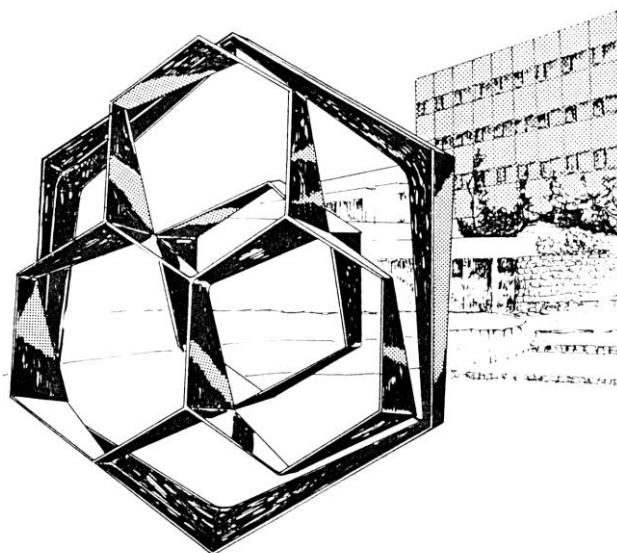
Par ailleurs, l'utilisateur s'engage à respecter les droits moraux de l'auteur, principalement le droit à l'intégrité de l'oeuvre et le droit de paternité et ce dans toute utilisation que l'utilisateur entreprend. Ainsi, à titre d'exemple, lorsqu'il reproduira un document par extrait ou dans son intégralité, l'utilisateur citera de manière complète les sources telles que mentionnées ci-dessus. Toute utilisation non explicitement autorisée ci-avant (telle que par exemple, la modification du document ou son résumé) nécessite l'autorisation préalable et expresse des auteurs ou de leurs ayants droit.

FACULTY OF SCIENCES
Chemistry Department

MS Lab

Dr. Delvaux, Dr. Far, Prof. de Pauw and Prof. Eppe

**Comparison of mobilities of peptides and
proteins by capillary electrophoresis and ion
mobility coupled to mass spectrometry**



Academic year 2023-2024

Dissertation submitted by
Simon Godaux
For the fulfilment of the degree of
Master in Chemistry

Résumé

La spectrométrie de masse native (nMS) couplée à la mobilité ionique (IM-MS) est une stratégie analytique permettant d'étudier les systèmes biologiques, notamment des protéines et des peptides, après les avoir transférés en phase gazeuse. Cependant, l'absence de certaines interactions en phase gazeuse par rapport à celles en solution peut-elle engendrer de nouvelles conformations par rapport à leurs états natifs ? Ou les conformations des ions sont-elles cinétiquement piégées ? Ce travail a pour but d'apporter des éléments de réponses à ces questions par l'étude de peptides obtenus à la suite d'une digestion à la trypsine d'une protéine connue qui est l'albumine de sérum bovin. Les peptides issus de cette digestion ont été étudiés grâce à deux méthodes de séparation, l'une en phase gazeuse (mobilité ionique) couplée avec une autre en solution (électrophorèse capillaire), permettant aussi d'obtenir des informations sur des paramètres structuraux des systèmes étudiés. Ces deux méthodes ont été testées dans différentes conditions (pH, interface entre les deux méthodes, régime d'activation des ions) afin de déterminer l'influence des paramètres expérimentaux. Après analyse et interprétation des résultats, il ressort que malgré des distributions conformationnelles similaires entre les deux phases pour la majorité des peptides. Certains peptides subissent des changements de conformations après désolvatation.

Summary

Native mass spectrometry (nMS) coupled to ion mobility (IM-MS) is an analytical strategy for studying biological systems, particularly proteins and peptides, after transferring them to the gas phase. However, can the absence of certain interactions in the gas phase compared to those in solution result in new conformations compared to their native states? Or are ionic conformations kinetically trapped? The aim of this work is to provide some answers to these questions by studying peptides obtained following trypsin digestion of a well-known protein, bovine serum albumin. The peptides derived from this digestion were studied using two separation methods, one in the gas phase (ion mobility) coupled with another in solution (capillary electrophoresis), which also provided information on the structural parameters of the systems studied. Both methods were tested under different conditions (pH, interface between the two methods, ion activation regime) to determine the influence of experimental parameters. After analysis and interpretation of the results, it was found that despite similar conformational distributions between the two phases for the majority of peptides. Some peptides undergo conformational changes after desolvation.

Acknowledgements

The purpose of this section is to thank all the people who contributed to the completion of this master's thesis, and without whom I would not have got this far. First of all, I would like to thank my professor and thesis promotor Gauthier Eppe for welcoming me into his research laboratory. A good working environment and the opportunity to have access to all kinds of leading-edge equipment is the basis of a master's thesis, and I was able to find all those ingredients at the Mass Spectrometry Laboratory. I would also like to thank Prof. Edwin de Pauw, who is still very involved in all matters relating to the laboratory and with whom I have had some very fruitful conversations.

Among all the people I must thank, there is of course Prof. André Matagne and Dr. Christopher Kune who agreed to be part of my jury and to read this manuscript so that I could defend it to complete my studies in Chemistry.

I must also extend a heartfelt thank you to my two supervisors, Dr. Johann Far and (Dr.) Cédric Delvaux, who guided me day by day for many months and spent a considerable amount of their valuable time offering advice when I veered off the right path. Johann, may you maintain your sincere desire to help others and your kind heart despite your unorthodox methods. Cédric, I hope you will always keep this overflowing energy that characterizes you and seems to make you tireless.

I would also like to express my gratitude to all those who made my laboratory experiences so enjoyable. That is why I thank Nancy and Lisette who trained me as a technician even though I had very little experience and without whom I would have had great difficulty in producing my samples. What is more, life in the lab would not have been nearly as much fun without my MSLAB friends and colleagues, with whom I have had many serious discussions, and sometimes a lot less. So, a special thanks to Bastien, Charles, Evan, Matthieu, Maxime, Vincent and Zeina. I wish you all the best for your future projects, whatever they may be.

Enfin, j'aimerais adresser la fin de ces remerciements en français à ceux qui me sont le plus chers à commencer par ma grand-mère qui est sans aucun doute ma plus ancienne supportrice, à ma marraine qui m'a toujours prodigué de bons conseils et enfin à mes parents qui ont vécu toutes mes victoires et tous mes échecs avec moi et sans lesquels ma vie aurait été bien plus terne. Il y a tellement de choses à dire, tellement de gens à remercier et si peu de place, je veux donc leur dire « Merci à vous tous pour tout ».

Table of content

Contents

1. Proteins and peptides.....	4
2. Protein structure characterization methods.....	7
3. The rise of Native MS and related issues	21
4. Capillary electrophoresis.....	22
5. Ion mobility.....	25
6. Objectives and strategy.....	27
7. Material and methods.....	31
7.1. Ion mobility determination in the gas phase and solution by capillary electrophoresis coupled with ion mobility mass spectrometry (CE-IM-MS):	31
7.2. Electrophoretic mobility determined in solution by capillary electrophoresis:.....	32
8. Ion mobility parameters of the Synapt G2 HDMS.....	32
9. Sample preparation.....	33
10. Data processing.....	34
11. Library of studied peptides	34
12. Orthogonality of the CE-IMS coupling.....	37
13. Multiple conformations identified in CE	41
14. Multiple conformations identified in IMS	43
15. Conformation(s) in solution versus conformation(s) in IMS: the different observed cases:	45
16. Soft ion activation prior to the IMS analysis	49
17. Hyphenation of CE to ESI-IM-MS: impact of the CE-IM-MS interface.....	54
18. Influence of the BGE's pH.....	58
19. Conclusions.....	61
20. Bibliography.....	62

1. Proteins and peptides

Proteins (also known as polypeptides) constitute a family of biomolecules that perform a series of biological functions of major importance. They play an important structural role in the cytoskeleton¹ and in tissues² (e.g. actin, collagen), act as molecular transporters³ (e.g. porins, carnitine-acylcarnitine translocase), and ensure catalytic functions⁴ (e.g. proteases) by regulating reactions necessary for the metabolism. For example, about ten enzymes are necessary to perform the anoxic glycolysis cycle, which is essential for the production of ATP and intermediates for the Krebs cycle⁵. Proteins and peptides are chains of amino acids, which constitute their building units. 22 proteogenic (*i.e.* incorporated in proteins during the biosynthesis by the ribosomes) amino acids appear in the genetic code⁶ of eukaryotes, fungi, archaea and bacteria (Fig.1), while there is the 20 most common residues (*i.e.* the 22 residues from (Fig.1) excepted selenocysteine and pyrrolysine) used by all the lifeforms known on Earth.

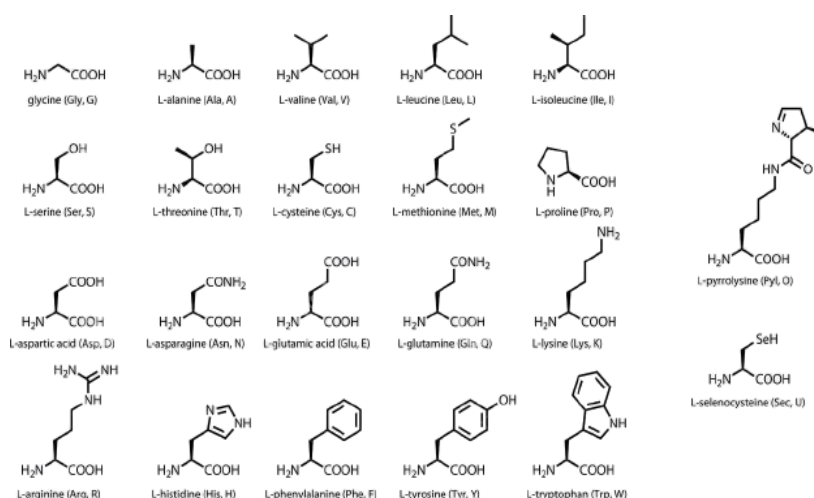


Fig.1 Representation of the 22 amino acids (from the site www.dreamstime.com)

Table 1 Amino acid's 1 letter and 3 letters codes

Amino acid	1 letter code	3 letters code
Alanine	A	Ala
Arginine	R	Arg
Asparagine	N	Asn
Aspartic acid	D	Asp
Cysteine	C	Cys
Glutamic acid	E	Glu
Glutamine	Q	Gln
Glycine	G	Gly
Histidine	H	His
Isoleucine	I	Ile
Leucine	L	Leu
Lysine	K	Lys
Methionine	M	Met
Phenylalanine	F	Phe
Proline	P	Pro
Serine	S	Ser
Threonine	T	Thr
Tryptophan	W	Trp
Tyrosine	Y	Tyr
Valine	V	Val
Selenocysteine	U	Sec
Pyrrolysine	O	Pyl

The amino acids are termed “residues” when they are engaged from their N-terminus and C-terminus in bonding with other molecules. In peptides and proteins, the residues are linked by the “peptide bond”, which is an amide bond, and the lateral chains of the residue can interact with the solvent or other residues from the same (poly)peptides or from other (poly)peptides, nucleic acid, small molecules or any other type of matter. These interactions can impose the tridimensional structures to the polypeptides which are more or less flexible or organized. Proteins present a wide range of structures: some proteins such as PTP1B⁷ entirely lack defined structural features and are referred as “intrinsically disordered”, while cytochrome P450s⁸ present precise, defined structures. In that context, protein structures can be described according to several levels from primary to quaternary (Fig.2). The primary level of a protein describes the sequence (order of linking of the residues from the N-terminus to the C-terminus) of the residues that constitutes the main chain of the protein, which then folds into a 3D structure comprising the secondary, tertiary, and quaternary levels. Those levels of structures are often referred to as “higher order structure (HOS)”. The secondary level describes the locally adopted structures of the primary chain such as beta sheets, alpha helices (on average composed by 11 amino acids)⁹, and beta loops. The tertiary level describes the structure globally adopted by the protein and is the result of the assembly in space of the different secondary structures. Finally, the quaternary structure (if present) is composed of several polypeptides and proteins interacting together to form a complex (for example: *Haemoglobin*).

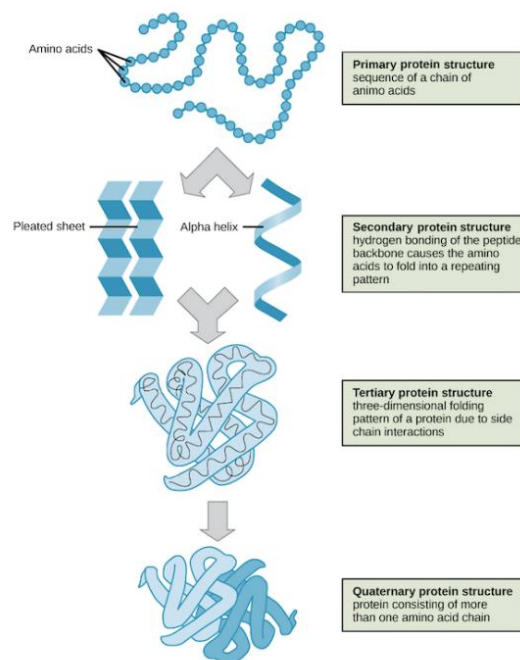


Fig.2 Representation of the different structural levels of proteins (from microscopiaiwm.wordpress.com)

The function of a protein relies on its amino acid composition but also on its 3D structure, which is often referred to as the “structure/activity relationship”. The “lock and key” model^{10,11} (Fig.3) is the historical model introduced to provide a theoretical explanation of that “structure/activity relationship” by assimilating a ligand to a key and a protein to its padlock perfectly shaped as rigid bodies to interact.

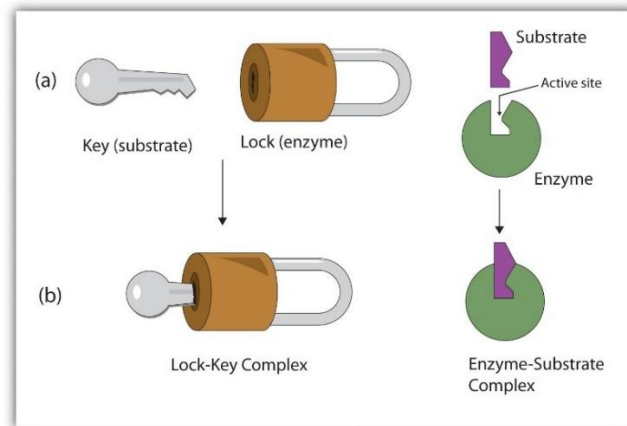


Fig.3 Representation of the lock and key model (from socratic.org)

Over the years, that model evolved to take into account the dynamics of both partners into the unfolding/folding model (Fig.4). Both models imply that the protein structure intrinsically contains the information to ensure its structures and activity. Denatured proteins usually experience a drastic reduction of their biological activity¹².

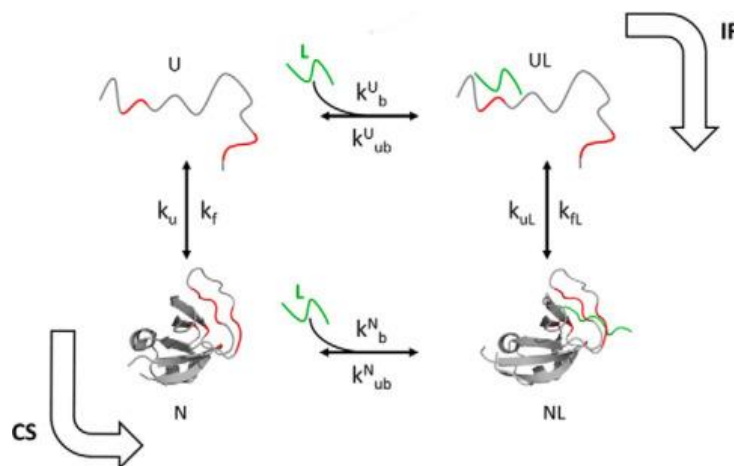


Fig.4 Representation of the Unfolding/Folding model (from [Sen, S.; Udgaonkar, J. B. Binding-Induced Folding under Unfolding Conditions: Switching between Induced Fit and Conformational Selection Mechanisms. J. Biol. Chem. 2019, 294 \(45\), 16942–16952.](#))

Hédoux *et al.*¹³ showed that denatured lysozyme using urea and guanidine hydrochloride resulted in loss of hydrolytic activity of the peptidoglycan (calculated by measuring the decrease in absorbance of a suspension of *Micrococcus lysodeikticus* Gram positive bacteria due to its lysis) that was correlated to conformational changes of the lysozyme. Understanding the information contained in the structures of proteins is therefore of high importance to preserve or even optimize their functions such as catalytic capabilities¹⁴. The improper folding of specific proteins cause the degeneration of cognitive cells such as Parkinson and Alzheimer diseases¹⁵. Over the last 30 years, subtilisin proteases and other enzymes were genetically engineered to fit the purpose of additional ingredient in laundry detergent

especially in terms of *e.g.* thermal resistance or *in-situ* peroxy-carboxylic acids production as mild bleaching agent¹⁶.

2. Protein structure characterization methods

Nowadays, the study of protein structures is a vast subject of research which mobilises many different characterization methods. The most popular methods include Infrared Spectroscopy (IR), Circular Dichroism (CD), X-ray crystallography, Nuclear Magnetic Resonance (NMR), Fluorescence Resonance Energy Transfer (FRET), Cryo-Electron Microscopy (Cryo-EM), Atomic Force Microscopy (AFM), Surface Plasmon Resonance (SPR), and finally computer simulation (*in silico* methods). An overview of those major techniques, along with their respective advantages and drawbacks is provided in the following section:

Infrared spectroscopy^{17,18} is the measurement of the absorbance of infrared light radiation characterized by a wavelength between 0.7 μm and 100 μm by a sample which was first described by Abney and Festing in 1882¹⁹. The energy carried by such wavelength is of the same order of magnitude as the energy differences that exists between molecular levels of vibrational energy. In the case of proteins, the carbonyl bonds (C=O) of amides absorb at wave numbers between 1600 and 1700 cm^{-1} but those vibrational frequencies are influenced by the presence of near secondary structures. The observation of absorbance shifts allows to highlight the presence of secondary structures (Fig.5) and quantitative study (which reveals the percentage of a certain type of secondary structure in the protein) can be calculated based on peak deconvolution and peak area integration. Similar to circular dichroism methods, this method allows the global study of secondary structures of proteins in native conditions. A major drawback of the technique is its global characterization aspect, preventing precise positioning of amino acids involved in the characterized secondary structure. However, the samples do not require complex preparation prior to the analysis and IR experiments allow both qualitative and quantitative analysis.

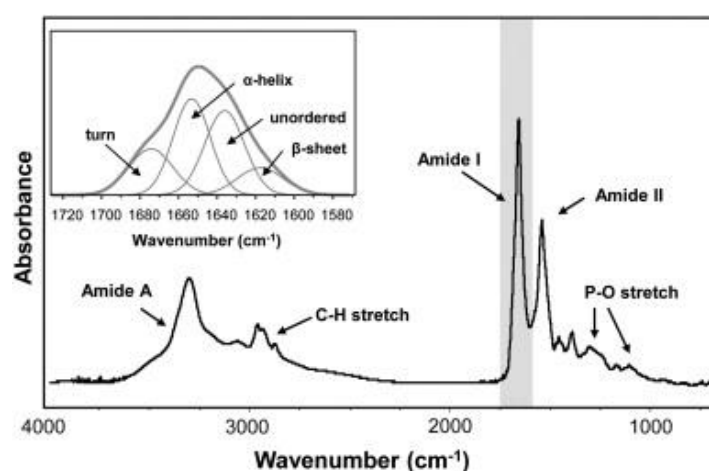


Fig.5 Structural analysis of a typical protein by infrared spectroscopy (from Miller, L. M.; Bourassa, M. W.; Smith, R. J. FTIR Spectroscopic Imaging of Protein Aggregation in Living Cells. *Biochim. Biophys. Acta BBA - Biomembr.* **2013**, *1828* (10), 2339–2346.)

In this context, IR spectroscopy have been successfully used by Carissimi *et al.*²⁰ to study the composition in secondary structures of silk fibroin fibres as their properties such as strength, flexibility, and degradability are directly depend on the secondary structure composition (Fig.6).

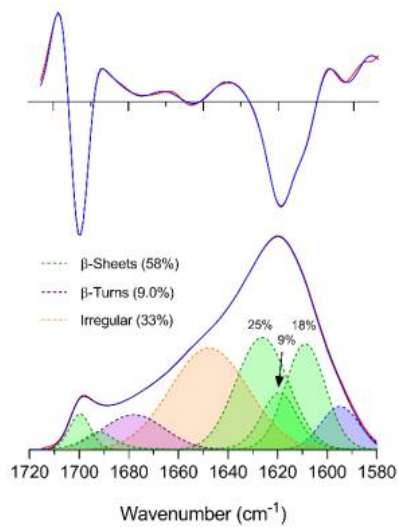


Fig.6 Band fitting of the amide I band and its second derivative of SF fibers. Top: second derivative of absorbance; bottom: ATR absorbance spectrum. Blue: Experimental spectrum and experimental second derivative; Red: fitted spectrum and fitted second derivative (from Carissimi, G.; Baronio, C. M.; Montalbán, M. G.; Villora, G.; Barth, A. On the Secondary Structure of Silk Fibroin Nanoparticles Obtained Using Ionic Liquids: An Infrared Spectroscopy Study. *Polymers* **2020**, *12* (6), 1294.)

Circular Dichroism^{21,22} is a phenomenon that was discovered in 1895 by Aimé Cotton²³, which is based on differential molecular absorption between right and left circularly polarized electromagnetic waves. A linear electromagnetic wave is composed of an electric field and a magnetic field oscillating in phase. The passage of this wave through a circular polarizer generates a 90-degree phase shift between these two fields, which creates a circularly polarized wave. The secondary structures of proteins such as alpha helices and beta sheets show characteristic absorbances of those polarized waves, allowing their identification (Fig.7). Consequently, CD is perfectly suited to quantify secondary structures in proteins and peptides in native conditions. The tertiary level can also be studied by near ultraviolet CD²⁴. It is however more limited for the other levels of structures and does not allow their precise localisation within the structure. On top of that, typical buffers used for this type of experiment can absorb light in the range of molecule's absorption spectrum and cover important peaks.

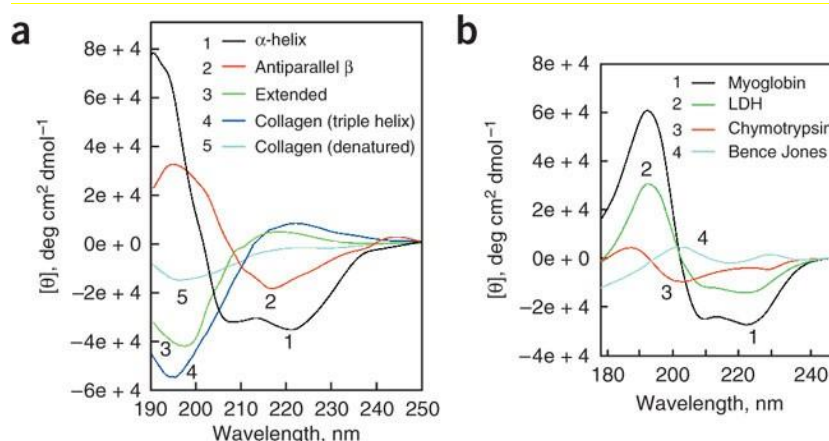


Fig.7 CD spectra of polypeptides and proteins with representative secondary structures. (a) CD spectra of poly-L-lysine at pH 11.1 in the (1, black) α -helical and (2, red) antiparallel β -sheet conformations and at pH 5.7 in the (3, green) extended conformations and placental collagen in its (4, blue) native triple-helical and (5, cyan) denatured forms⁶⁴. (b) CD spectra of representative proteins with varying conformations: 1 (black), sperm whale myoglobin; 2 (green), chicken heart lactate dehydrogenase; 3 (red), bovine α -chymotrypsin and 4 (cyan), human Bence Jones protein REI light chain, which is a human immunoglobulin light chain of κ type (from Greenfield, N. J. *Using Circular Dichroism Spectra to Estimate Protein Secondary Structure. Nat. Protoc.* **2006**, *1* (6), 2876–2890.)

Circular dichroism has been used by Miles and Wallace²⁵ to study the secondary structure compositions of membrane proteins by studying their characteristic absorbance (Fig.8).

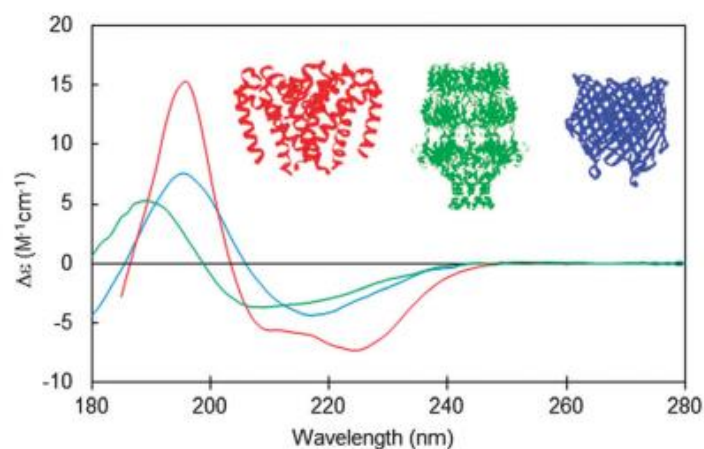


Fig.8 Circular dichroism spectra typical of membrane proteins composed of different secondary structural types: predominantly antiparallel α -helical bundle (red: a sodium channel pore⁴⁸); predominantly β -barrel (blue: BTUB outer membrane cobalamin transporter²³), mixed helical, β sheet and unordered structure (green: WZA translocon for capsular polysaccharides²³). Inset are the crystal structures of these proteins depicted in the same colour scheme (from Miles, A. J.; Wallace, B. A. *Circular Dichroism Spectroscopy of Membrane Proteins. Chem. Soc. Rev.* **2016**, *45* (18), 4859–4872.)

X-ray crystallography^{26,27} is a more recent spectroscopic method (1912) that can reach spatial atomic resolution to structurally assess crystals by using X-rays (wavelengths between 10^{-8} to 10^{-12} m). The compound to be analysed is first crystallized and then bombarded by an incident X-ray beam that diffracts in several directions in space. The diffracted X-rays are detected to provide a diffractogram. The diffraction pattern and the intensities of the diffracted rays depend on the crystal lattice, from which the locations of the different atoms composing the crystal can be determined (see Fig.9). The

crystallization step can be (very) difficult in the case of proteins as they are large biomolecules that contain many repulsive forces and present many degrees of freedom. The solution containing the ideally pure protein must crystallize under precise conditions of pH, ionic strength and temperature (often obtained empirically)²⁸. The main drawback of X-ray crystallography is that the analysis is carried out in state that is far from the physiological environment, which prevent the native study. Moreover, information about the dynamics of the system is not straightforward to obtain.

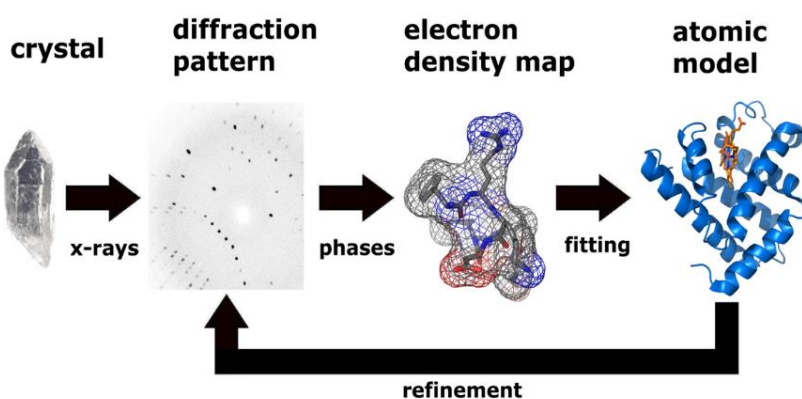


Fig.9 Structural analysis of a protein by X-ray crystallography (from elearning.bits.vib.be)

In a recent example, Handing *et al*²⁹. used X-ray crystallography for studying the zinc-binding site of equine serum albumin and its dependence to the pH of the crystallization solution (orientation of histidine residues) (**Fig.10**).

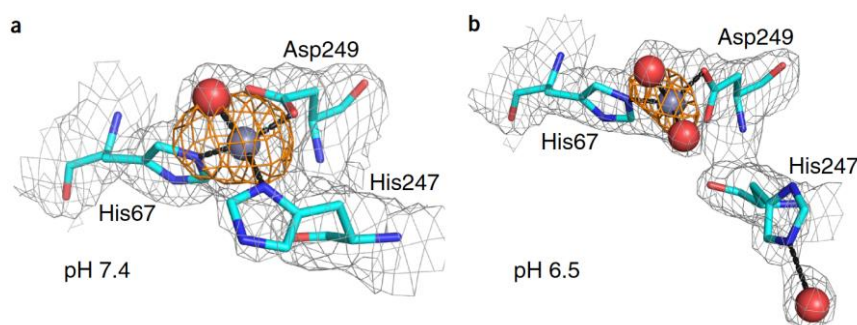


Fig.10 Representative structures of ESA–Zn²⁺ complexes showing the dynamic behaviour of His247. Both structures were crystallized in 100 mM Tris buffer, and the pH refers to the final pH in the crystallization drop. (a) ESA–Zn²⁺, 2.5 mM Zn²⁺, pH 7.4; PDB 5III. (b) ESA–Zn²⁺, 15 mM Zn²⁺, pH 6.5; PDB 5IIX. Sticks, residues; grey, zinc ion; red, oxygen; dark blue, nitrogen; green, carbon; black dashed lines, coordination bonds. The grey grid represents the 2mFo – DFc map (1.0σ); orange, anomalous map (3.0σ). (from Handing, K. B.; Niedzialkowska, E.; Shabalin, I. G.; Kuhn, M. L.; Zheng, H.; Minor, W. Characterizing Metal-Binding Sites in Proteins with X-Ray Crystallography. *Nat. Protoc.* **2018**, *13* (5), 1062–1090.)

Nuclear Magnetic Resonance^{30,31} is a method of structural analysis that was introduced in the 1940s. Several types of NMR experiments were developed, which makes it a versatile technique widely used for structural analysis of (bio)molecules³², including proteins until the atomic level^{33,34}. While one-

dimensional experiments (^{13}C , ^1H , ^{15}N , ^{31}P) provide general information such as the number of carbons, nitrogens and hydrogens in a molecule, two-dimensional and multi-dimensional experiments can unravel much more detailed information such as correlations and spatial positions. For example, correlation spectroscopy (COSY) correlates two adjacent types of hydrogen. Heteronuclear single quantum coherence (HSQC) (Fig.11) correlates hydrogens to the carbons (or nitrogen) that are bound to them. Heteronuclear multiple bond correlation (HMBC) can correlate a hydrogen to a carbon (or nitrogen) in the close environment but not directly attached to it. NMR can also be used to harvest structural information (Fig.12), such as the spatial proximity between two groups using experiments such as nuclear Overhauser spectroscopy (NOESY) or paramagnetic resonance enhancement (PRE).

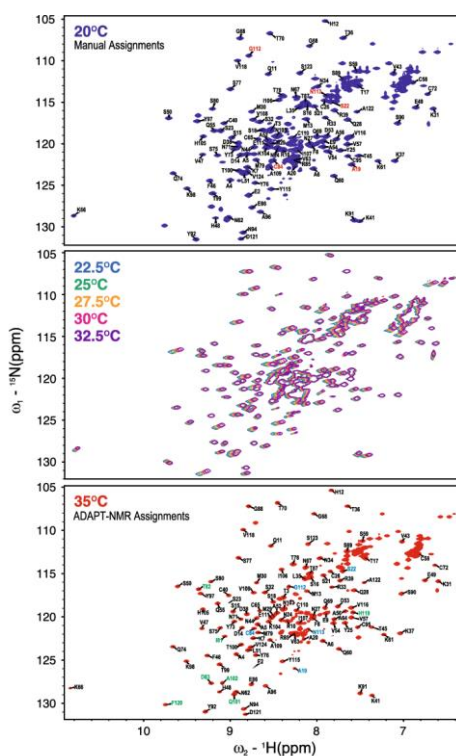


Fig.11 Temperature dependence of 2D H-N HSQC of RNase A showing the influence of temperature on its conformation (from Tonelli, M.; Eller, C. H.; Singarapu, K. K.; Lee, W.; Bahrami, A.; Westler, W. M.; Raines, R. T.; Markley, J. L. Assignments of RNase A by ADAPT-NMR and Enhancer. *Biomol. NMR Assign.* **2015**, *9* (1), 81–88.)

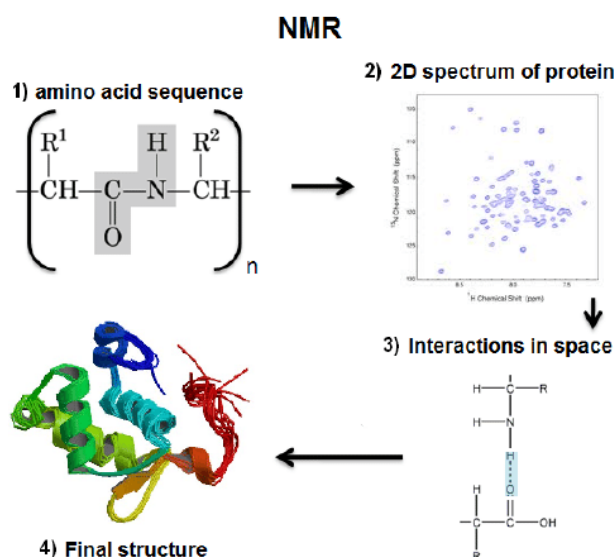


Fig.12 Structural analysis of a protein performed by NMR (from Kumar, S.; Demo, G.; Koca, J.; Wimmerova, M. In *Silico Engineering of Proteins That Recognize Small Molecules*. In *Protein Engineering*; Kaumaya, P., Ed.; InTech, 2012.)

Two experiments particularly useful in NMR for the study of proteins are the HNC α C β and the HN(C=O)C α C β , which allow the characterization of the primary structure of a protein^{35,36} (Fig.13).

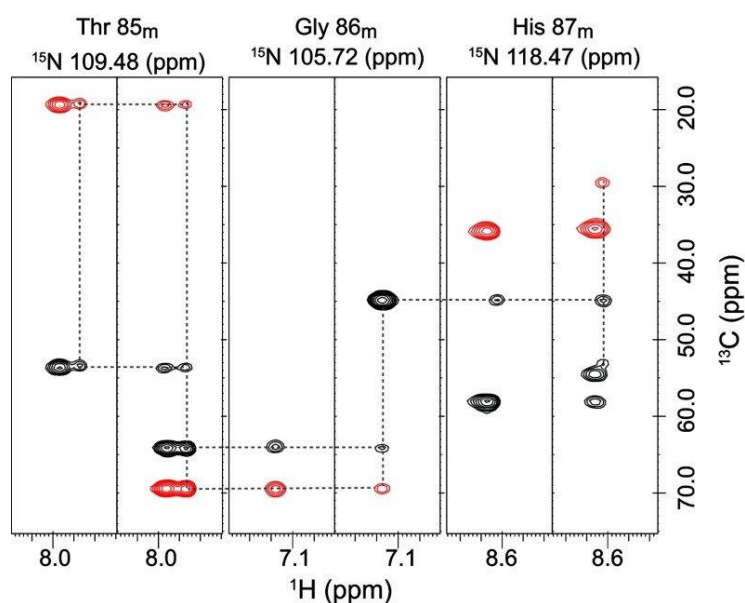


Fig.13 Backbone assignment with HNCOC α C β and HNC α C β in the C22V variant of human FKBP12 (from Mustafi, S. M.; Chen, H.; Li, H.; LeMaster, D. M.; Hernández, G. *Analysing the Visible Conformational Substates of the FK506-Binding Protein FKBP12*. *Biochem. J.* **2013**, 453 (3), 371–380.)

NMR is a technique that provide a close-to-atomic resolution in addition to the dynamics of the system. Several methods allow the characterization of the dynamics of a protein, such as measuring the relaxation times of the spins of ^{13}C and ^{15}N or studying dipolar coupling because as those phenomena directly depend on the orientations of the nuclei involved. Despite those very attractive assets, NMR

suffers from several limitations. First, the size of the molecule is limited, to avoid too complex correlation spectra to resolve. The size limit was initially close to 10 kDa and has evolved up to 100 kDa nowadays³⁷. Then, NMR experiments often require a relatively high amount of sample of high purity (often at concentration in the millimolar range).

Fluorescence (or Förster) Resonance Energy Transfer spectroscopy^{38,39} is a technique that was developed during the 20th century based on the "Förster resonance energy transfer" (FRET) mechanism. In that phenomenon, two fluorophore groups separated by a distance of less than a hundred Angstroms (a distance compatible with most biological molecule diameters) can interact to provide information about their respective spatial positions. It relies on a non-radiative energy transfer via dipole-dipole coupling where the energy is transmitted from the excited donor group to the acceptor group. The prerequisite for this energy transfer is that the emission spectrum of the donor must (at least partially) superimpose on the excitation spectrum of the acceptor (see Fig 14).

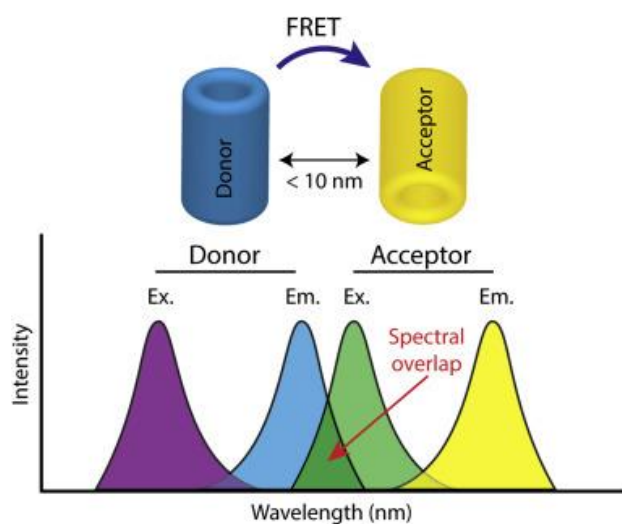


Fig.14 Structural analysis of a protein by FRET (from Bonardd, S.; Díaz Díaz, D.; Leiva, A.; Saldías, C. Chromophoric Dendrimer-Based Materials: An Overview of Holistic-Integrated Molecular Systems for Fluorescence Resonance Energy Transfer (FRET) Phenomenon. *Polymers* **2021**, *13* (24), 4404.)

The efficiency of that energy transfer is inversely proportional to the power six of the distance between the two fluorophores. That technique is therefore widely used in the structural analysis of biomolecules such as proteins since it allows the measurement of inter- and intramolecular distances by functionalizing the residues of interest with fluorophores and measuring the efficiency of their energy transfer. Santini *et al.*⁴⁰ were able to measure the distance in Human Serum Albumin (HSA) between Trp-214 (donor) and Cys-34 labelled with 1.5-iaedans (acceptor) (Fig.15). The major drawback of this technique is the required functionalizing step if fluorophores are not naturally present in the molecule. As a result, the functionalizing step can modify the probed interaction(s) and therefore affect the investigated structure.

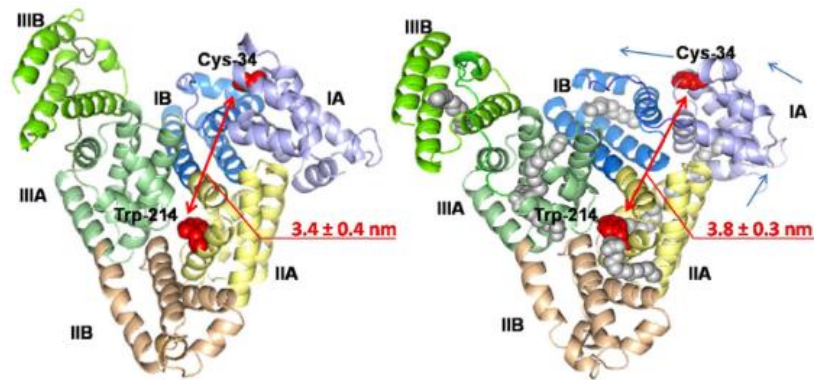


Fig.15 Crystallographic structure of human serum albumin (HSA) (A) and HSA complexed with palmitic acid (B). Trp-214 in sub-domain IIA and Cys-34 in sub-domain IA are represented as red spheres (from Santini, S.; Bizzarri, A. R.; Cannistraro, S. Revisitation of FRET Methods to Measure Intra-protein Distances in Human Serum Albumin. *J. Lumin.* **2016**, *179*, 322–327.)

Cryogenic Electron Microscopy^{41,42} is a microscopy technique allowing to obtain an "almost-atomic" resolution (4\AA) which was developed in the 1970's as an alternative method to the structural characterization by X-ray diffractions. The electron microscope is composed of an electromagnetic lens that focuses an accelerated electron beam and the interactions between the sample and the beam provide a detailed image that can be used to extract structural information. The preparation of Cryo-EM samples has remained unchanged from that developed in the 1980's and consists in the application of a sample containing the purified protein of interest to an electron microscopy grid. The sample is then processed to leave only a thin aqueous layer which is then immersed in a powerful cryogen, often liquid ethane (-190°C)⁴³ cooled by liquid nitrogen (Fig.16). The rapid cooling of the sample avoids the formation of ice crystals that can damage the sample. Moreover, fast freezing provides the sample a better resistance to electron bombardment and thus improved conservation of the sample during the imaging experiment. Cryo-EM requires much less sample than NMR (typically a few microliters at a concentration of $0.05 - 5\mu\text{M}$ of proteins)⁴⁴. However, like X-ray crystallography, proteins are no more in a physiological environment when they are structurally assessed, which prevents the study of their native conformations.

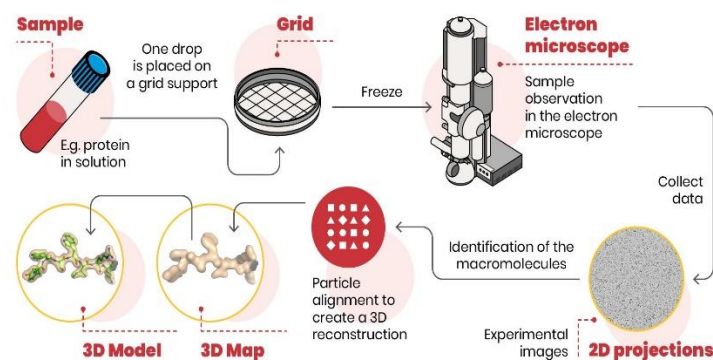


Fig.16 Structural analysis of proteins by Cryo-EM (from www.gsdiinternational.com)

Cryo-EM can be used for intramembrane molecule imaging as shown by Thonghin *et al.*⁴⁵. That method has been used, among others, to resolve the structure of an endo-lysosomal protein named TRPL1 (Fig.17).

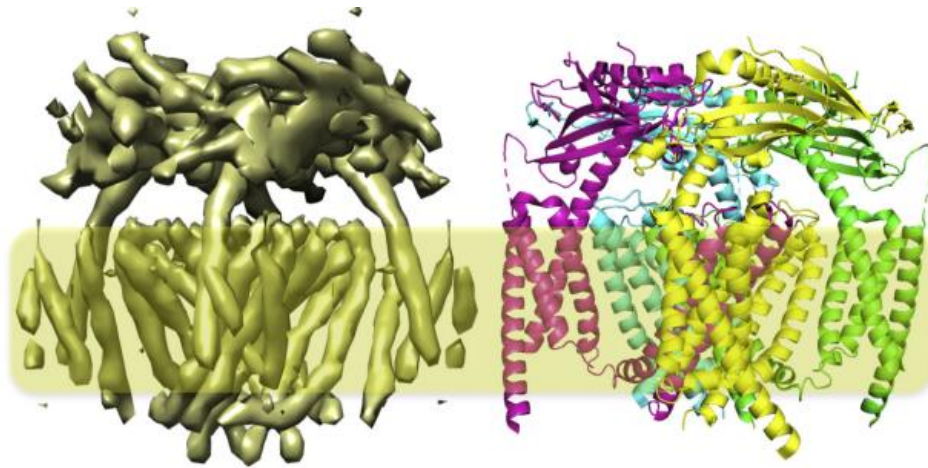


Fig.17 Cryo-EM of membrane proteins. Endo-lysosomal TRPL1 channel protein (EMD-6823) in amphipol A8-35. Strong structural features such as transmembrane helices (yellow transparent box) can be easily distinguished from the amphipol at a high-density threshold (left) allowing a molecular model to be built (right) (from Thonghin, N.; Kargas, V.; Clews, J.; Ford, R. C. *Cryo-Electron Microscopy of Membrane Proteins. Methods* **2018**, *147*, 176–186.)

Atomic force microscopy (AFM)^{46,47} is a microscopy technique that was developed in 1986⁴⁷ which allows the determination of the topography of an isolated molecule with a spatial resolution close to the atom. To this end, the sample is scanned by a stylus mounted on a cantilever whose deflection is quantified by the means of a laser. The laser's force sensitivity is of the order of a piconewton, and the deflection of the cantilever can be used to image the topography of the sample. It is important that the force experienced by the sample should be sufficiently high to perform the measurements but avoid the degradation of the sample (or the cantilever). To this end, the cantilever is mounted on a piezoelectric material whose height can be adjusted with a precision under the Angstrom and the stylus thus constantly sends feedback to maintain the right height (Fig.18). One important feature of the AFM hardware is to measure with the finest probe possible since the resolution of the image obtained directly depends on it. The scanning speed is lower than for other types of microscopies (about 10 frames per seconds for high-speed imaging AFM⁴⁸ against a femtosecond temporal resolution in high-speed transmission electron microscopy⁴⁹).

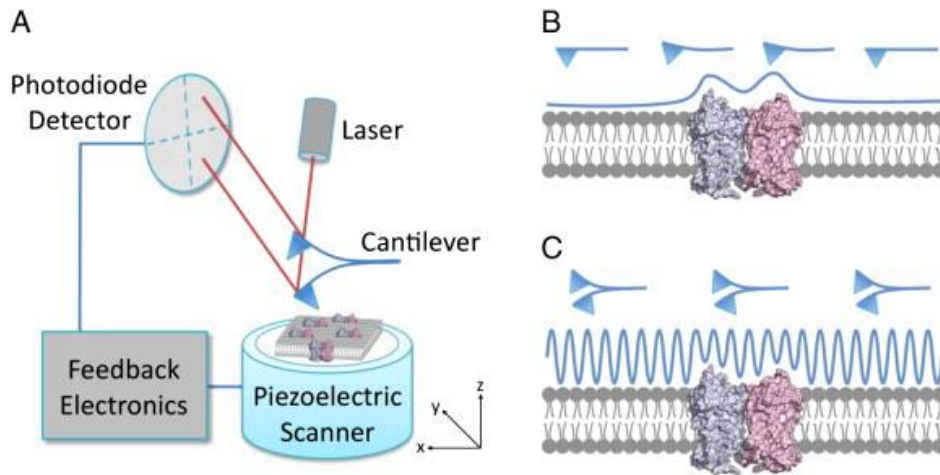


Fig.18 Structural analysis of proteins by AFM. A) General principles of the apparatus. B and C) topology measurement of the surface of membrane with the cantilever (from Whited, A. M.; Park, P. S.-H. *Atomic Force Microscopy: A Multifaceted Tool to Study Membrane Proteins and Their Interactions with Ligands. Biochim. Biophys. Acta BBA - Biomembr.* **2014**, *1838* (1), 56–68.)

AFM experiments can be performed to image but also to study inter- and intra- protein interactions by applying a stretching force to one or many proteins. For example, that technique has been used by McAllister *et al.*⁵⁰ to study the aggregation forces that take place between proteins and peptides such as Amyloid Beta peptides (Fig.19).

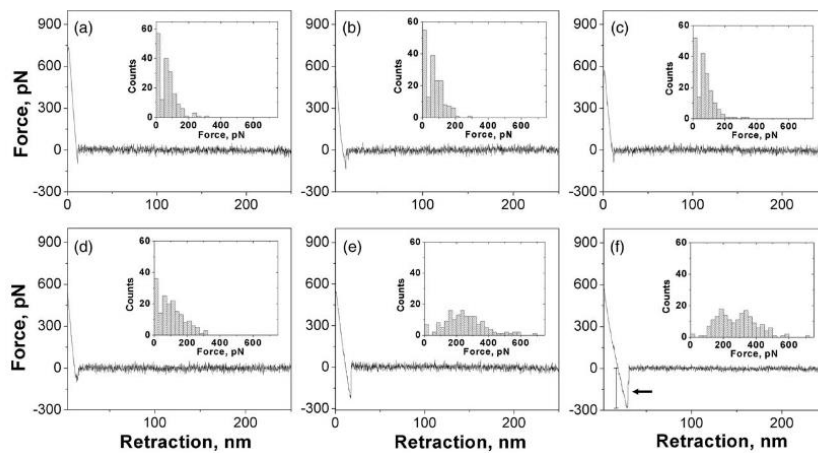


Fig.19 Typical force curves and histograms summarizing all force curves taken at (a) pH 9.8, (b) pH 7.0, (c) pH 5.1, (d) pH 3.7, (e) pH 2.0, and (f) pH 1.0. (from McAllister, C.; Karymov, M. A.; Kawano, Y.; Lushnikov, A. Y.; Mikheikin, A.; Uversky, V. N.; Lyubchenko, Y. L. *Protein Interactions and Misfolding Analyzed by AFM Force Spectroscopy. J. Mol. Biol.* **2005**, *354* (5), 1028–1042.)

Surface Plasmon Resonance Spectroscopy (SPR)^{51,52} is an optical technique that has mainly been developed during the 20th century to study intramolecular interactions. In this technique, a thin gold film is functionalized with a ligand that binds to the analyte(s) of interest. A polarized light beam is sent on this surface, causing the excitation of the free surface electrons. Then, these excited electrons oscillate, and that oscillation can be detected to characterize the interactions taking place at the

surface. Surface Plasmon Resonance occurs only for a certain value of the incident angle of the polarized light and the value of this angle called "resonance" varies according to the refractive index of the medium near the metal surface. It is therefore possible to determine the refractive index of the analyte-ligand medium by measuring the resonance angle and thus to study their interactions since those interactions are responsible for the variation of the optical properties of the medium. The main drawback of that method is that, as said before, the ligand must be grafted to the surface, which can modify its interactions with the analyte (Fig.20).

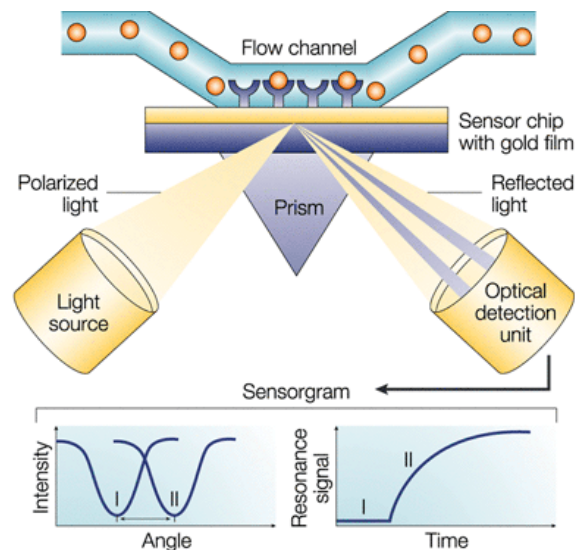


Fig.20 Analysis of molecule/ligand interaction by SPR (from Mitchell, J. *Small Molecule Immunosensing Using Surface Plasmon Resonance. Sensors* **2010**, *10* (8), 7323–7346.)

As said before, the SPR technique allows to study interactions and has been used by Omar *et al.*⁵³ to detect interactions between the dengue virus (DENV) and an immobilized monoclonal antibody (IgM) to assess its viral concentration (Fig.21).

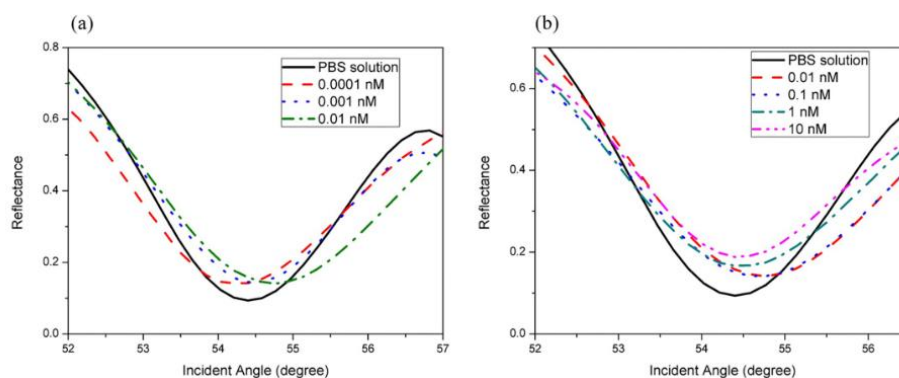


Fig.21 SPR reflectivity curves for Au/Fe-MPA-NCC-CTAB/EDC-NHS/IgM thin film in contact with different concentrations of DENV E-protein solution ranged from (a) 0.0001 nM to 0.01 nM and (b) 0.01 nM to 10 nM (from Omar, N. A. S.; Fen, Y. W.; Abdullah, J.; Chik, C. E. N. C. E.; Mahdi, M. A. *Development of an Optical Sensor Based on Surface Plasmon Resonance Phenomenon for Diagnosis of Dengue Virus E-Protein. Sens. Bio-Sens. Res.* **2018**, *20*, 16–21.)

In silico methods^{54,55} can also be used to resolve the structure of a protein or the interactions between several proteins by theoretical modelling. When using theoretical calculations, two alternative approaches can be performed: the comparative model or the minimisation of the free energy of the protein and its environment. In the comparative model, the sequence of the protein whose structure must be determined is compared to the sequences of a protein with well-characterized 3D structures. In that approach, the working hypothesis states that the amino acid sequence provides the structure to the protein and consequently, two sequences of high homology in amino acids present the same structure⁵⁶. The second approach does not rely on a comparison with a database. The aim is to minimize the free energy of the protein and its environment to identify the most stable 3D structure(s). Density functional theory (DFT), molecular mechanics (MM) and molecular dynamics (MD) are the most used methods in addition to quantum mechanics/molecular mechanics (QM/MM) which combine ab-initio and MM. Despite being more computationally demanding, this second approach does not require homologue sequences of known structures. The in-silico methods are implemented in many fields but are not self-sufficient and need to be verified experimentally, ideally by several orthogonal methods described above.

More recently, the introduction of artificial intelligence and machine learning algorithms allow some accurate prediction of the folding of proteins initiated by the AlphaFold project. In their paper, Pearce and Zhang⁵⁷ describe the evolution of protein structures and showed different protein structures that were calculated using AlphaFold2 software and their template modelling score (TM-score) with the experimental structures (Fig.22).

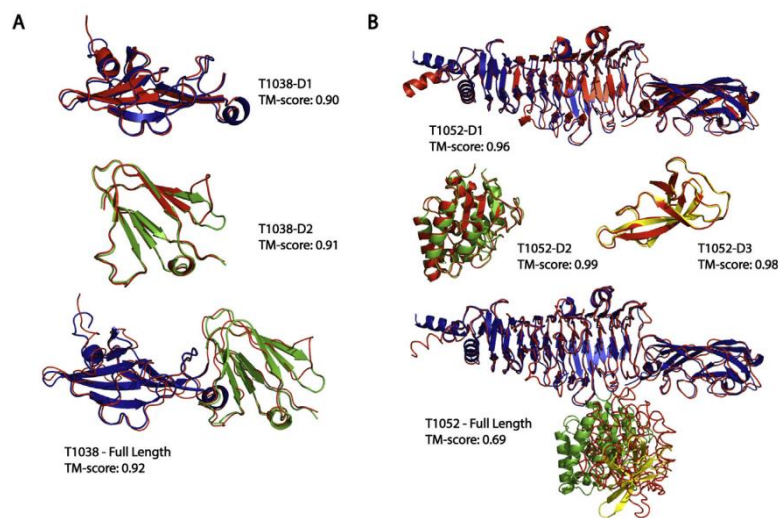


Fig.22 Representative examples of AlphaFold2 on multidomain protein structures in CASP14. The experimental structures are shown in red cartoons, while the predicted models are shown in different colours for different domains. A) modelling results for T1038, where AlphaFold2 achieved excellent performance on both the domain-level and full-length models. B) modelling results for T1052, where the domain-level models achieved an extremely high accuracy, but the full-length assembled structure had incorrect domain orientations. (From Pearce, R.; Zhang, Y. *Toward the Solution of the Protein Structure Prediction Problem. J. Biol. Chem.* **2021**, *297* (1), 100870.)

Mass Spectrometry (MS): Among those different characterization techniques, MS plays a key role in the structural analysis of proteins. The sequencing of proteins is routinely performed by MS based methods nowadays^{58,59}. That type of MS experiment aims at the determination of the primary structure of the studied protein and are generally classified as 3 general approaches referred as “bottom-up”, “middle-down” and “top-down”. The “bottom-up” and “middle-down” approaches are

relatively similar since they rely on the digestion of the protein(s) by a protease (or in some case, a combination of enzymes⁶⁰) to analyse the generated peptides typically by liquid chromatography coupled to MS (LC-MS). The major difference between these 2 approaches lies in the targeted lengths of the peptides: while the bottom-up approach aims at the complete digestion of the target protein (therefore generating peptides with relatively short sequences), the middle-down approach usually involves an incomplete digestion, leading to the production of peptides of longer sequences, typically several dozens of residues (Fig.23). Finally, those peptides are generally analysed by LC-MS/MS, which is currently considered as the gold standard method for such analyses. The top-down approach is fundamentally different since it does not involve any digestion step. In this method, the intact protein of interest is ionized, and its sequence is determined based on the fragments generated inside the MS instrument using different ion activation methods to generate product ions. These fragmentations techniques are based on electron activation such as Electron Transfer Dissociation (ETD) and Electron Capture Dissociation (ECD), photoactivation such as Ultraviolet Photodissociation (UPVD) and Infrared Multiphoton Dissociation (IRMPD), or collision with neutral gas such as Collision Induced Dissociation (CID) or Higher-energy C-trap Dissociation (HCD).

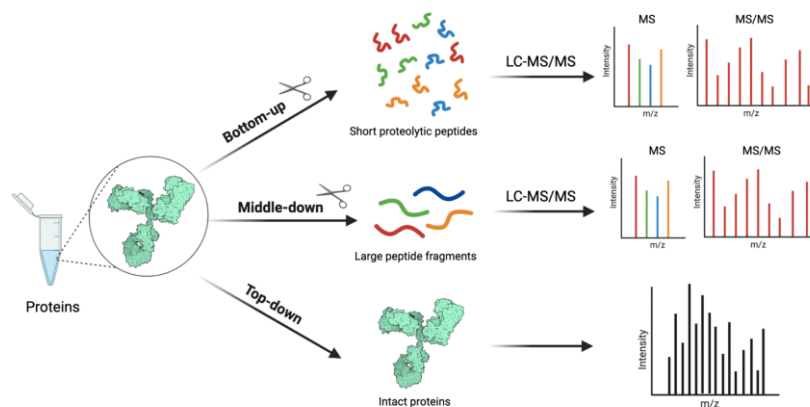


Fig.23 MS based sequencing of a protein based on the bottom-up, middle-down and top-down approaches (adapted from www.rapidnovor.com)

Liquid chromatography is a liquid phase separation technique based on a difference of partition coefficient of an analyte between the mobile phase and the stationary phase in a column. High-Performance Liquid Chromatography (HPLC) and ultra-high performance LC (UHPLC and UPLCTM) in 1 or 2 dimension are frequently used to separate a mixture of peptides in a bottom-up approach⁶¹ or proteins in a complex mixture⁶² which is often hyphenated to MS for detection. In their study, Xingkai Hao *et al.*⁶³ have studied the peptide composition of a milk digested with trypsin using bottom-up LC-MS/MS proteomics (Fig.24).

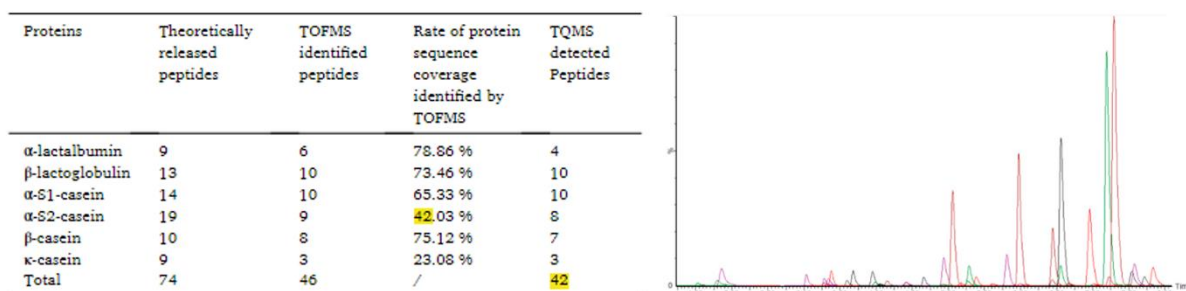


Fig.24 On the left, table of all the peptides that can theoretically be found in milk and on the right, the total ion chromatogram of the 42 peptides detected by LC-MS. (From Hao, X.; Fu, L.; Shao, L.; Chen, Q.; Dorus, B.; Cao, X.; Fang, F. Quantification of Major Milk Proteins Using Ultra-Performance Liquid Chromatography Tandem Triple Quadrupole Mass Spectrometry and Its Application in Milk Authenticity Analysis. *Food Control* **2022**, *131*, 108455.)

From the structural point of view, MS can also be used for the study of inter- and intra-proteins interactions by Hydrogen Deuterium eXchange (HDX) ^{64,65} or cross-linking (XL)^{66,67}. In a HDX experiment, the protein of interest is placed into a medium rich in deuterium (often using D₂O as source of deuterium), an exchange equilibrium is established between the hydrogens of the protein backbone (uniformly distributed on the proteins, sensitive to perturbations of the higher order structure and presenting a measurable exchange rate)⁶⁵ and lateral chains of the residues (extremely fast exchange, not accessible for HDX-MS) and the deuteriums of the solution (termed H/D exchange). As a result, H/D exchange occurs on the “exposed” parts of the protein, which can then be measured by MS due to the observable mass shifts (Fig.25) between ¹H and ²H (as deuterium). On the other hand, cross-linking involves the use of difunctional molecules of variable lengths (linkers) allowing to covalently bind two spatially close amino acids within the protein. As the linker is covalently attached, tandem mass spectrometry can be used to determine the position of the interaction within the sequence by typically using a bottom-up approach (Fig.26). Despite being powerful structural techniques, those techniques also present drawbacks. The HDX performed in solution can be perturbed during the ionisation step and reach a different distribution of deuterons that the one relevant in solution (this phenomenon is called “scrambling”)⁶⁸. On the other hand, cross-linking can create aberrant cross-links due to the intrinsic dynamics of the system, leading to misguided structural conclusions. Moreover, those two techniques require extensive data treatments.

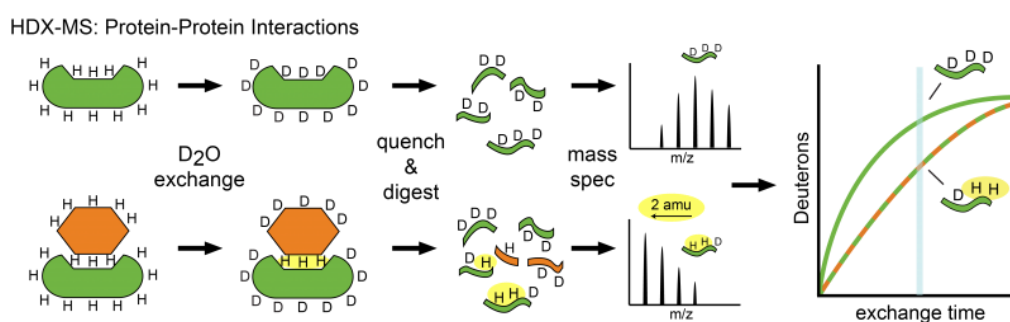


Fig.25 Hydrogen Deuterium Exchange on proteins (from www.underbakkelab.org)

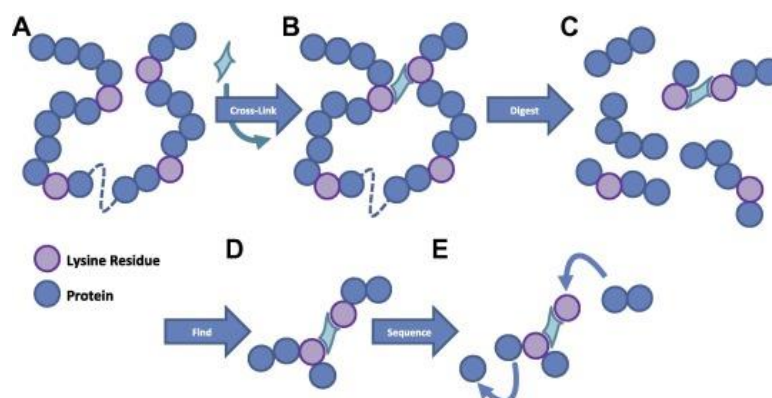


Fig.26 Cross-Linking of a protein (from Holding, A. N. XL-MS: Protein Cross-Linking Coupled with Mass Spectrometry. *Methods* **2015**, *89*, 54–63.)

3. The rise of Native MS and related issues

More recently, native MS was introduced as a MS technique aiming at maintaining structural features of biologically relevant macromolecules such as proteins or nucleic acids from solution to the gas phase during the desolvation by electrospray ionisation. The general idea of native MS is that the system to be sprayed should be placed in a solution as close as possible to the native conditions of the system and the obtained MS data reflect the structure of the biomolecule in solution. Within this hypothesis, various studies showed that native MS could be used to determine stoichiometry⁶⁹ of complexes and supra-molecular assemblies or dissociation constant⁶⁹ (Fig.27).

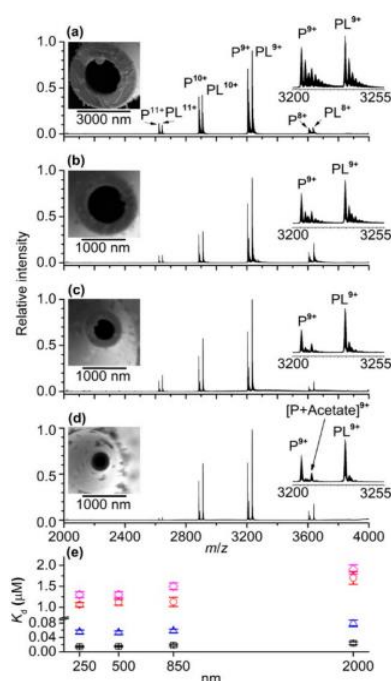


Fig.27 Narrow-bore nano electrospray ionization emitters with inner tip diameters less than 1000 nm used to obtain K_d values for carbonic anhydrase (P) inhibitors (L) (from Tamara, S.; den Boer, M. A.; Heck, A. J. R. High-Resolution Native Mass Spectrometry. *Chem. Rev.* **2022**, *122* (8), 7269–7326.)

However, a major issue with this type of workflow is that the electrospray ionisation and subsequent MS analysis are performed in vacuum while proteins in their native environments are almost exclusively functioning in aqueous conditions (exceptions can be found for proteins contained in nails and hair or acting as pores in the lipidic bilayer). As the 3D structure of a protein is determined by the balance between its different covalent and non-covalent intramolecular interactions, such a drastic change of environment (transfer from solution to the gas phase) must disturb, at least partially, those different interactions. It is therefore legitimate to wonder if the obtained results observed in native MS truly represents the studied systems in their native state or are a superimposition of these with the perturbations produced by the electrospray ionisation.

4. Capillary electrophoresis

Electrophoresis is an analytical method that was first used by Tiselius in 1930 when he described the separation of blood plasma proteins, namely albumin from α -, β - and γ -globulin. First performed in sieved medium such as agarose and polyacrylamide gel, the method was operated in open tubular devices, improving the cooling of the system and the global performance of electrophoresis-based separation methods. Over time, the technique improved, and in 1981⁷⁰, Jorgenson and Lukacs showcased the exceptional separation capabilities of high performance capillary zone electrophoresis (CZE) (Fig.28). The name electrophoresis includes together several types of separation methods based on the use of an electric field applied to charged or ionized species contained either in a buffer solution or a gel (agarose or polyacrylamide)⁷¹.

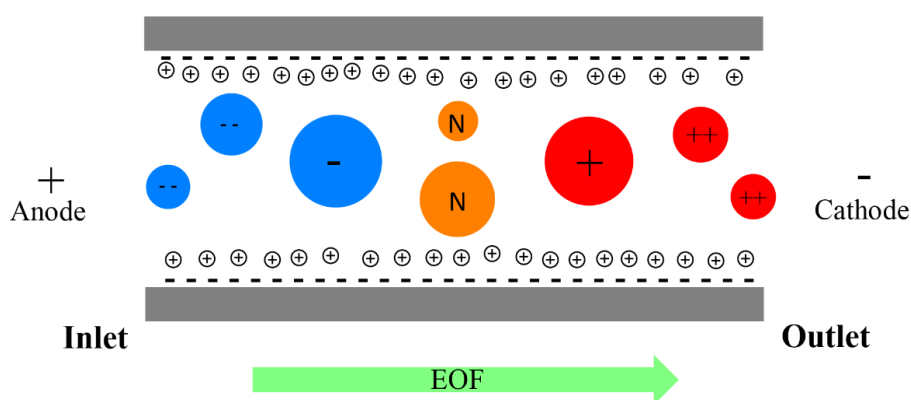


Fig.28 Representation of a capillary electrophoresis separation

Capillary electrophoresis can be used for 2 distinct purposes, either in an analytical approach to analyse the composition of a complex sample by separating its compounds, or to carry out physical chemistry studies. One major advantage of capillary electrophoresis is the versatility of the method offered by the different available modes : capillary gel electrophoresis (CGE), capillary zone electrophoresis (CZE), isotachopheresis⁷² (iTP), micellar electrokinetic chromatography (MEKC)⁷³ (separation caused by a difference in partition coefficient between the mobile phase and a stationary phase composed of suspended micelles), capillary electrochromatography (CEC), affinity CE (ACE), and different variants of kinetic capillary electrophoresis (KCE) . Additionally, CE can be coupled with different type of detectors offering good to excellent limit of detection and linearity, from optical detection such as UV and fluorescence, to conductivity (contactless conductivity detector, C4D), also including mass

spectrometry detection. For analytical applications, CE showed successful applications in the sequencing of DNA^{74,75} (Fig.29) and the analysis of the Chloroplast GrpE proteins from *Arabidopsis*⁷⁶.

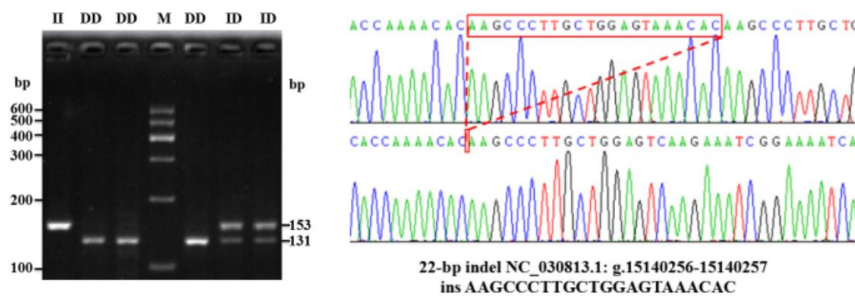


Fig.29 Agarose gel electrophoresis and DNA sequencing of 22 bp indel of the goat PITX2 gene (left panel) and result of DNA sequencing using capillary gel electrophoresis with light induced fluorescent (LIF) detector (right panel) (from Yan, H.; Jiang, E.; Zhu, H.; Hu, L.; Liu, J.; Qu, L. The Novel 22 Bp Insertion Mutation in a Promoter Region of the PITX2 Gene Is Associated with Litter Size and Growth Traits in Goats. *Arch. Anim. Breed.* **2018**, *61* (3), 329–336.)

On the other hand, CE can also be used for physical chemistry applications involving CZE and kinetic capillary electrophoresis. In kinetic capillary electrophoresis, a KCE modes called "equilibrium capillary electrophoresis of equilibrium mixture" (ECEEM)⁷⁷ and "non-equilibrium" (NECEEM)^{77,78} allow the study of the thermodynamics of a reaction by measuring the migration times and the areas under the peaks of interest, the mobility of an analyte being correlated to its equilibrium constant. The analytes are placed in presence of a ligand with which they reach an equilibrium, then the analytes migrate differentially under the influence of an electric field according to the dissociation constants with the ligand. For example, Krylov and Berezovski⁷⁹ have used NECEEM experiments with fluorescent detection to study the equilibrium dissociation constant of a protein-DNA complex and the monomolecular rate constant of complex decay (Fig.30).

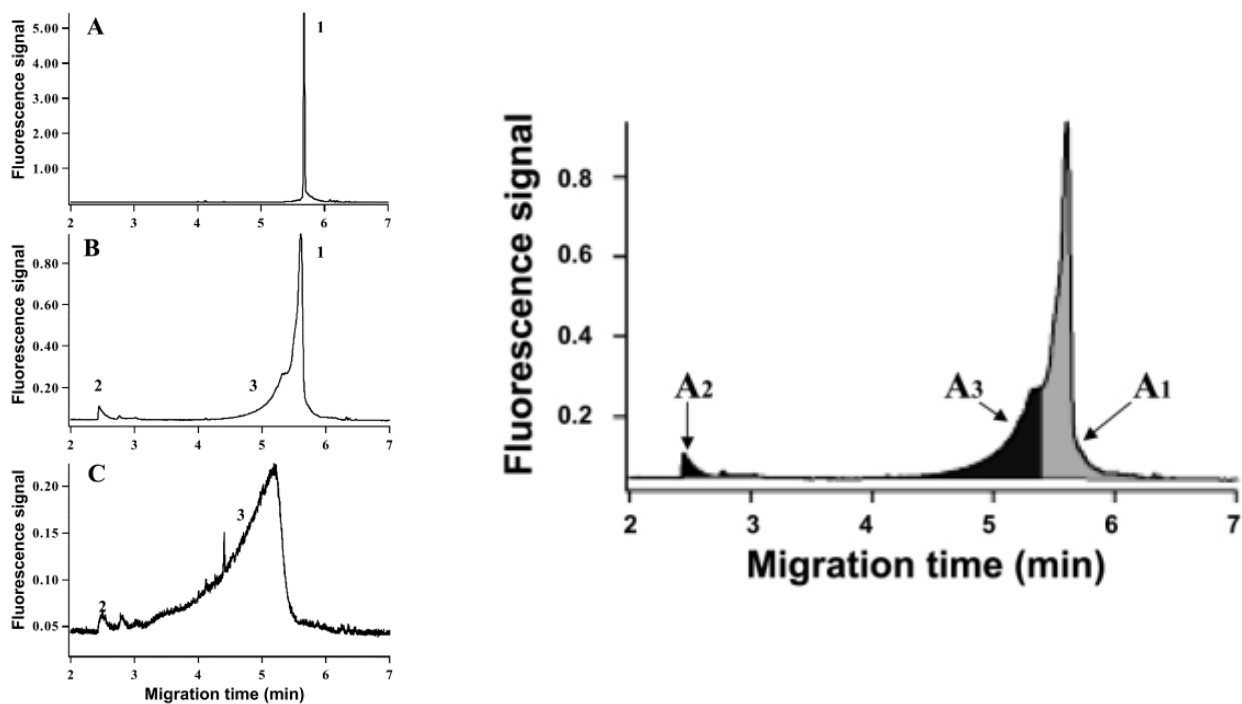


Fig.30 NECEEM of SSB and fdDNA. The total concentrations of SSB and fdDNA in the mixtures were: (A) $[SSB]_0 = 0$, $[fdNA]_0 = 0.20 \mu\text{M}$; (B) $[SSB]_0 = 0.32 \mu\text{M}$, $[fdNA]_0 = 0.16 \mu\text{M}$; (C) $[SSB]_0 = 0.80 \mu\text{M}$, $[fdNA]_0 = 0.10 \mu\text{M}$. The run buffer was 25.0 mM borate at pH 9.4. (from Krylov, S. N.; Berezovski, M. Non-Equilibrium Capillary Electrophoresis of Equilibrium Mixtures—Appreciation of Kinetics in Capillary Electrophoresis. *The Analyst* **2003**, *128* (6), 571–575.)

Capillary zone electrophoresis (CZE)⁸⁰ can be used to obtain some structural information as the mobility of a protein directly depends on its average charge in solution (q) and its hydrodynamic radius (R_h). R_h is a structural parameter that represents the radius of a sphere composed of the charged protein and all the water molecules interacting with it. The average charge in solution of a protein can be estimated based on the pK_a values of its constitutive residues which allows to determine the R_h value). Zhang *et al.*⁸¹ have used this method for structural purposes to study proteins such as lysozymes or bovine serum albumin (Fig.31).

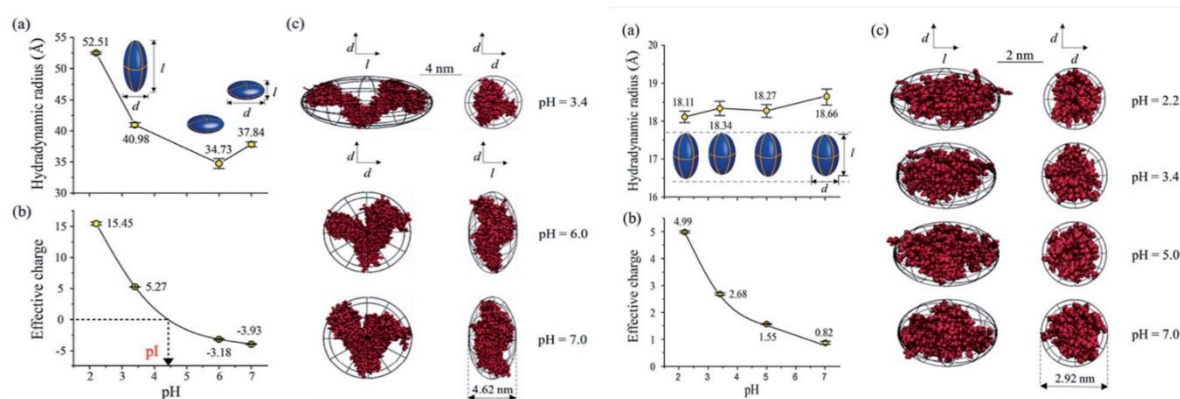


Fig.31 Conformation and charge state variations of BSA (on the left) and lysozyme (on the right) under different pH conditions. (a) Hydrodynamic radii and (b) effective charges of BSA at different pHs, and pI indicates the isoelectric point of BSA. (c) Side and top views of BSA conformations under different pH conditions (from Zhang, W.; Wu, H.; Zhang, R.; Fang, X.; Xu, W. *Structure and Effective Charge Characterization of Proteins by a Mobility Capillary Electrophoresis Based Method. Chem. Sci.* **2019**, *10* (33), 7779–7787.)

Based on this workflow, it is also possible to perform thermal or chemical denaturation to follow the evolution of R_h induced by the thermal or chemical unfolding. The great advantage of that last type of experiment is the possibility of studying the structure of a protein in its native environment (*i.e.*, in solution) but the obtained structural information is at the global level (overall shape and trends of folding and unfolding).

5. Ion mobility

Ion mobility spectrometry (IMS) designed since the 1890's⁸² is a separation technique then revisited in the 1970's by Cohen and Karasek^{83,84}, based on the separation of ions in a cell filled with a drift gas under the influence of an electric field. The ions are separated according to both their charge (z) and a structural parameter, the collision cross section (CCS). The CSS of an ion represents the momentum transfer between ion and gas particles averaged over all gas-ion relative thermal velocities (Fig.32).

The CCS can be deduced from the mobility coefficient in the gas phase using the Mason Schamp equation (Eq. 1). Keep in mind that this equation used the CGS (centimeter-gram-second) system of unit instead of the SI based units⁸⁵.

$$\Omega = \frac{3ez}{16N} \left(\frac{2\pi}{\mu \cdot K_B \cdot T} \right)^{0.5} \frac{1}{K} \quad (eq1)$$

where Ω is the collision cross section in cm^2 (the usual subunit is \AA^2), e is the elementary charge in statcoulombs, z is the absolute number of charge of the ion, N is the density number as the number of particles per cm^3 of buffer gas, μ is the reduced mass in g, K_B is the Boltzmann constant in CGS unit ($1.3807 \times 10^{-16} \text{ cm}^2 \cdot \text{g} \cdot \text{s}^{-2} \cdot \text{K}^{-1}$), T the temperature of the buffer gas in K, and K is the mobility coefficient of the ion in the gas phase in $\text{cm}^2 \cdot \text{V}^{-1} \cdot \text{s}^{-1}$. Usually, one prefers to use the reduced ion mobility coefficient K_0 .

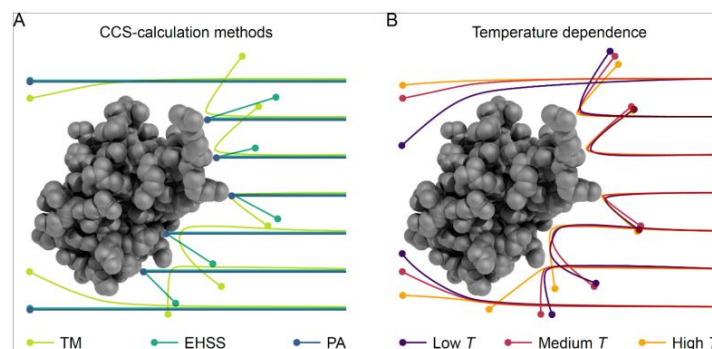


Fig.32 Representation of the concept of collision cross section (from Gabelica, V.; Marklund, E. *Fundamentals of Ion Mobility Spectrometry. Curr. Opin. Chem. Biol.* **2018**, *42*, 51–59.)

In the specific field of protein analysis, IMS coupled with mass spectrometry detection was used to characterize proteins structures such as the structural behaviours of bradykinin sprayed from several solvent compositions (Fig.33).

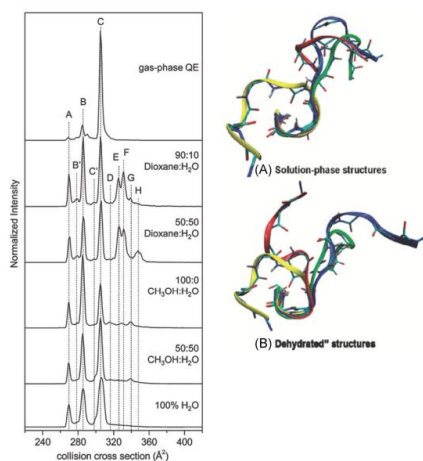


Fig.33 Solvent-dependent CCS profiles and examples of four low-energy structures for bradykinin 3+ ions in solution phase and “dehydrated” states. The solvent composition used for each solvent system is shown to the right of each plot (from McCabe, J. W.; Hebert, M. J.; Shirzadeh, M.; Mallis, C. S.; Denton, J. K.; Walker, T. E.; Russell, D. H. *THE IMS PARADOX: A PERSPECTIVE ON STRUCTURAL ION MOBILITY-MASS SPECTROMETRY. Mass Spectrom. Rev.* **2021**, *40* (3), 280–305.)

Activation methods can be used to study the unfolding of the ion, known as collision induced unfolding (CIU)^{86,87}. Alternatively, the fragmentation pathway can also be studied by using (energy resolved) collision induced dissociation (CID)^{86,88}, electron transfer dissociation (ETD)^{86,89}, electron capture dissociation (ECD)^{86,90} and even ultraviolet photodissociation (UVPD)^{86,91}. Overall, IMS presents the same disadvantage as CE, namely that the obtained structural information is global and described as the CCS, a bidimensional projection of the initial tridimensional structure. Activation methods allow a better understanding of the mechanisms of unfolding and refolding and to compare similar molecular structures. CIU-IMS experiments have been used by Phetsanthad *et al.*⁹² to compare the unfolding mechanism of Human Serum Albumin (HAS) and Bovine Serum Albumin (BSA) (Fig.34).

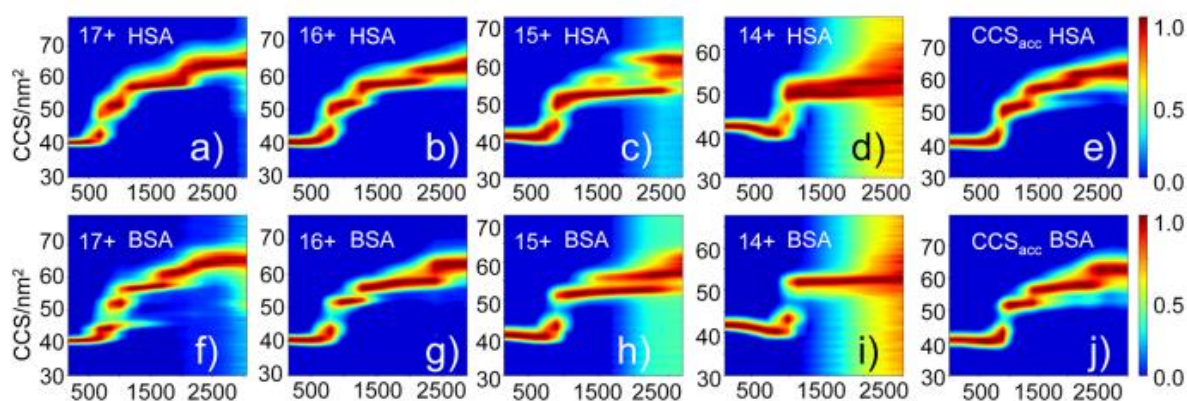


Fig.34 Comprehensive structural comparison between HSA and BSA using collision induced unfolding and ion mobility mass spectrometry. Unfolding fingerprints for individual charge states and CCS evolution as a function of the lab-frame energy provided to the ionized proteins transferred into the gas phase generated of (a–e) HSA and (f–j) BSA (from Phetsanthad, A.; Li, G.; Jeon, C. K.; Ruotolo, B. T.; Li, L. Comparing Selected-Ion Collision Induced Unfolding with All Ion Unfolding Methods for Comprehensive Protein Conformational Characterization. *J. Am. Soc. Mass Spectrom.* **2022**, *33* (6), 944–951.)

6. Objectives and strategy

As mentioned in previous sections, the electrospray ionization process is possibly at the origin of structural perturbations because the intramolecular forces responsible for the adoption of the structure in solution are different from those present in the gas phase. The absence of the counterions in the gas phase could also induce ion stretching due to Coulomb repulsion. On the other hand, the time required for the electrospray ionisation process (millisecond timescale) may be too rapid for the ionized protein to undergo significant structural change (by exploring its energy landscape). Consequently, structural features of proteins present in solution may be preserved during ionization and (IM-)MS analysis, confirming the hypothesis postulated in native MS topics. The aim of this master's thesis is to bring some elements of answer to that question by comparing the structures of different peptides in solution and in the gas phase. The general idea is to structurally assess different peptides in solution and in the gas phase to reveal if changes in their migration behaviours can be observed from one phase to the other. Similarities and deviations can be classified based on different physico-chemical properties such as the percentage of hydrophobic residues or the presence of specific secondary structures that type of classification could be very interesting but will only be carried out if the necessary time is available.

The experimental workflow will be based on the use of two electrophoretic migration methods mentioned above, namely capillary electrophoresis (CE) and ion mobility spectrometry (IMS) both coupled to high resolution mass spectrometry (HR-MS). Capillary electrophoresis-mass spectrometry experiments will be performed using 2 different technologies of CE-IM-MS interface: one will be based on the use of a microfluidic sheath liquid (SL) interface (that assists the ionization process using additional liquid also containing organic modifiers), and the other will be performed without sheath liquid (the so-called sheathless interface (which produces droplets of significantly smaller size than the SL interface) to prevent any structural alteration of the peptides and proteins caused by the organic modifier from the sheath liquid. As described in previous sections, CE allows the study of peptides in solution while IMS performs the structural assessment in the gas phase (Eq.2).

$$\mu_e = \frac{q}{6\pi \cdot \eta \cdot R_h} \quad (eq2)$$

where μ_e is the electrophoretic mobility in $m^2/(V.s)$, q is the (averaged) charge in solution in C, η is the (dynamic) viscosity in Pa.s, and r_h is the hydrodynamic radius in m. ($V = (kg.m^2)/(A.s^3)$) and ($Pa = kg/(m.s)$)

The determination of the average charge in solution of the species will be performed using the pK_a values of the different residues composing the peptides using their distribution functions. A combination of those results with computational chemistry tools to estimate the exposure to the solvent of the ionizable lateral chain of the residues could be interesting but will only be realised if the required time is available. A comparison of CCS values and hydrodynamic radii gathered from both CE and IMS techniques will be used for the comparison of structures in solution and the gas phase. The mobility trends μ_e versus K of the peptides/proteins obtained from CE and IMS will be compared. Different pH values of the BGE solution in capillary electrophoresis will be tested during coupling with the IMS to vary the orthogonality of those two methods and compare R_h and CCS values at similar or different charges.

The first part of this work will focus on the study of peptides derived from the digestion of reduced and alkylated BSA. The aim of this digestion is to create large libraries of peptides which will be investigated by CE-IM-MS to compare their respective mobilities in solution (μ_e) and in the gas phase (K) (Fig.35). The IMS mobility (K) of an analyte is obtained from the drift time of this analyte (t_d), the length of the drift cell (L) and finally the applied electric field (E) according to

$$K = \frac{v_d}{E} = \frac{L}{t_d \cdot E} \quad (eq3)$$

where E is the electric field in $V.m^{-1}$, v_d is the (drift) velocity of the ion in $m.s^{-1}$, L is the length of the drift cell in m, and t_d is the drift time of the ion in s.

The mobility K of a specific analyte can then be converted into the corresponding CCS value according to the Mason-Schamp equation (equation 4) when rearranging equation 2, knowing the charge state (determined by the mass spectrum due to the ESI process)

$$K = \frac{3}{16N} \cdot \left(\frac{2\pi}{\mu k_B T} \right)^{1/2} \cdot \frac{q}{\Omega} \quad (eq4)$$

The CE electrophoretic mobility (μ_e) can also be calculated from the migration time of the analyte (MT), the effective length of the capillary to the detector (l), the electric field (E) and the mobility of the electroosmotic flow (μ_{EOF}) according to the following equations:

$$\mu_{app} = \frac{l}{MT \cdot E} \quad (eq5)$$

where μ_{app} is the apparent electrophoretic mobility ($m^2 \cdot V^{-1} \cdot s^{-1}$), l is the length of the capillary in m, MT is the migration time in s, and E is the electric field applied on the CE capillary in $V \cdot m^{-1}$.

$$\mu_{app} = \mu_e + \mu_{EOF} \quad (eq6)$$

The value of the electroosmotic flow (EOF) mobility can be determined by using a neutral marker such as sucrose but was not required in this paper because I only searched to observe relative changes. The apparent electrophoretic mobilities is the contribution of the true electrophoretic mobilities of the peptides summed to the value of the EOF. The electrophoretic mobility μ_e depends on the analyte's average charge in solution (governed by the pH of the BGE for ionizable moieties) and its hydrodynamic radius according to equation (2) (provided again for your convenience):

$$\mu_e = \frac{q}{6\pi \cdot \eta \cdot R_h} \quad (eq2)$$

Using this workflow, the mobilities K (gas phase) and μ_e (solution) can be determined after normalisation of the charge for all the studied species and reported in a plot K/q as a function of μ_e/q :

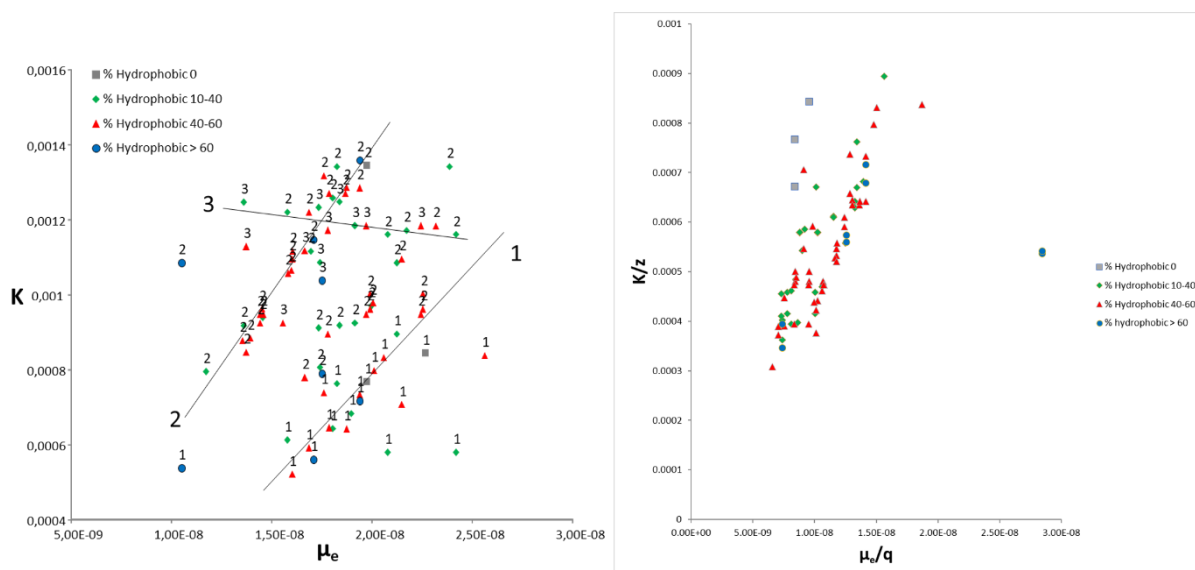


Fig.35 Comparison of CCS and R_h of BSA tryptic peptides obtained by CE and IMS: left without charge normalization, right with charge normalization

In this type of plot, where only the structural parameter is assessed, differential behaviours can be observed, with peptides presenting 2 structures in solution while only 1 in the gas phase (Fig.36) peptide SLHTLFGDELCK for example) or 2 structures in solution and 2 structures in the gas phase (Fig.36) peptide ECCDKPLLEK for example).

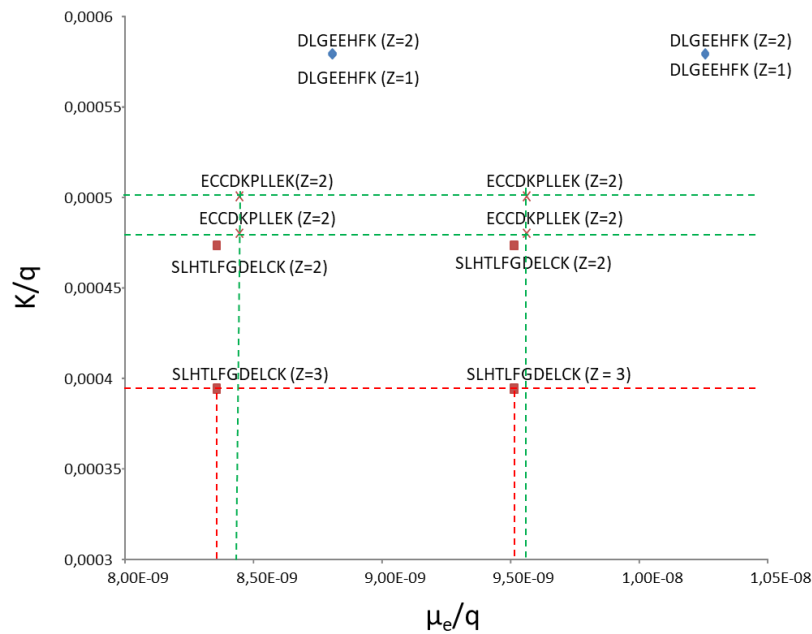


Fig.36 Normalized mobility/charge in CE and IMS for some peptides which appeared to have 2 conformations in solution and in the gas phase (SLHTLFGDELCK and ECCDKP LLEK) or 2 conformations in liquid phase but 1 in the gas phase (DLGEEHFK)

That type of CE versus IMS experiment (or to be precise, mobility comparison between solution and gas phase) enables the comparison of the behaviour of peptides in solution (as reflected by their peaks in CE) and in the gas phase (as revealed by the arrival time distribution or ATD) in IMS. This comparison allows to assess the populations of structures observed in both media.

Thereafter, the unfolding of those peptides will be investigated by chemical activation experiments in CE and by collision induced unfolding in IMS⁹³. Activation experiments are widely used in IMS as they allow to link the evolution of the CCS (evolution of percentages between the different conformation populations present) as a function of the energy supplied to the ions (Fig.34). That type of approach is much less common in CE. The obtained results will then be compared in order to spot the differences and similarities between the two phases. If a peptide exhibits different behaviours in one of those two experiments, we will be able to conclude that there is a loss of structural information during the phase transfer. Conversely, if both experiments yield the same type of results for multiple types of activation, we can conclude that there is, at least partially, retention of structural features.

7. Material and methods

7.1. Ion mobility determination in the gas phase and solution by capillary electrophoresis coupled with ion mobility mass spectrometry (CE-IM-MS):

Experiments were carried out using two kinds of electrophoresis systems, either a Beckman electrophoresis system coupled to a Waters Synapt G2 HDMS via a home-made CE-IM-MS interface using a sheath liquid (electrolyte solution used to close the capillary electrophoresis electrical circuit in our case composed of 50 % isopropanol and 50 % water, with a formic acid concentration of 10 mM to obtain optimum viscosity for a stable Taylor cone, detailed starting on page 56) or a SCIEX electrophoresis system (CESI8000) using a commercially available OptiMS sheathless interface (SCIEX) to assess the impact of the interface on the results. Peptide migration comparison was performed using different mixtures of peptides. The first peptide mix (residue sequences using the 1-letter provided in Table 1) was composed of “MRFA”, [Glu¹]-Fibrinopeptide B human (thereafter referred as Glufib) and various pI markers (CIEF pI markers from Beckman Separations) and was used as quality control for the CE-IM-MS setup. This is a simple mixture allowing fast data processing to evaluate the optimization of the experimental conditions. The different important features of this mix are summarized in the following (table 2):

Table 2 sequences of the model peptides used to optimize the CE-IM-MS experiments

Peptide	Sequence	Molecular mass (Da)	[M+H]⁺	[M+2H]²⁺
MRFA (pI 9.5)	MRFA	524.26	524.265	262.64
Glufib* (pI 4.0)	EGVNDNEEGFFSAR	1569.65	1570.68	785.84
pI 4.1	WDDD	590.24	591.25	296.13
pI 5.5	WEH	470.19	471.2	236.10
pI 7.0	WEHR	626.29	627.3	314.15
pI 9.5	WYYYKK	949.47	950.48	475.74
pI 10.0	WYKK	623.74	624.35	312.68

* [Glu₁]-fibrinogen human peptide

The second peptide mix for this work was composed of the reduced and alkylated peptides generated by the tryptic digestion of mature Bovine Serum Albumin (BSA, uniprot as ALBU_BOVIN). BSA is a 66,433Da protein composed of 582 residues (607 residues if including signal and propeptide) characterized by the sequence provided in (Annex 1).

The list of the theoretical tryptic peptides of BSA (after reduction and cysteine carbamidomethylation, i.e. sulfhydryl or thiol derivatization with iodoacetamide ICH₂CONH₂, 3 missed cleavages authorized) can be found in the annex to this document ([Annex 1](#)) (generated using UniProt, ExPASy Peptide Mass tool). This mix of peptides was used to perform the migration comparison of peptides between CE and IMS based on a higher number of peptides presenting very different physico-chemical properties ([Annex 2](#)).

7.2. Electrophoretic mobility determined in solution by capillary electrophoresis:

First, the pH of the background electrolytes (BGE) of the CE experiments was selected to match the averaged charge states in solution (as far as possible) to the charge states distributions of the peptides generated by the electrospray ion source in the mass spectra. This strategy should prevent any structural change due to the difference of charge between the liquid and the gas phase. To this end, a background electrolyte composed of 100mM formic acid (FA) at pH 2.4 was used.

These different peptide mixes were investigated by CE-IM-MS where peptide migration times (CE) and arrival time distributions (ATD) from IMS were reported. Both mobility values were then converted into their respective mobility values normalized by the charge (μ_e/q for CE and K/q for IMS) using the equations described in the “Objectives and strategy” section (page 27 to 29).

These samples were later investigated at different pH values to assess the charge/structure relationship. To this end, BGE based on pH 2.4 (obtained with a formic acid-based BGE), pH 4.0 and pH 6.5 using 25mM ammonium formate-based BGE were tested. Changing the pH of the BGE also affect the orthogonality of the CE separation compared to ion mobility, as the average charges of the peptides in CE (solution) are dictated by the pH of the solution, whereas the charge in the gas phase is dictated by proton affinity imposed by the ESI process.

The bare fused silica capillary dimension used for the sheathless experiments was 91cm length for OptiMS Sheathless experiments and 30 μ m as internal diameter (150 μ m outer diameter) for a total volume of 0.643 μ L. Bare fused silica capillary dimension used with the sheath liquid interface were 90cm length and 50 μ m internal diameter (375 μ m outer diameter) for a total volume of 1.76 μ L.

The CE runs were performed at +30kV (i.e. normal polarity) with a voltage ramping from 0 to 30kV of 1 minute. The background electrolytes concentration was optimized to provide a CE current of approximately 10 μ A of CE current for the entire set of experiments to avoid different Joule heating effects between experiments, which could lead to changes in the observed conformations.

The samples were hydrodynamically injected inside the capillary. The pressure and duration of injection was set to reach 2% of the capillary volume, considering a relative viscosity of the BGE as 1 at +25°C for any experimental conditions. The same parameters were used with sheathless and sheath liquid.

8. Ion mobility parameters of the Synapt G2 HDMS

A Waters Synapt G2 HDMS (Waters) ion mobility mass spectrometry was used. Briefly this instrument uses an ion stacked-rings IMS cell design (called Tri-Wave) to produce voltage waves that elute the ion from the IMS cell toward a Time of Flight (TOF) mass analyzer. The Synapt G2 HDMS was fitted with an

electrospray Z-spray geometry ion source limiting the injection of neutral species inside the instrument. A quadrupole allows the selection of precursor ion if required. The Trap and Transfer sections are located before and after the IMS cell, respectively. Trap and Transfer cell are also using the ion stacking ring geometry to perform collision induced dissociation with collision with Ar. An He cell filled with helium is located prior the IMS cell filled with nitrogen to limit the fragmentation of ions during their injection in the Tri-Wave.

The ESI voltages applied to the CE-IM-MS interface were either +1.2kV for the sheathless interface and +2.8kV for the sheath liquid CE-IM-MS interface to produce a stable spray when the CE voltage was applied. The sampling cone value was 20V and extraction cone was 2V. The mass range was 50-2000 m/z . The Tri-Wave ion mobility parameters were 180mL/min of He in the He window while a flow of 120mL/min of N₂ was used in the ion mobility cell. A flow of 4mL/min of Ar was used in both Trap and Transfer cells. The wave velocity was set at 750m/s and wave height to 37V those two parameters were chosen after pre-optimization on a mixture of MRFA and (Glu1)-Fibrinopeptide B to elute all ion within the 200 bins of the ion mobility mass spectrometry scans. All other parameters (MassLynx v4.1) were the default parameters, except for specified values.

The "Trap Bias" parameter of the Synapt G2 was also modified. At each pH value, the parameter was set to 40V (default value), 65V, and 75V. Trap bias affect the kinetic energy of the ion provided during the transfer between the outlet of the Trap collision cell and the inlet of the helium window of the ion mobility cell. In other words, the soft collision of the ion with He during the introduction in the ion mobility cell will affect the ion heating, i.e. the effective temperature of the ions.

9. Sample preparation

Several aliquots of 50µg of Bovine Serum Albumin (BSA) were digested according to a standard protocol carried out in 50mM NH₄HCO₃ buffer at pH 7.8. Reduction of disulfide bonds of BSA was performed using dithiothreitol (DTT) at a concentration of 10 mM, followed by cysteine alkylation (cysteine carbamidomethylation) with 20mM of iodoacetamide (IAM) and a further "reduction" with DTT (at 11mM added) to deplete the excess of IAM. The sample was then treated with a 2-D Cleanup kit (ReadyPrep 2-D Cleanup kit from BIO-RAD) to purify the sample by precipitating quantitatively the target proteins and removing the supernatant which could contain detergents, salts, lipids, phenolics or nucleic acids. Once the cleanup stage was completed, a dry pellet was obtained which could either be stored for several weeks in the freezer or directly digested to obtain the peptide sample for the analysis by CE-IM-MS. The trypsin digestion step is in fact a succession of two digestions to achieve a complete digestion (i.e. in theory without miscleavage). First, the pellet is solubilized in 50mM NH₄HCO₃ pH 7.8 buffer before submitted to porcine trypsin digestion (Trypsin Gold mass spectrometry grade, Promega, witch briefly consists of lysine methylated trypsin and tosyl phenylalanyl chloromethyl ketone (TPCK) chymotrypsin inactivation, then purified by affinity chromatography) using a ratio of 1µg of trypsin for 50µg of protein. The digestion was performed at 37 degrees Celsius overnight. Then a second digestion step is performed. The sample was solubilized in 80% acetonitrile and digested during 3 hours at 37°C, using a trypsin/BSA ratio of 1:100. Finally, the digestion is stopped by boiling the samples for two minutes before evaporation using a speed vacuum instrument to recover the digested peptides pellets. The peptides were finally solubilized in the 10-times diluted background electrolytes before their analyses by CE-IM-MS.

10. Data processing

The in-silico digestion was performed either using peptide-mass tool from ExPASy website (https://web.expasy.org/peptide_mass/), Protein Prospector MS-Digest web tool (<https://prospector.ucsf.edu/prospector/cgi-bin/msform.cgi?form=msdigest>). A spreadsheet software was used for the statistics of the generated peptides (average/median length, occurrences ...). All MS data were processed manually.

The MS and IM-MS data obtained from the Synapt G2 HDMS were processed using MassLynx v4.1. The peptide list generated from [Table 2](#) and [Annex 1](#) were monitored in the raw data in the CE dimension (CE migration time, MT), the ion mobility dimension (ATD), and the MS dimension. The peptides were identified according to their exact masses and their experimental isotope patterns in the mass spectra (matched with the theoretical ones).

The MTs, ATDs, m/z ratios (charge states in the mass spectra), and average charge state computed in solution were reported in a spreadsheet software (e.g. Microsoft Excel) for each detected peptide. The charge states distribution of the peptide in solution were computed using the Henderson-Hasselbalch charge states distribution equations encoded in an Excel spreadsheet. Briefly, assuming that all the residues are exposed to the solvent, it reads the 1-letter sequence of the peptide and computes the average charge due to the linear (i.e. sum) contribution for each residue based on the pH of the solution and the pK_a of the N-ter, C-ter, and the side chains of the residue.

For peptides detected at several migration times and/or arrival time distributions, Driftscope (proprietary software from Waters) and a home-made Python Script (courtesy of Dr. Christopher Kune) were used to produce the 2D ion heatmaps (MT vs ATD vs ion intensity color-coded).

11. Library of studied peptides

The choice of BSA as the model protein was based on its extensively characterized sequence and its tendency to generate mis-digested peptides (referred to as mis-digests) when subjected to trypsin digestion under specific experimental conditions. This propensity is attributed to the presence of prolines, as well as consecutive lysins and arginines in its sequence, which hinder trypsin from cleaving certain sites. Consequently, this phenomenon leads to the production of a larger peptide library. The digestion of BSA has the potential to yield 307 distinct peptides with zero to three miscleavages, and these are detailed in the document's annex ([Annex.1](#)). The obtained peptides were however less numerous than expected, as presented in ([Fig.37](#)).

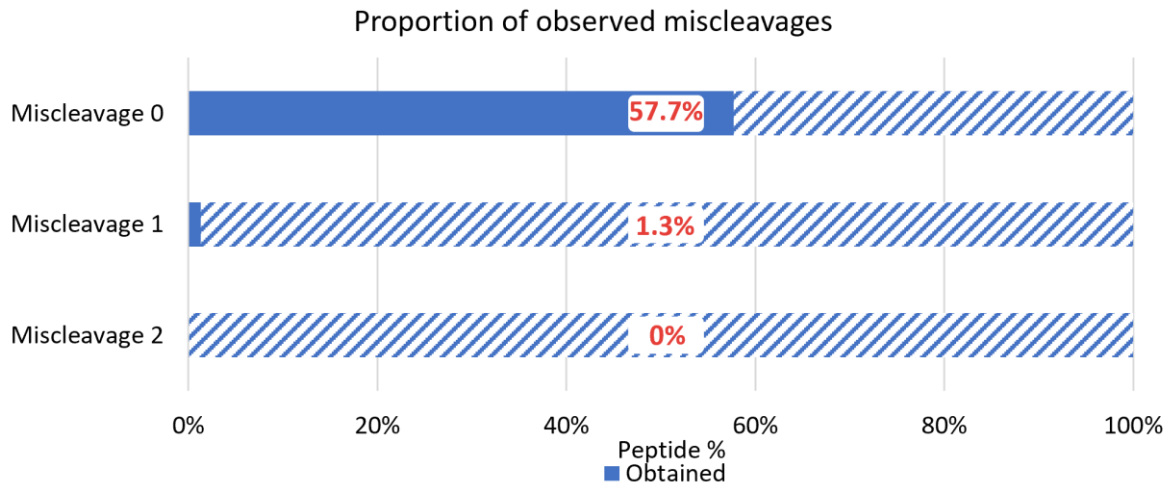


Fig.37 Histogram representing the number of peptides observed on the total number of theoretical possible peptides in regards of the number of potential miscleavages

46 unique peptides were detected and confidently identified in the CE-IM-MS data. Performing in-silico digestion on the mature BSA (Uniprot identifier P02769) with trypsin and assuming no miscleavage results in the generation of 73 peptides, each containing a minimum of 2 residues. These peptides have an average length of 7.9 residues (with a median of 7) and a maximum length of 20 residues (**Fig.38**)

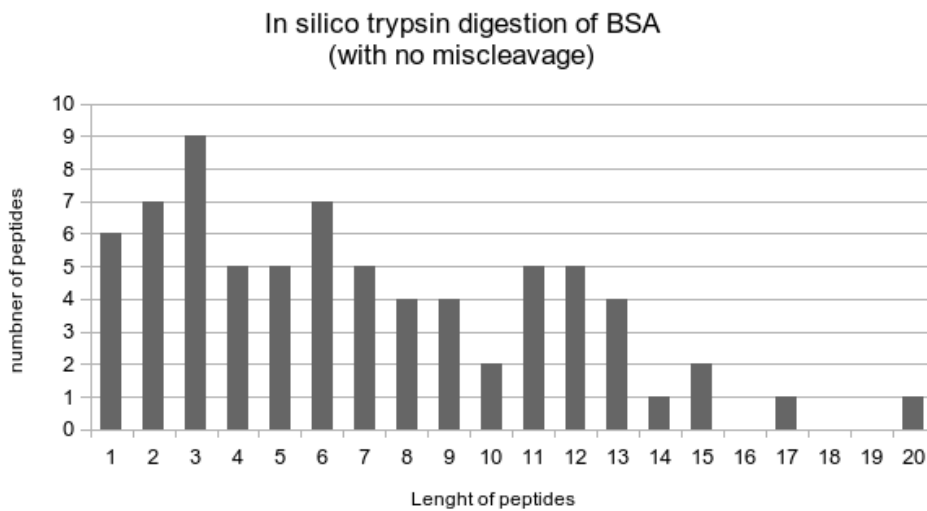


Fig.38 Histogram representing the number of peptides and length of peptide obtained from in silico digestion with no miscleavage allowed.

In the case of allowing a maximum of one miscleavage, the in-silico digestion with trypsin anticipates the creation of 150 distinct peptides. These peptides exhibit an average length of 12.3 residues (with a median of 11) and can extend up to a maximum length of 31 residues. (**Fig.39**).

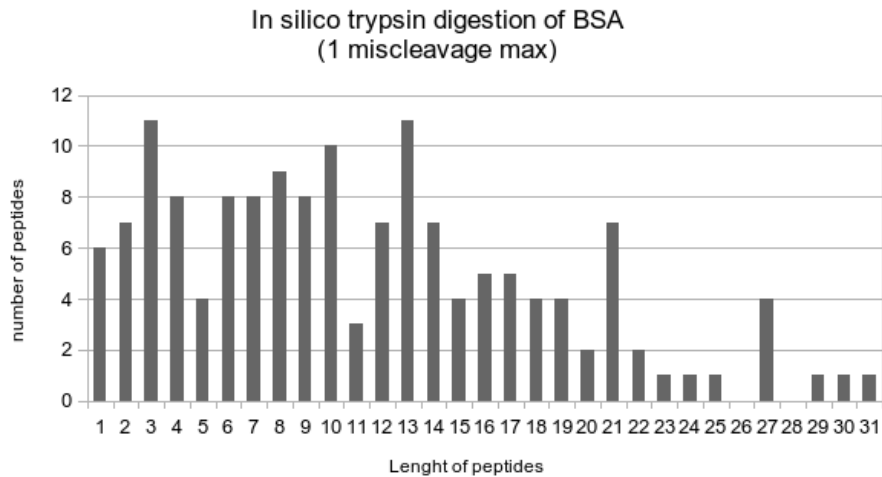


Fig.39 Histogram representing the number of peptides and length of peptide obtained from in silico digestion with maximum 1 miscleavage allowed.

As a reminder, trypsin is an endopeptidase utilizing a catalytic triad (Histidine-Aspartic acid-Serine, or H-D-S) to catalyze the hydrolysis of a polypeptide on the carboxyl side of basic residues, namely lysine (K) and arginine (R). Trypsin miscleavage may occur in the presence of a C-terminal proline (i.e., "after" lysine or arginine) or when multiple consecutive K and/or R residues are present in the sequence. In (Fig.37), it is evident that nearly all identified peptides are sequences without miscleavage, with only one exception. This suggests that the digestion conditions resulted in a nearly complete digestion of BSA, yielding an average of 9.69 residues per peptide (Fig.40). This result supports that the standard protocol employed to perform the digestion is well optimized to prevent miscleavage. The standard protocol (refer to Materials and Methods for specifics) served as the initial framework for developing a robust method to generate a substantial peptide library. Subsequently, various experimental conditions were explored to induce additional miscleavage. The use of a lower quantity of trypsin or the decrease of the digestion duration were explored to increase the number of digestion peptides. In this regard, a pre-optimization step concerning the quantity of trypsin was already investigated using the rabbit muscle phosphorylase B. Because this protein does not contain any disulfide bridge, the alkylation and reduction steps can be skipped, therefore accelerating sample preparation. Several conditions were tested: digestion for 30 and 15 minutes with trypsin/Phosphorylase B ratios of 1/5000 or 1/1000. Those different experiments provided various amounts of miscleavage (data not shown), as the 1/5000 cases showed poorly digested proteins, while the 1/1000 cases provided the most promising results, containing both short and large peptides.

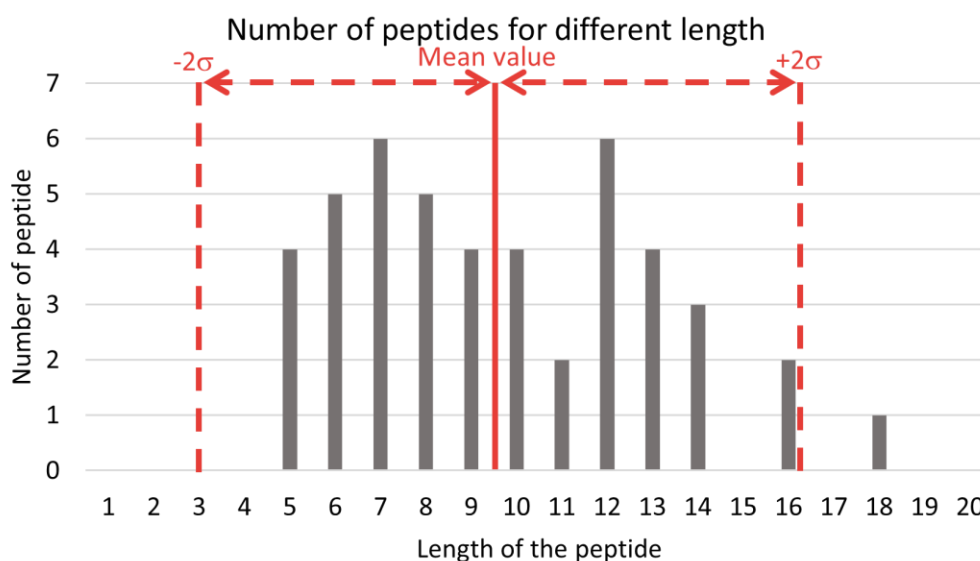


Fig.40: Histogram representing the number of peptides observed and their number of residues

12. Orthogonality of the CE-IMS coupling

The charge state distributions in solution and in the gas phase are due to different physico-chemical properties.

Amino acids and their residues included inside peptides and proteins are zwitterionic species. It means that such molecules have functional groups which are partially ionized in solution (i.e. positive and negative charge co-exist within the species at various degree of dissociation α , also described as the Van't Hoof factor). The functional groups with partial dissociation found in the peptides, proteins, and proteogenic residues are mainly the carboxylic acids and amines, even though the hydroxyl moieties of serine and tyrosine, and thiol moieties of cysteine are weak acids and subjected to deprotonation. All these functional group have pK values (dimensionless) which can be found in chemistry handbooks or in the literature.

In solution, the ionization of the side chains of the residues, as well as the N-ter and C-ter, is pH dependent. Note that the exposition to the solvent or interaction between residues, cations (e.g. Ca^{2+} ...) within the tridimensional structure of the (poly)peptides and proteins, as well as supramolecular assemblies, also affect the dissociation factors of these functional groups⁹⁴. Below is a table published by Grimsley and coworker⁹⁵ in the journal Protein Science in 2009 reporting pK consensus values of the side chains and N-ter/C-ter of the amino acidic residues in folded proteins.

Table.3 Table of published pK values of side chain residues and N-ter and C-ter of the proteogenic alpha amino-acids, according to Grimsley and coworkers (2009)

Summary of 541 pK Values for 78 Proteins Tabulated from the Literature^a

Group	pK value in alanine pentapeptides ^b	Average pK value	Low pK value	High pK value	Number of measurements
Asp	3.9 ^c	3.5 ± 1.2	0.5	9.2	139
Glu	4.3	4.2 ± 0.9	2.1	8.8	153
His	6.5	6.6 ± 1.0	2.4	9.2	131
Cys	8.6	6.8 ± 2.7	2.5	11.1	25
Tyr	9.8	10.3 ± 1.2	6.1	12.1	20
Lys	10.4	10.5 ± 1.1	5.7	12.1	35
C-term	3.7	3.3 ± 0.8	2.4	5.9	22
N-term	8.0	7.7 ± 0.5	6.8	9.1	16

^a The values were reported under various conditions for 78 folded proteins. The individual measured values can be found in Table 1 of our Supporting Information.

^b From Ref. 1.

^c This value is higher than the one previously reported in the reference above. See text for a discussion of this value.

In the gas phase, the ionization occurring e.g. as proton adduct(s) in positive ionization mode is depending on a value called proton affinity (PA) or gas phase basicity (GB). Contrary to the pK, PA is non dimensionless value but instead expressed in kJ/mol (or any related unit). Nevertheless, absolute and relative scales of proton affinity of the functional group available in residues can be found in the literature (Table.4), such as the article published by Bleiholder and coworkers in 2006⁹⁶. In this context, it is noteworthy that, for instance, the amide moieties in the glutamine side chain (approximately 231 kJ/mol determined by Density Functional Theory), exhibit a proton affinity that is nearly comparable to the primary amine in the lysine side chain (approximately 237 kJ/mol)! The proton mobility within a sequence (proton migration from site to site) can be explained, at least in part, by value of the PA energies (local minima) of the various protonable sites. Crossing the activation energy barrier would depend, at least, on the internal energy (effective temperature) provided to the ion inside the mass spectrometer.

Table.4 Table of published proton affinities values of side chain residues of the proteogenic alpha amino acids, according to Bleiholder and coworkers (2006)

Proton affinity scales for the naturally occurring α -amino acids

AA	Harrison	Hunter/Lias ^a	Maksic	Tabet	Bouchoux	DFT ^d	G2(MP2) ^d
Gly	210.5	211.9	210.5	212.3	211.1 ^a ,211.8 ^b	211.4	211.8
Cys	214.0	215.9	213.2	214.4		214.4	214.1
Ala	214.2	215.5	214.0	214.0	213.8 ^a	215.0	215.2
Ser	215.2	218.6	216.0	216.4	216.2 ^a	217.3	217.7
Asp	216.4	217.2	217.3	217.4	221.5 ^b	218.0	218.5
Val	216.5	217.6	215.2	217.6		217.7	218.0
Leu	217.4	218.6	216.8	217.8		218.2	218.2
Ile	218.6	219.3	216.5	218.4		218.7	218.8
Thr	219.5	220.5	217.5	218.5		218.7	218.5
Phe	219.9	220.6	223.3	219.8		220.6	219.8
Asn	220.6	222.0	223.2	223.0	230.7 ^b	224.2	222.4
Tyr	220.9	221.3	221.9	220.3		221.2	220.2
Met	221.1	223.6	221.7	221.7		224.0	223.7
Gln	222.0	224.1	233.0	226.2	236.2 ^b	231.9	230.5
Pro	222.1	220.0	221.9	223.9,225.7 ^a	221.3 ^a	224.0	223.8
Glu	223.4	218.2	225.9	223.3	234.7 ^b	225.8	224.7
Trp	223.9	226.8	220.7	223.8		223.8	-
His	231.5	236.1	229.8	229.2	236.5 ^a ,238.1 ^b	233.7	231.8
Lys	235.6	238.0	237.8	228.6	237.7 ^a ,237.6 ^b	237.3	237.1
Arg	244.8	251.2	248.6			253.3	250.2

All values in kcal/mol. Those PAs that differ more than 2.5 kcal/mol from the Harrison values are underlined.

^aValues taken from Reference [14].

^bValues taken from Reference [15].

^cValues taken from Reference [19].

^dThis work.

^eReference [29].

The key takeaway is that the charge state in both the gas phase and solution, along with the distribution of these partial charges within peptides and proteins—regulated by diverse physicochemical properties—can exhibit notable distinctions. The conformation of peptides and proteins is still influenced by Coulombic repulsions and/or attractions. Therefore, the assurance of maintaining the 3D structures of peptides and proteins after desolvation is uncertain. To assess the conformation of peptides in solution and the gas phase, the MSLab introduced the on-line coupling of capillary electrophoresis (CE) and ion mobility mass spectrometry (IM-MS) fitted with an electrospray ion source adapted on CEMS interfaces. The electrophoretic mobility (“ion mobility” in solution) of the peptides in solution is monitored by CE using different pH values for the background electrolytes. The ion mobility coefficient in the gas phase was monitored by IM-MS, using several kinetic energies for the injection of ion inside the mobility cell. The orthogonality of the both ion mobility techniques, i.e. CE and IM-MS, will be evaluated for potential analytical chemistry applications.

Several buffers were prepared as background electrolytes (BGE) to vary the pH of the migration solution and therefore monitor the impact of the average charges of the peptides in solution, which is governed by the acido-basic equilibrium constants of their constitutive residues (table 3). Three BGE were used during this study:

- a 100 mM formic acid BGE, providing a pH value of 2.40.
- an 8 mM ammonium formate BGE, providing a pH value of 6.52.
- a 5.5 mM ammonium formate BGE acidified by an excess of formic acid to lower the pH to a value of 3.84.

All CE separations were carried using a 30 kV voltage in normal polarity, The concentration of the different BGEs were optimized to provide a comparable current intensity (around 11 μ A) to the CE current observed for the formic acid BGE at 100mM to avoid any thermal denaturation caused by the Joule effect during the migration. The various pH conditions were specifically selected to ensure variations in peptide charges among the three conditions. Around a pH of 3, the pK_a values of a carboxylic acid present in an amino acid result in partial protonation of the carboxylic acid functional groups. As the pH increases, this equilibrium shifts towards greater deprotonation, leading to a more pronounced negative charge. In contrast, the N-terminus is predominantly protonated at acidic pH, while the amine group remains protonated close to neutral pH values.

Table.5 Evolution of the average charge in solution of peptides from BSA tryptic digest as a function of the pH of the BGE. Comparison with the charge states obtained in the gas phase provided by the electrospray ionization process in positive ionization mode.

	<u>pH 2.40</u>	<u>pH 3.84</u>	<u>pH 6.52</u>
<u>Average charge in solution</u>	1-2-3 2 prevails	0 to +3	-3 to +1
<u>ESI(+) charge state</u>	1-4, 2 prevails	1-3	1-2

Table.5 summarizes the average charge in solution obtained by calculating the acido-basic distribution functions of the studied peptides and the charge states obtained in the gas phase imposed by the electrospray ionization processes. The results show that the average charge in solution ranges from +1 to +3 at pH 2.4 and from -3 to +1 at pH 6.52. On the other hand, the detected charge states in the gas phase are much more consistent, ranging from +1 to +4 but mainly $[M+2H]^{2+}$ ions. As a result, the orthogonality of CE and IMS increases from pH 2.4 to pH 6.52 (and reasonably at higher values), as the two separation methods depend on the analyte's charge (average in solution or ESI charge state) and structure (hydrodynamic radius in solution and CCS value in the gas phase). The presence of distinct charges hinders the correlation of the two mobilities, as the number of charges is likely to impact the peptide's structure influenced by Coulomb forces. If the Coulomb forces differ between the two phases, the orthogonality between the separations increases, and therefore the distribution of MTs versus ATDs also varies (Fig.41).

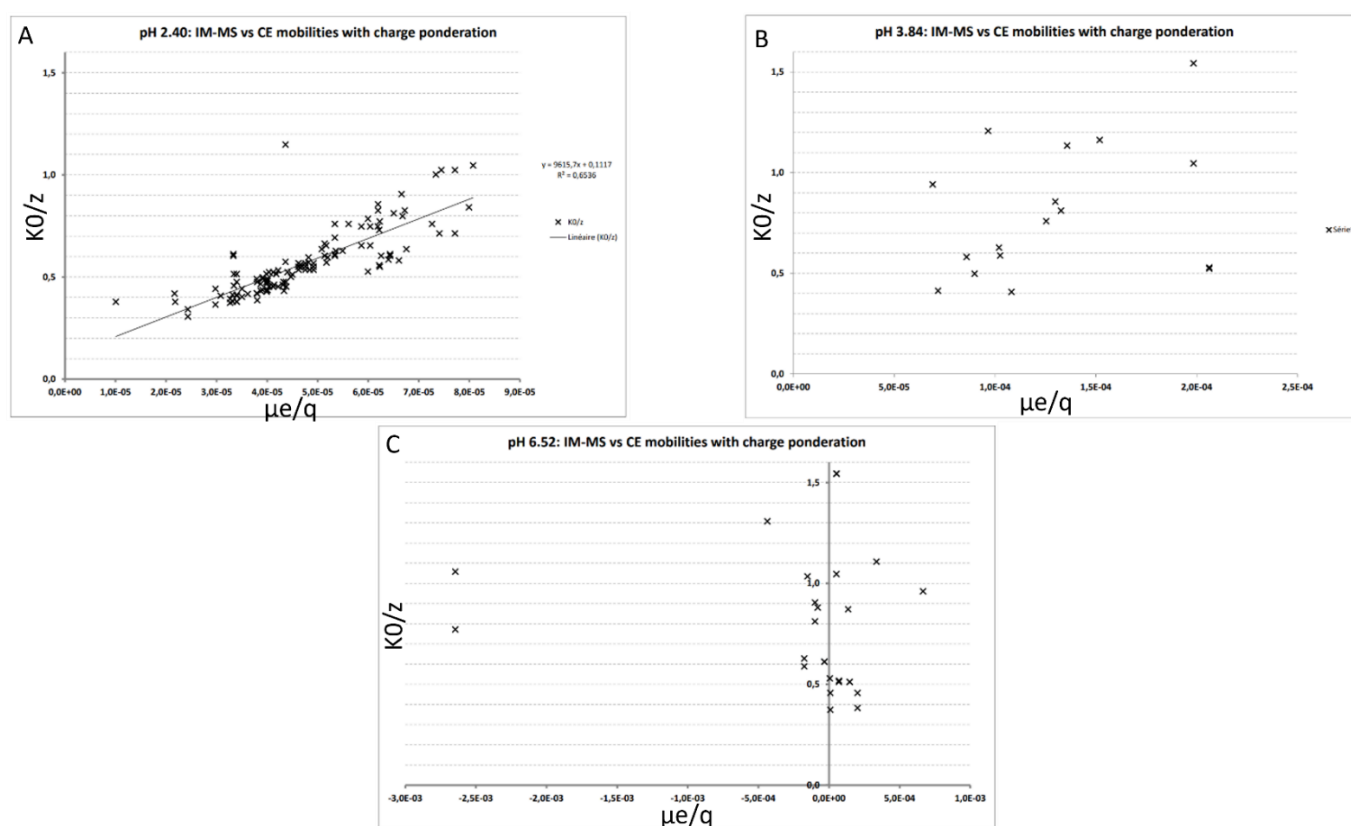


Fig.41 A: Plots of the charge-normalized electrophoretic mobilities in solution as a function of the charge state-normalized ion mobility in the gas phase for different peptides from BSA trypsin digestion at pH 2.4, B at pH3.84 and C at pH 6.52

Increasing the orthogonality of the CE-IM-MS coupling represents an interesting application in the separation field, in the same way as two-dimensional gas or liquid chromatography techniques. However, one should note that the ionization efficiency by the CE-IM-MS interfaces in positive ionization mode is negatively impaired when the pH of the background electrolytes increases. This is especially true for the sheathless CE-IM-MS interfaces while the sheath liquid interface is less affected. For analytical applications, the optimization of the method is a trade-off between orthogonality and sensitivity and detection limit of the CE-IM-MS method.

In the present study, we will focus on conditions where orthogonality is absent (or almost absent) for comparing the structural features of peptides before and after desolvation. To this end, separations will be carried out at pH2.4 where the orthogonality with the IMS separation is reduced. The type of CEMS interface will be also evaluated in terms of the potential impact of the arrival time distribution.

13. Multiple conformations identified in CE

In most cases, the CE separation of peptides produce individual electrophoretic peaks with varying degrees of resolution, depending on the number of theoretical plates (N) provided by capillary electrophoresis, typically $N > 10^5$ (Fig.42).

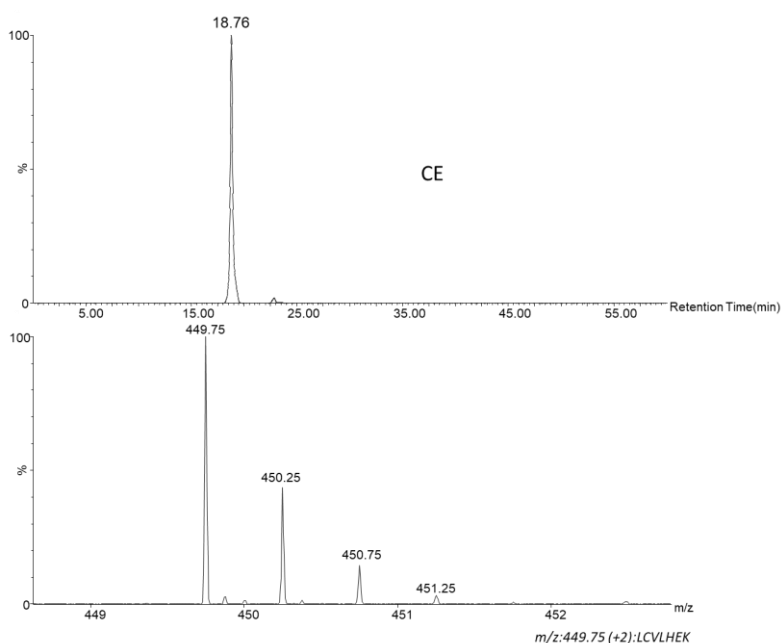


Fig.42 Single electrophoretic peak obtained in CE for a peptide with the sequence (LCVLHEK) and associated mass spectrum at the corresponding migration time at 18.76 minutes.

When working in the separation of peptides by CZE, the experimental results sometimes show the presence of two (or sometimes multiple) electrophoretic peaks corresponding to a unique peptide sequence. An example of such result is provided in (Fig.43).

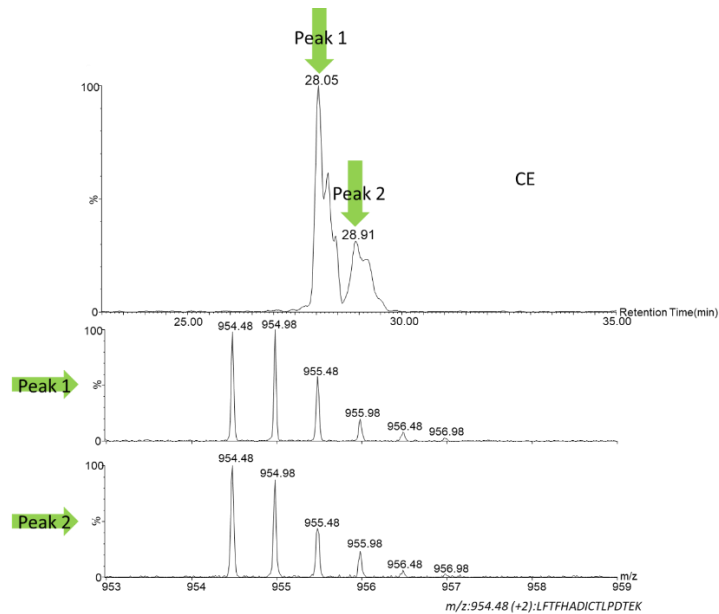


Fig.4.3 Example of two electrophoretic peaks obtained for the same peptide sequence in CE showing a ~1min separation window with the mass spectrum provided. Both electrophoretic peaks are correlated to identical mass spectra

Given the equation of the electrophoretic mobility ([Fig.4.4](#)), the presence of two peaks in the electropherogram implies that the peptide of interest either presents 2 distinct, non-convertible (or poorly convertible) average charges in solution or different hydrodynamic radii, or both at the same time ([Fig.4.4](#)).

$$\mu_{EP} = \frac{q}{6\pi \cdot \eta \cdot R_h}$$

Population 1
 $q_1 \neq q_2$
And/Or
 $R_{h1} \neq R_{h2}$
Population 2

Fig.4.4 Equation of the electrophoretic mobility reflecting the presence of 2 populations of average charge in solution and/or hydrodynamic radii for 2 separate peaks observed in CE for the same peptide.

It is important to acknowledge that the average charge of a peptide in a solution is additionally influenced by its structure, particularly through steric hindrances. When an exchangeable proton is located within the peptide chain's core, it directly affects the acid-base equilibrium constant of the functional group. This is a result of the limited accessibility of the solvent to exchange the acidic proton. As a result, the protonation state of a peptide is intrinsically linked to its structure and vice-versa ([Fig.4.5](#)). The averaged charge difference in solution between two peptides sharing the same sequence is therefore necessarily linked to their structures.

The coexistence of electrophoretic peaks for the same peptide sequence suggests that (at least, under the resolution of separation of the CE method) 2 conformations in solution are thermodynamically

stable, i.e. local minima with a relatively high activation energy barrier between the 2 populations of conformation, or slow kinetics of conversion.

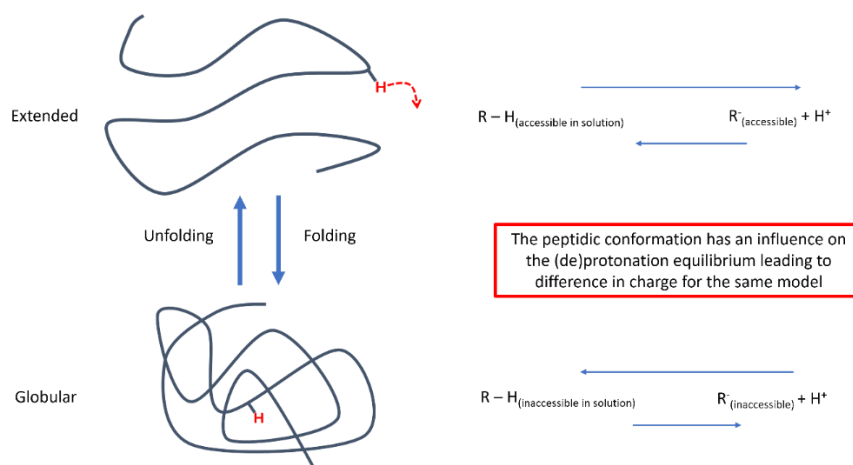


Fig.45 Representation of the link between the average charge in solution of a peptide and its structure

14. Multiple conformations identified in IMS

In general, ion mobility experiments using the Tri-Wave design typically yield a single ion mobility peak for a specific peptide sequence (Fig.46). The resolving power of the Tri-Wave design, which is approximately $CCS/\Delta CCS=50$ (according to the manufacturer specifications), is relatively low compared to more recent IMS designs such as trapped ion mobility spectrometry (TIMS).

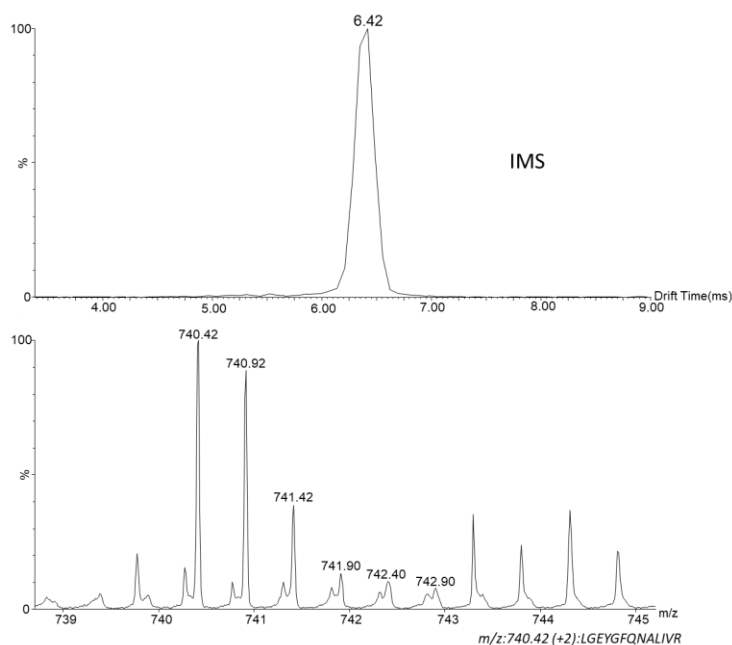


Fig.46 One peak obtained for the peptide with the sequence (LGEYGFQNALIVR) in IMS showing a ~ 0.55 ms separation window

However, akin to the occurrence of multiple peaks in CE, we occasionally observed two (or more) ion mobility peaks for a specific peptide sequence, as illustrated in (Fig.47):

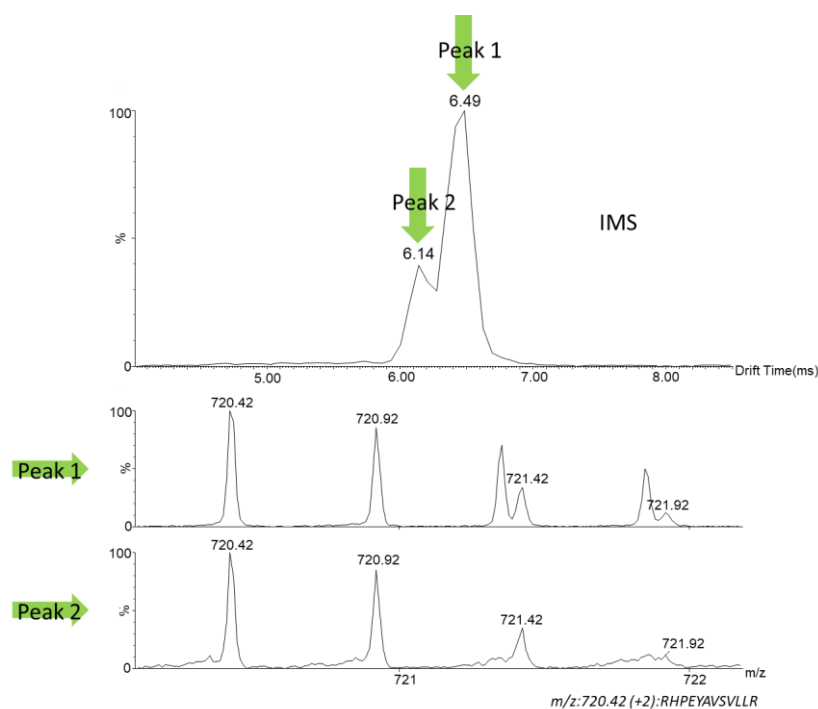


Fig.47 Two peaks obtained for the same peptide in IMS showing a ~0.35ms separation window

Similar to the CE equation, the equation for the mobility constant K in IMS, as depicted in (Fig.48), reveals that the presence of two (or multiple) peaks in IMS can only be attributed to a disparity in the experimental CCS values for a specified charge state. The difference of rotationally averaged collision cross section could result of:

- Different atoms coordinated, i.e. different 3D rotationally averaged conformation.
- The same rotationally averaged conformation but different positions of the charges that induced different dipole moments within the ion, affecting how the ion interacts with the polarizable gas inside the ion mobility cell (nitrogen here). When the position of the proton is different, one can meet in the literature the terms of “protomer”.

Protomer is a term designing either the difference of the position of protons within a molecule, or improperly designing the tautomerization of the proton, e.g. aniline ion⁹⁷. The presence of protomers of peptide was suggested to exist in cyclic lipopeptides in a recent work⁹⁸.

$$K = \frac{3}{16N} \left(\frac{2\pi}{\mu k_B T} \right)^{\frac{1}{2}} \frac{q}{\Omega}$$

Population 1
 $q_1 = q_2$
 $\Omega_1 \neq \Omega_2$
 Population 2

Fig.48 Equation of the mobility constant in IMS reflecting the presence of 2 populations of different collision cross section values for 2 separate peaks observed in IMS for the same peptide.

Based on the identification of these multiple conformations in CE and/or IMS, it is therefore of high interest to directly couple a CE separation with an IMS characterization to assess the potential links between these different population of detected peptides. The objective of this approach is to investigate whether a correlation exists between the number of populations observed in solution and those in the gas phase. This aims to provide insights into the influence of the ESI process on maintaining the structural integrity of biomolecules from the solution to the gas phase during ionization. One will note that the most majority of the published articles focusing on peptides mention 1 peak in the liquid phase (1 electrophoretic peak from CE but most commonly 1 chromatographic peak obtained from liquid chromatography which is a gold standard method nowadays), and 1 arrival time distribution detected for the same peptide by ion mobility.

15. Conformation(s) in solution versus conformation(s) in IMS: the different observed cases:

When examining peptides derived from the tryptic digestion of BSA using CE-IM-MS, various scenarios were identified. Some peptides exhibited a single electrophoretic peak in CE and one ATD peak in IMS, referred to as "case 1/1" (which is the expected main behavior). Additionally, instances were observed where there was a single peak in IMS and two peaks in CE, as well as the reverse situation, denoted as "case 1/2" and "case 2/1" respectively. Furthermore, there were cases where both solution and gas phases displayed two peaks, termed "case 2/2." It is noteworthy that the occurrences of cases 2/2, 2/1, and 1/2 were notably less frequent in our dataset compared to the more prevalent 1/1 cases. It is important to note that CE experiments typically span dozens of minutes, whereas ion mobility measurements are conducted in a matter of milliseconds. Both mobility methods do not investigate the kinetics of conformational equilibrium, if present, at the same time frame. In other words, these methods do not cover a comparable range of kinetic rates. Consequently, ion mobility may reveal kinetically trapped conformations, a scenario that is less likely in CE when applied to oligopeptides like the trypsin-generated peptides from BSA. Those cases were investigated using heatmaps revealing the gas phase conformational populations as a function of the conformational populations present in solution. The heatmaps plot of the CE-IM-MS data allows to monitor the fate of the population of conformation of the peptides in solution after the transfer in the gas phase, as presented in the following section:

- A. Cases 1/1: Examples: HLVDEPQNLIK, YICDNQDTISSK:** The case of 1 electrophoretic peak in CE and 1 ATD peak in IMS is the standard case, and it is the expected behavior for the majority of the analyzed peptides (Fig.49):

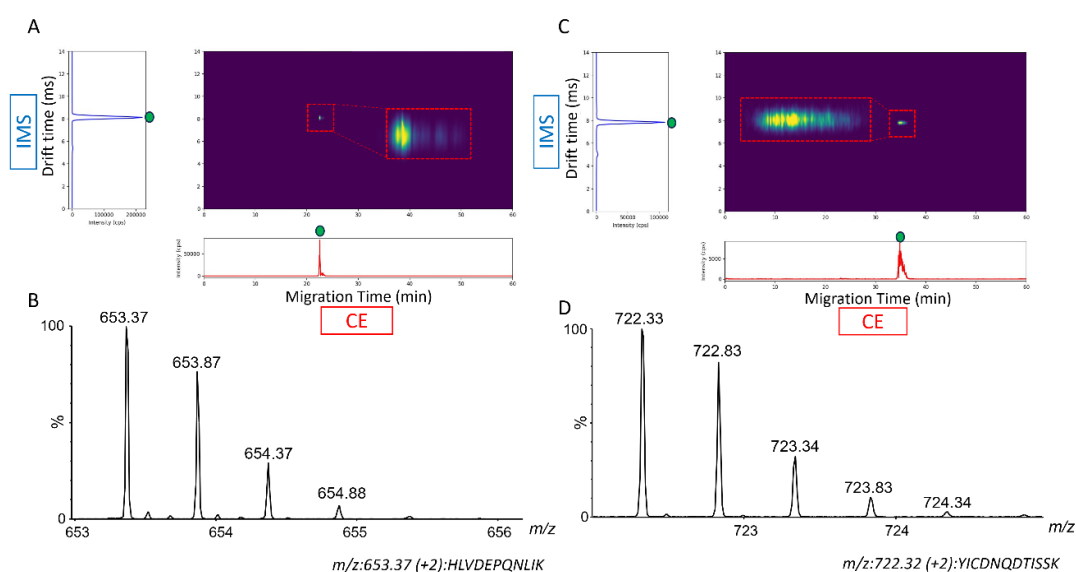


Fig.49 A and C: Heatmaps of peptides belonging to the case 1/1 composed of the IMS experiment on the y-axis and the CE experiment on the x-axis with their respective mass spectra (B and D). The insets show the arrival drift time obtained from ion mobility and the electropherogram obtained from the CE experiments in their respective axes. The heatmap were zoomed in red inset for clarity.

The interpretation of those cases is the simplest, where a single peak in CE and in IMS indicates the presence of a single stable population of conformation in the gas phase and in solution, under the limitation of the experimental resolving power of the CE and the IM-MS, respectively. This general case however must be mitigated by the potential presence several populations of conformations that are separated by low activation barriers (and therefore in rapid equilibrium), resulting in the observation of a single average peak in each phase. This case supports the hypothesis of the structural preservation between the two phases after the desolvation. In the case of peptides displaying this behavior, there is a possibility that the ATD peak observed in ion mobility spectroscopy (IMS) and the electrophoretic peak in capillary electrophoresis (CE) correspond to the same conformational population. At this point in the analysis, no definitive conclusions can be drawn. Additional experiments, such as spectroscopy and action spectroscopy for the solution and gas phase, respectively, would be essential for a more comprehensive understanding of the conformation.

- B. Cases 2/2: Examples: ECCDKP LLEK, LKPD PNTLCDEFK:** Interpreting the instances where two peaks are observed in CE and two in IMS is somewhat more intricate compared to the 1/1 case. In this scenario, two distinct conformational populations are observed in solution, perhaps in equilibrium with slow kinetic rates (possibly due to a high activation barrier) or existing as independent conformers. Additionally, there are two stable gas-phase conformational populations, potentially kinetically trapped following the ionization process, as depicted in (Fig.50).

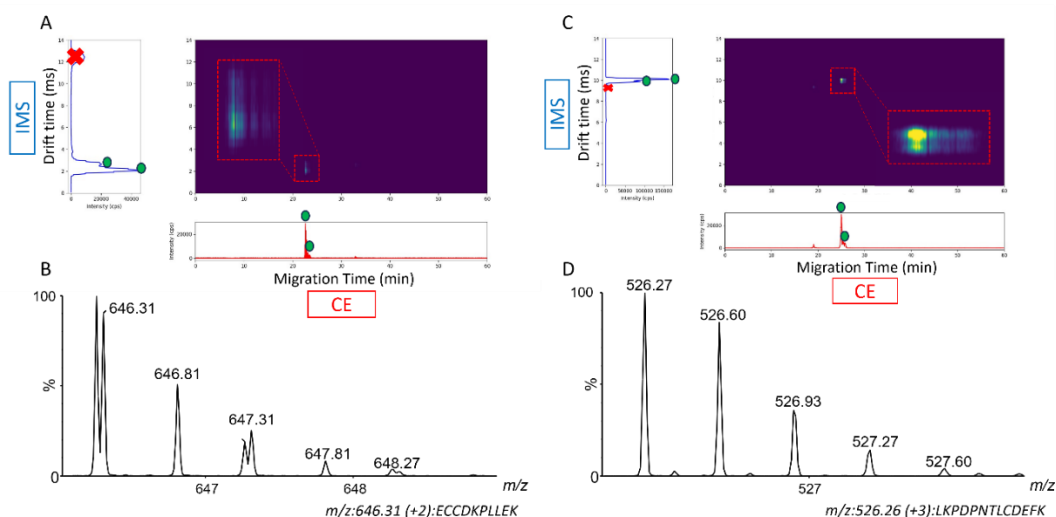


Fig.50 A and C: Heatmaps of peptides belonging to the case 2/2 composed of the IMS experiment on the y-axis and the CE experiment on the x-axis with their respective mass spectra (B and D). The insets show the arrival drift time obtained from ion mobility and the electropherogram obtained from the CE experiments in their respective axes. The heatmap were zoomed in red inset for clarity.

In principle, the “2/2” cases are also not necessarily inconsistent with the hypothesis of structure preservation upon ESI desolvation. It is conceivable that each conformational population identified in CE aligns with a corresponding population identified in IMS. Nevertheless, there is also the possibility that the multiple conformations observed in each separation medium do not mirror those in the other phase, and instead, represent distinct conformational populations in solution and in the gas phase. Once more, additional experiments are needed to draw robust conclusions.

- C. Cases 1/2: Examples: RHPEYAVSVLLR, HPEYAVSVLLR:** the scenario of having one electrophoretic peak in CE and two ATD peaks in IMS emphasizes the presence of two stable or kinetically trapped conformational populations in the gas phase, contrasting with only one such population in solution (Fig.51).

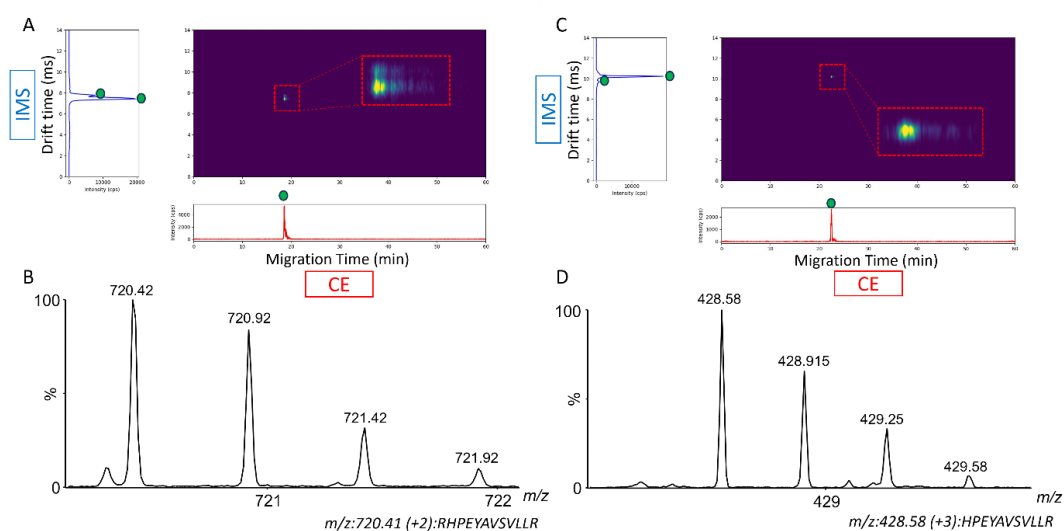


Fig.51 A and B: Heatmaps of peptides belonging to the case 1/2 composed of the IMS experiment on the y-axis and the CE experiment on the x-axis with their respective mass spectra (B and D). The insets show the arrival drift time obtained from ion mobility and the electropherogram obtained from the CE experiments in their respective axes. The heatmap were zoomed in red inset for clarity.

In contrast to the “1/1” and “2/2” cases discussed earlier; this particular case poorly supports the structural preservation hypothesis. The extra population revealed by the IMS data cannot be associated with the single population observed in CE. It is reasonable to propose that this additional population is generated during the ESI process. However, the “1/2” case does not completely refute the structural preservation hypothesis, as there is a possibility that the single peak observed in solution may encompass multiple closely related conformations in rapid equilibrium. These conformations could then be kinetically trapped in the gas phase and separated by IMS. Nevertheless, this scenario is unlikely, given that CE separations are characterized by significantly higher separation efficiency compared to IMS.

- D. Cases 2/1: Examples: QNCDQFEK, LFTFHADICTLPDTEK:** he case where two peaks are observed in CE and only one in IMS emphasizes the presence of two stable conformational populations in solution, contrasting with only one population in the gas phase (Fig.52):

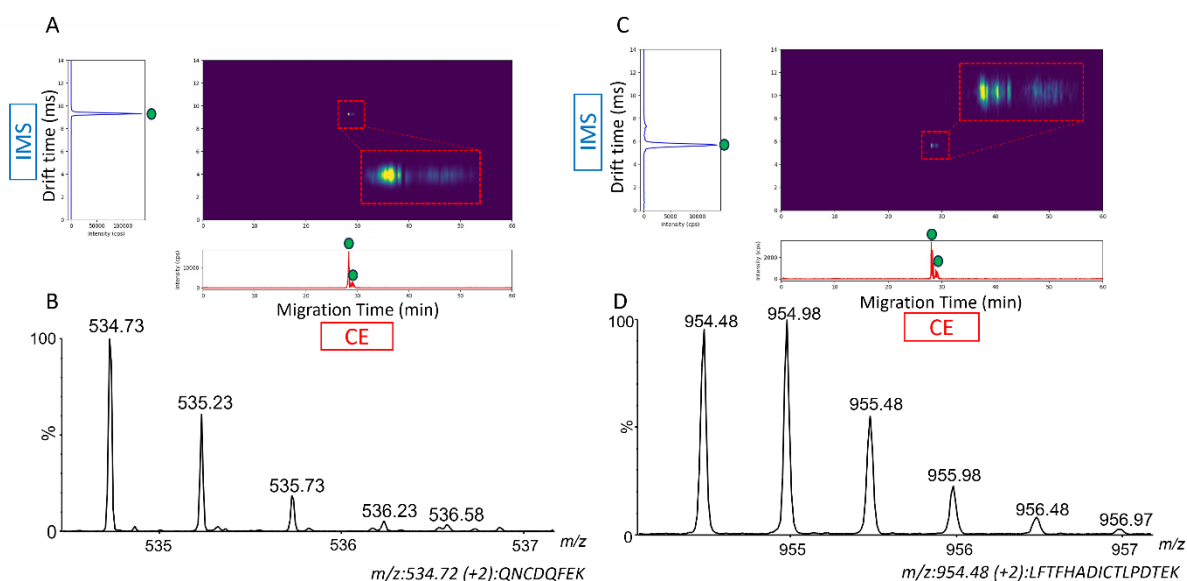


Fig.52 A and B: Heatmaps of peptides belonging to the case 2/1 composed of the IMS experiment on the y-axis and the CE experiment on the x-axis with their respective mass spectra (B and D). The insets show the arrival drift time obtained from ion mobility and the electropherogram obtained from the CE experiments in their respective axes. The heatmap were zoomed in red inset for clarity.

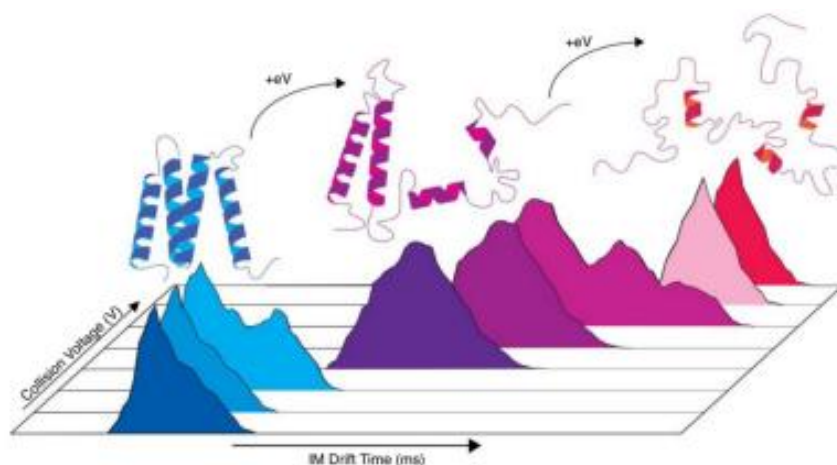
Similar to the “1/2” cases, the “2/1” cases do not lend strong support to the structural preservation hypothesis. Notably, in this particular situation, a conformation present in solution is not identified in the gas phase, suggesting the potential disappearance of one population during the ionization process and transfer into the gas phase. However, these cases do not entirely invalidate the hypothesis because the conformations revealed in CE might have closely similar collision cross-section (CCS) values, generating a single peak in IMS due to the considerably lower resolving power of IMS compared to CE. To draw more definitive conclusions, reproducing the experiment using an instrument with higher ion mobility resolving power would be beneficial. These experiments are more feasible than implementing on-line spectroscopy with CE or action spectroscopy of ion resolution through ion mobility.

16. Soft ion activation prior to the IMS analysis

Soft ion activation can be implemented to increase the internal energy of the ions of interest prior to the IMS separation. The aim of these experiments is to provide sufficient energy to induce structural rearrangements (or induce proton mobility) while remaining below the energy threshold required to induce dissociation (Fig.53A and Fig.53B). Such experiments are also called “Collision Induced Unfolding” (CIU), as an analogy of the Collision Induced Dissociation (CID) but without reaching the energy to induce the fragmentation of the ions. In this experiment, certain ions may experience changes in their collision cross-section (CCS) values due to the gentle collision energy introduced by

the progressively increasing acceleration of ions (Trap bias voltage) in the helium cell before entering the ion mobility cell filled with nitrogen.

A/ ^a



B/ ^a

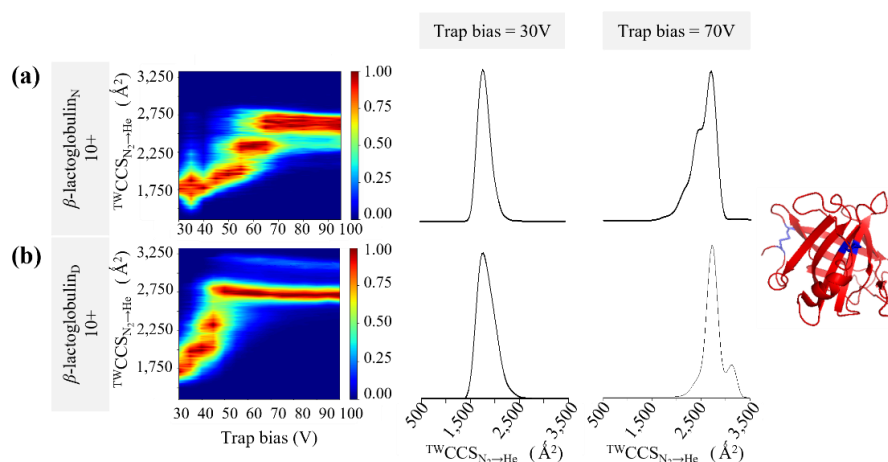


Fig.53 A/ Diagrams and cartoons depicting the CIU of proteins and common methods of analysis. As collision energy (eV) is increased, an isolated protein ion unfolds in the gas phase (From Dixit, S. M.; Polasky, D. A.; Ruotolo, B. T. *Collision Induced Unfolding of Isolated Proteins in the Gas Phase: Past, Present, and Future. Curr. Opin. Chem. Biol.* **2018**, *42*, 93–100.). B/ Heatmaps of native (a) and reduced(b) β -lactoglobulin ($z=+10$) submitted to Collision Induced Dissociation using Trap Bias acceleration voltage (from 30V to 100V). Courtesy of Grifnée and coworkers, article accepted with revisions, submitted to the Journal of the American Society for Mass Spectrometry (Manuscript ID: js-2023-003985).

That energy input takes place just before the ion mobility cell as shown in the (Fig.54), with the ions accelerated against a thin cell filled with helium gas (helium cell). The control parameter managing this acceleration is referred to as the "Trap Bias Voltage," which regulates the acceleration of ions between the trap and the helium cell. Its purpose is to enhance the transfer of ions into the mobility cell without causing fragmentation (Fig.54). The soft activation energy for CIU is allowed by collision on He (mass = 4 Da) instead of N_2 (mass = 28 Da). As a remind, the transferred energy during the collision depends on the reduced mass of the two-body system, and the reduced mass strongly converge to the lower mass of the two-body system.

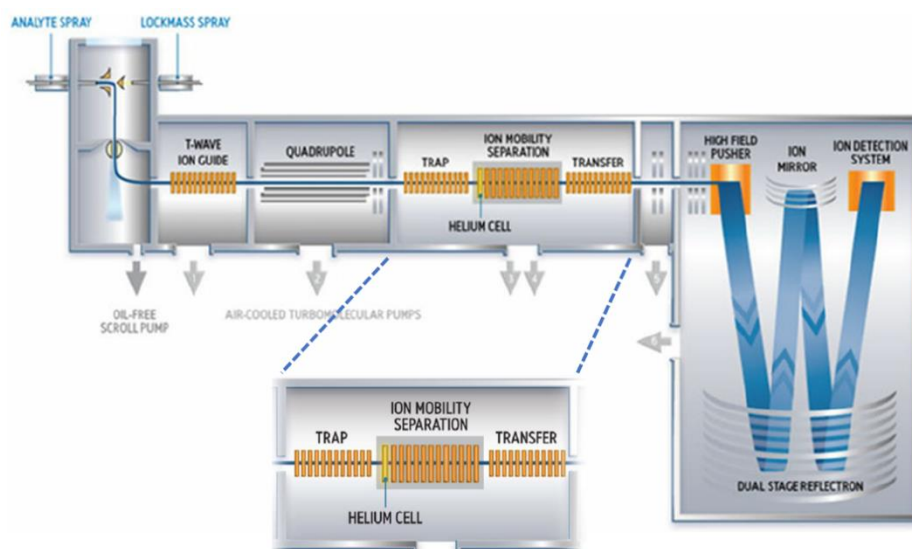


Fig.54 Scheme of a Synapt G2 HDMS with a highlight on the IMS cell (Waters.com)

Soft ion activation was implemented within the same CE-IM-MS experiments used in the previous experiments to assess the impact of CIU on the observed population of conformers. In many cases, no influence or neglectable influence of CIU could be observed on the conformational populations and their relative ratios, as depicted in (Fig.55).

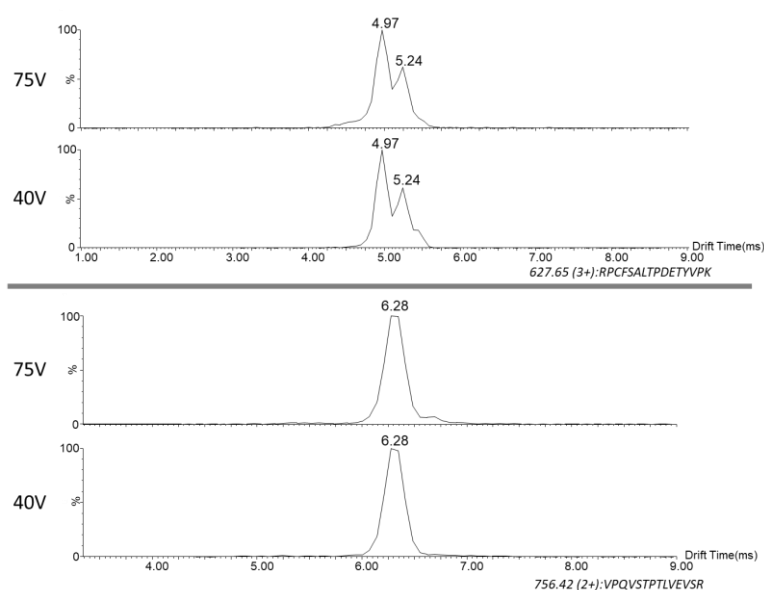


Fig.55 Examples of two arrival time distribution of peptides submitted to CIU using trap bias by default value (40V, bottom position) and 75V (top position), generated from MassLynx v4.1 for m/z 627.65 (RPCFSALTPDETYVPK) and m/z 756.42 (VPQVSTPTLVEVSR). Both peptides present two peaks in CE.

Conversely, certain peptides are significantly influenced by an increase of their internal energy. The alteration in relative intensities between two IMS peaks suggests a shift in the relative structural populations during ion activation or an impact on the population of protomers. Furthermore, specific cases reveal the emergence or disappearance of IMS peaks, indicating the generation or

transformation of conformational populations. In the first example in (Fig.56), a decrease in the intensity of the mobility peak characterized by a drift time of 6.14ms is observed compared to the intensity of the peak at 6.42ms when increasing the trap bias value from 40V (default value) to 75V. This observation indicates that a part of the population at 6.14ms is converted into the population at 6.42ms, due to a collisional activation enabling the activation barrier between these two conformations to be surpassed (Fig.56).

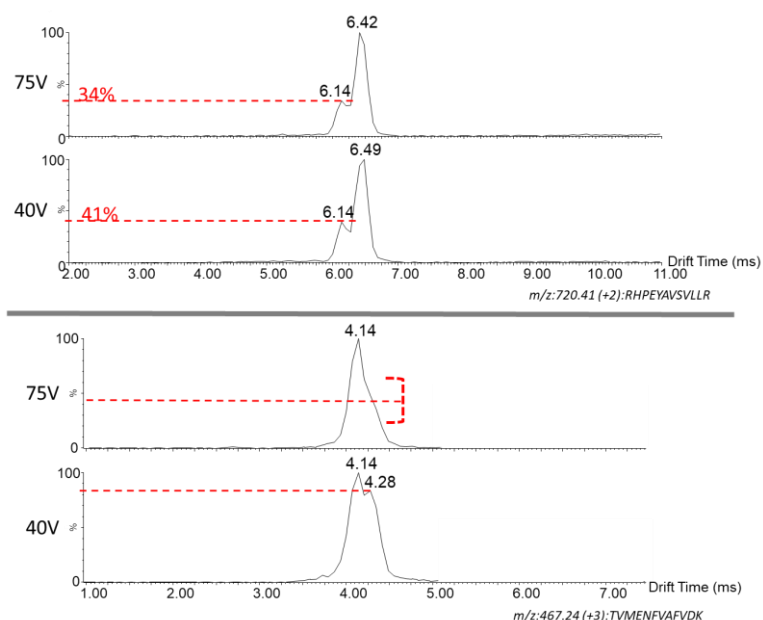


Fig.56 Examples of two arrival time distribution of peptides submitted to CIU using trap bias by default value (40V, bottom position) and 75V (top position), generated from **MassLynx** v4.1 for m/z 720.41 and 467.24. Both peptides present one peak in CE.

In the next example in (Fig.57) the IMS distributions are characterized by 2 peaks using the standard trap bias values. However, the distribution reveals a third conformation at 4.00ms upon activation. Interestingly, the ratio between the contributions at 3.52ms and 3.80ms is not preserved (from 1.1 to 1.28). There is therefore a conversion of the populations at 3.52ms and 3.80ms into a more extended population detected at 4.00 milliseconds. In this scenario, it can be inferred that one of the two initial populations undergoes conversion more readily than the other, likely owing to disparities in their respective energy landscapes. In the example, the energy needed to transition from the population eluting at 3.59 ms to the one eluting at 4.00 ms is presumably higher than that required for the population eluting at 3.80 ms. (Fig.57).

It is noteworthy that all the peptides depicted in (Fig. 54 to 56) contain a proline in their sequence, except for m/z 467.24, which instead features two closely located phenylalanine residues. The observed populations of conformers in ion mobility mass spectrometry may be attributed to the steric hindrance induced by the presence of either proline or the two adjacent phenylalanine residues.

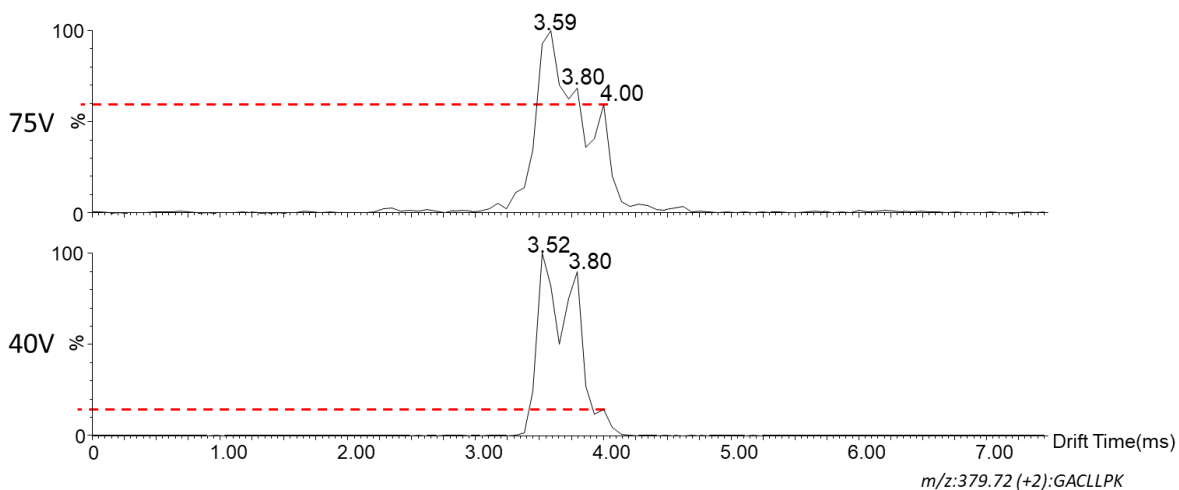


Fig.57 Example of a case with a change of ratio between three populations at a trap bias by default and adjusted at 75V generated from *Masslynx* v4.1 for m/z 379.72. This peptide presents two peaks in CE.

Finally, in some cases, a new peak appears upon activation. In the case presented in Fig. 57, there is a single peak at 3.52 ms at a low trap bias voltage (40V), but the increase of the trap bias voltage to 75V results in an increase in kinetic energy, giving rise to a new population that appears at 3.38 milliseconds. (Fig.58). It cannot be excluded that the emergence of this new ATD peak is a result of the formation of a new protomer. The hexapeptide CASIQK, which carries two protons, is expected to have one on the lysine side chain and the other either on the N-terminus of cysteine or on the carbodomethyl group of cysteine at the N-terminus. Introducing computational chemistry should help in this matter by providing additional evidence to either support or refute this hypothesis.

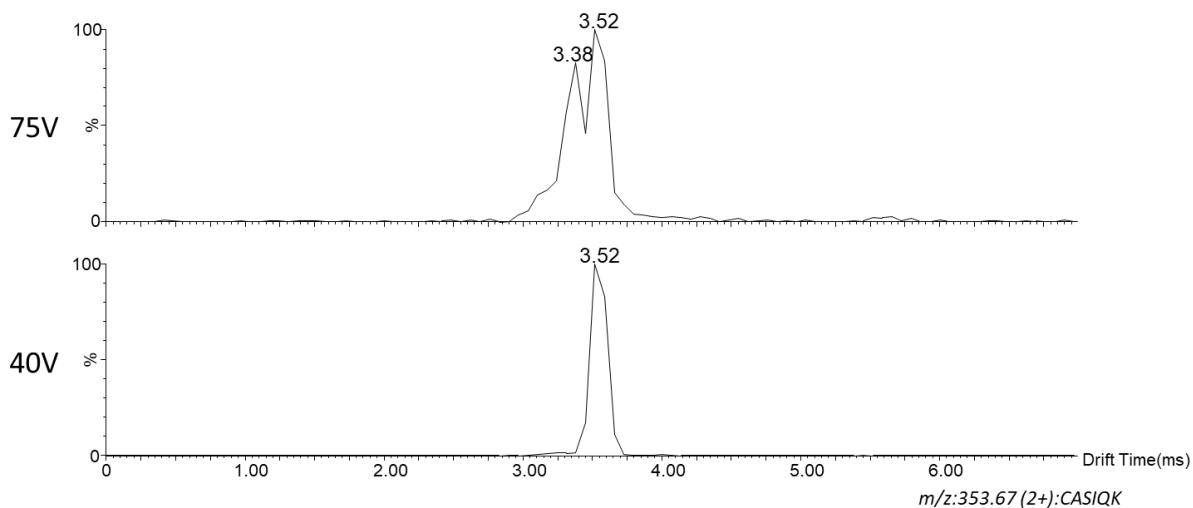


Fig.58 Examples of cases with an appearance of a peak between a trap bias by default and adjusted at 75V generated from *Masslynx* v4.1 for m/z 353.67. That peptide seems to present one peak in CE

For information, Paizs and Suhai (2003)⁹⁹ computed the delta of proton affinity within the O and N proton location in model dipeptides ranging from 23 to 88 KJ/mol (these values are converted from the energy provided in Hartree in the original publication), supported by the more recent publication

of Bythell and coworker¹⁰⁰ These authors also assessed the N-ter equivalent of a model compound and the delta proton affinity between N-ter equivalent and H proton location on the O/N of the amide moiety (peptidic bound) ranged from 8 to 80 KJ/mol. These delta PA values are quite low in regard of the energy deposited in the ions during collision with neutral gas (from few kJ/mol per Da to dozens of kJ/mol per Da, deduced from the literature¹⁰¹⁻¹⁰³. Consequently, one could speculate that the proton migration toward -CONH- peptide bounds and the N-ter or the carbamidomethyl group would be likely possible under CIU condition performed during this work.

A few conclusions can be deduced from the presented results regarding ion activation:

- When several conformational populations co-exist in the gas phase (as evidenced by the presence of multiple peaks in IMS for the same charge state of the same peptide), the relative proportions of each population can be modified by providing internal energy to the peptide through soft ion activation prior IMS separation (CIU). This workflow allows the determination of conformations which are favored at higher internal energy and therefore provides some insights into the peptide dynamics in the gas phase. Additional experiments to quantify the energy provided during the process of ionization and the CIU experiment to explore the energy landscapes explored would be of great interest. To achieve this goal, we suggest employing thermometer ions, a concept introduced by Collette and colleagues¹⁰⁴ allowing the determination of an effective temperature.
- The evolution of the ATD values can be structurally interpreted as unfolding or collapse of the ions after soft ion activation (CIU). This model is supported by the peptides presenting proline or phenylalanine in their sequences which affect the steric hindrance of the peptides. Nonetheless we cannot exclude that the change in the ATD value is due to proton mobility within the different favorable protonation sites, which is strongly suggested by the CASIQK peptides investigated in (Fig.58).
- Finally, it should be mentioned that the ratios determined in the present study are measured on a Synapt G2 HDMS and that the hardware of the MS instrument directly impacts the obtained results in the gas phase (differences can be generated due to differences in the hardware of the instrument). Consequently, results obtained from different instruments should be compared to allow a more comprehensive characterization of such peptides in the gas phase. The use of different IMS separation techniques based on trapped ion mobility (TIMS) or drift tube ion mobility should be explored to gain such insights.

17. Hyphenation of CE to ESI-IM-MS: impact of the CE-IM-MS interface

Since the introduction of the CE-ESI-MS, two major types of CE-ESI interface were developed (Fig.59). The first type of interface relies on the use of a sheath liquid to promote the ionization the analytes exiting the CE capillary after separation. Additionally, the sheath liquid acts as a saline bridge allowing to close the electric circuit between the inlet and the outlet of the CE capillary. In this work, a CE-MS sheath liquid operating at microfluidic flow rate developed in the MSLab was used. That interface takes the form of a needle pointing towards the MS detector, into which the capillary is inserted. A cavity filled with the sheath liquid, a solution composed of 50% isopropanol and electrolytes (10mM Formic Acid), surrounds the electrophoretic capillary filled with the BGE. These two solutions come into contact at the Taylor cone, closing the CE circuit and stabilizing the cone through the selection of an optimal viscosity. In another commercial sheath liquid CE-MS interface (triple tube SCIEX configuration), a third tube running parallel to the sheath liquid's needle, provides a high-pressure nebulizing gas to assist the ionization process.

The OptiMS™ sheathless interface from SCIEX relies on the use of a capillary that is porous at outlet to ensure electrolyte exchange between the BGE inside the capillary and a solution of identical composition to the BGE to ensure electrical closure. In this sheathless interface configuration, the Taylor cone is therefore solely composed of the solution inside the capillary, with no other contribution.

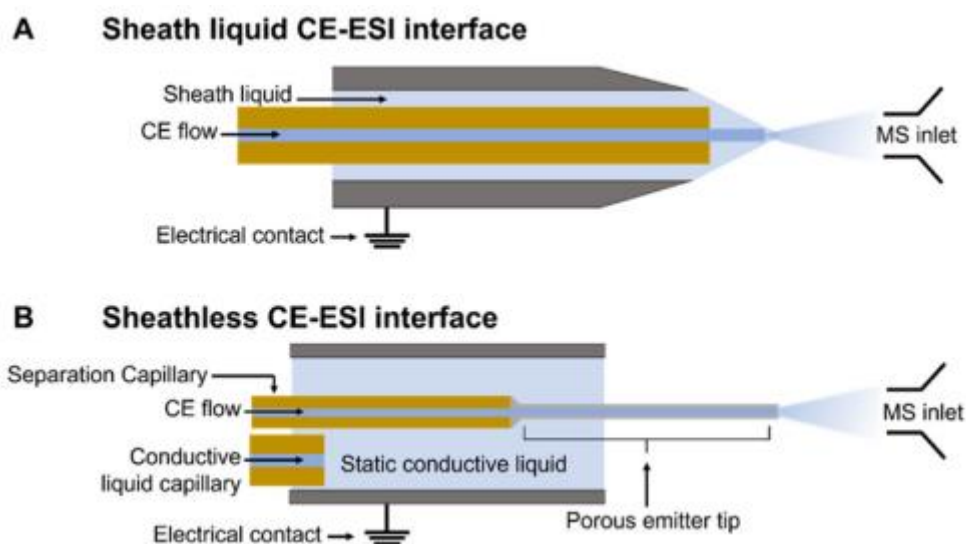


Fig.59 Representation of both types of interfaces between CE and ESI (From Bagwe, K.; Gould, N.; Johnson, K. R.; Ivanov, A. R. *Single-Cell Omic Molecular Profiling Using Capillary Electrophoresis-Mass Spectrometry. TrAC Trends Anal. Chem.* **2023**, *165*, 117117.)

Certainly, the depicted scheme above (Fig.59) outlines the fundamental concept of how these two interface types operate, although multiple variations exist. For the purposes of this study, the sheath liquid interface used is referred as the "Analis microfluidic interface". This interface was developed by a collaboration between Analis (Suarlée, Belgium) and the Mass Spectrometry Laboratory (MSLab) during a Wallonia FIRST Enterprise Project (6592). This interface can be described as a "low sheath-flow interface", as the sheath liquid flow rate is typically $1\mu\text{L}\cdot\text{min}^{-1}$ or lower, making it possible to couple this interface with a nano-ESI source without the need of nebulization gas, preventing the BGE suction effect in the interface due to Venturi effect.

As for the sheathless interface, SCIEX Separations has developed and marketed a kit called "OptiMS" for sheathless experiments (Fig.60). The use of a sheathless interface provides a better signal-to-noise ratio and therefore greater sensitivity, at the cost of lower sample injection volume due to a lower internal diameter of the capillary (i.e. $30\mu\text{m}$, as opposed to the typical $50\mu\text{m}$ I.D or even sometime $75\mu\text{m}$ I.D).

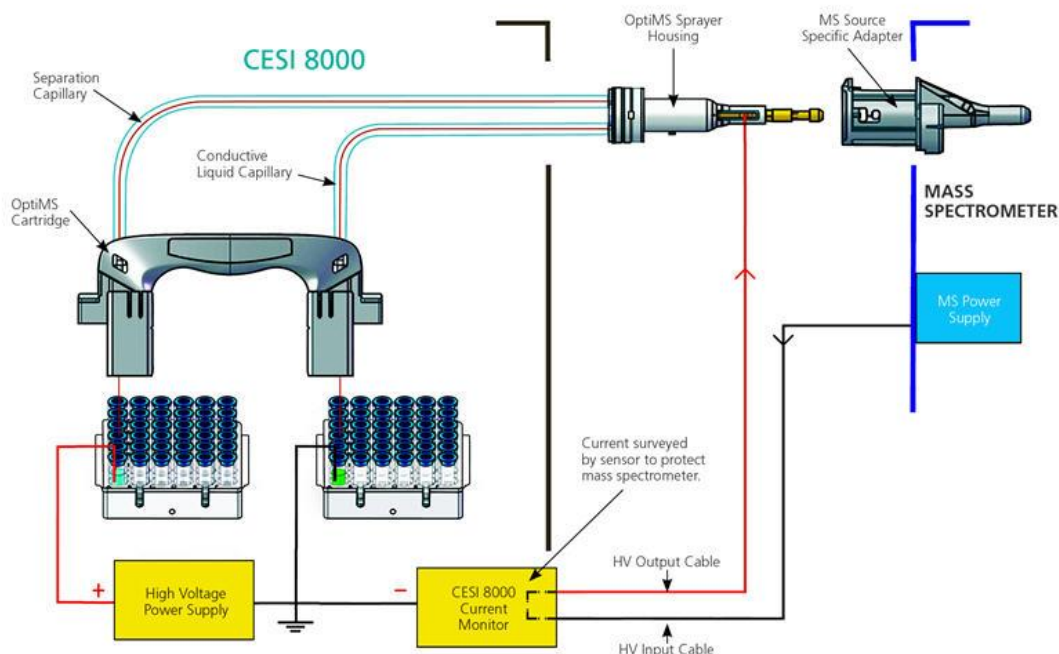


Fig.60 Scheme of the “CESI-OptiMS “kit by SCIEX Separations (from sciex.com)

Both types of interface present advantages and drawbacks. The sheathless configuration does not rely on the use of organic solvent such as methanol or isopropanol, which are well-known denaturing agent for biological macromolecules¹⁰⁵. As a result, the sheath liquid interface might present a chemical denaturing effect due to contact of the separated peptides by CE and this organic solvent before ionization. For the microfluidic sheath liquid interface that was used in this study, the contact time between the CE effluent and the sheath liquid was modelled by the group of Julie Schappler¹⁰⁶. However, the contact time between the isopropanol and the analytes is so short (in the order of milliseconds¹⁰⁷) that it may not impact the peptide conformation during the ESI process.

On the other hand, the organic solvent contained in the sheath liquid droplets quickly evaporate during the ionization process, which necessarily reduce the thermic energy within the droplets. Alternatively, the droplet generated by the sheathless interface (composed of 100% aqueous BGE) should present (much?) higher thermal energy upon evaporation due the sole presence of water and electrolytes. As a result, the sheath liquid approach might present a chemical denaturing effect due to the presence of organic solvent while the sheathless interface might induce thermal denaturation of the peptides.

In some cases, the number and shape of the ATD peaks remains unchanged regardless of the ionization interface used (Fig.61). It suggests that the ion heating experienced by the peptides under investigation would be similar between both CE-IM-MS interfaces, or at least neither CE-IM-MS interface is capable to induce the crossing of activation barrier(s). Nevertheless, the figure below is an example of the CE-IM-MS interfaces that affect the distribution of the ion populations in the gas phase. In section A of (Fig.61), peptide SLHTLFGDELCK presets a single, well-resolved IMS peak in each case, while in section B, two IMS peaks can be observed for peptide RPCFSALTPDETYVPK, which are partially resolved in the case of the ion generated by the sheathless interface. Note the presence of 3 prolines in this sequence.

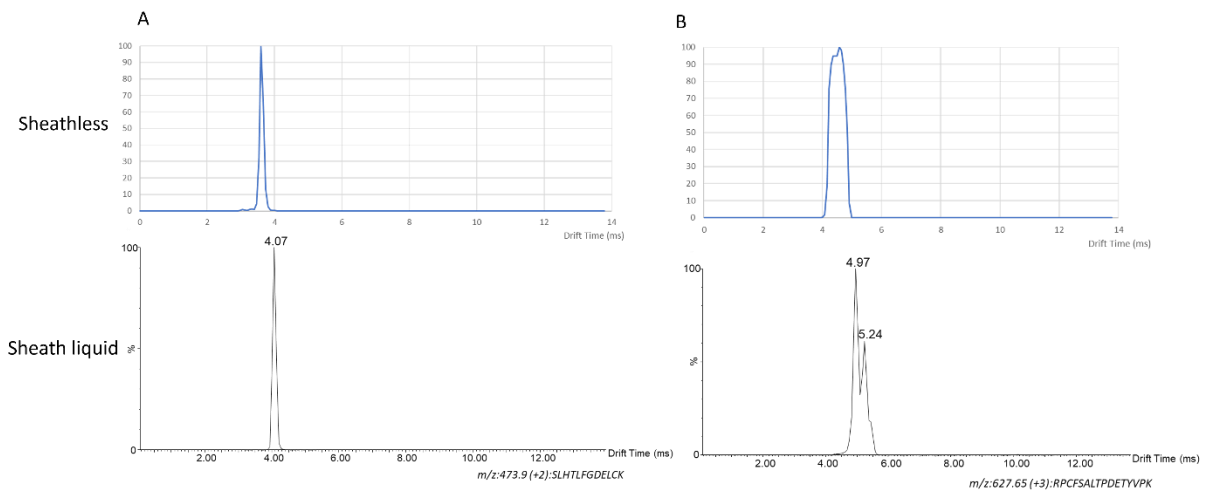


Fig.61 Example of conservation of peak number in IMS between the two types of interfaces for one peptide with the sequence SLHTLFGDELCK (A) and one peptide with the sequence RPCFSALTPDETYVPK (B)

Yet, in certain cases, the observed number of peaks is not constant between the two cases. For instance, two peaks may be detected with a sheathless interface, while only one is observed with a sheath liquid, and vice versa (Fig.62). This could be explained by a more stable total ion current typically obtained with the sheathless interface. The sheath liquid interface uses a syringe pump to feed the interface with the sheath liquid, consequently affected by Flicker noise due to the irregular rotation of the endless screw of the pump at such flow rate. In the figure below we can suspect the presence of two convoluted peaks in IMS for the sheathless interface while there is only one with a sheath liquid interface.

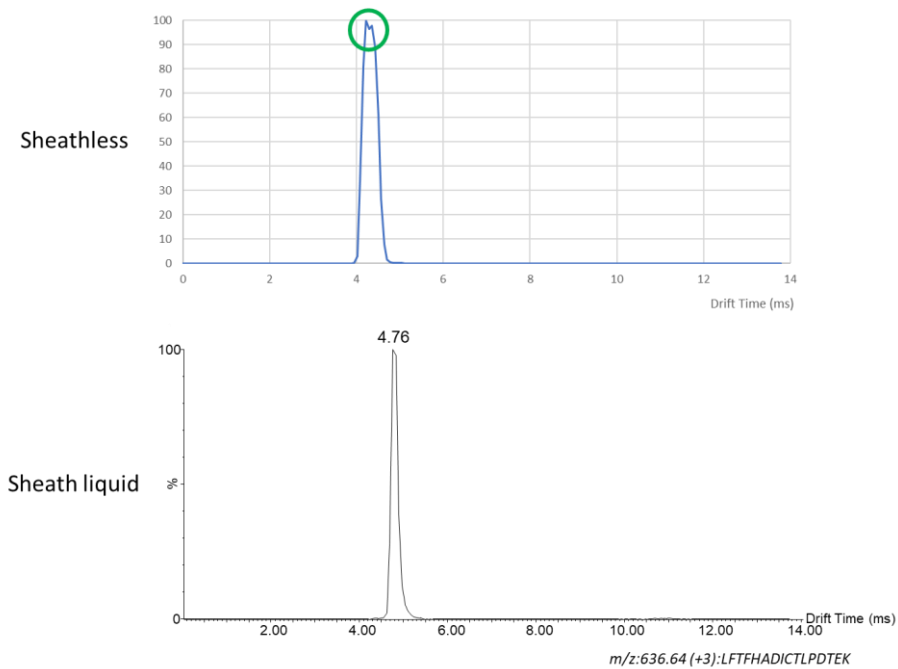


Fig.62 Difference in the number of IMS peaks between the sheathless and sheath liquid interfaces for the peptide LFTFHADICTLPDTEK

However, that phenomenon could also be explained by physical causes linked to the peptide structures. Indeed, the ionization process at a sheathless interface inherently involves a greater amount of thermal energy being imparted to the analytes. This is attributed to the generation of smaller droplets with this interface, resulting in reduced evaporation and, consequently, preventing the dissipation of energy. This elevated thermal energy may potentially facilitate overcoming the activation energy barriers within the peptide's energy landscape. Conversely, it is plausible to suggest that the sheath liquid interface introduces denaturing agents, such as isopropanol, with a capacity to influence the appearance or loss of specific conformations. In this study, definitive conclusions regarding the comparative energy contribution of the two interfaces are not drawn. However, conducting similar experiments on peptides with thermometer ions could enable a precise assessment of the actual energy supplied by both types of interfaces. This, in turn, would facilitate more accurate hypotheses regarding the potential pathways followed by peptide structures within their respective energy landscapes.

18. Influence of the BGE's pH

The pH of the background electrolyte (BGE) solution exhibits a close correlation with the migration times of the analytes, stemming from a combination of two primary effects. Firstly, variations in the averaged charge states of analytes lead to alterations in their electrophoretic mobility. Secondly, the electroosmotic flow (EOF) undergoes changes, contributing to the observed relationship. The EOF becomes more important with an increase of the pH of the BGE because the silanol groups at the surface of the capillary are more deprotonated, the negative charge of the surface increases and so the positive layer that create the EOF. In this section, some peptides with singular behaviors with the change of pH are presented. Additionally, the tridimensional structure of the peptide would also be affected by the pH due to the chemical denaturation, which in return should affect the hydrodynamic radius of the peptide. It is essential to emphasize that there is no pH value deemed "native" in our context, as our investigation focuses solely on peptides generated by trypsin from BSA, which lack biological activity.

The peptide with a mass of 1283.71 Da is a good example to illustrate the most common case. The peptide migrates faster at pH 6.52 than at pH 2.40 due to stronger EOF despite the negative average charge state and migrates much later at pH 4 due to lower average charge state despite the stronger EOF (Fig.63). The charge of this peptide was calculated at various pH values, revealing a reduction in charge as the pH increases (as could be expected). This charge decrease corresponds to an increase in the observed migration time. However, that effect is counterbalanced by the reinforcement of the EOF engendered by the rise of the pH. As a result, the peptide at pH 3.84 has the highest migration time because neither the EOF nor its average charge in solution has a high enough contribution to its migration.

In terms of peak shape, the electrophoretic peak obtained at pH 2.4 seems to a bit thicker, while the electrophoretic peak shape seems well defined as a single peak.

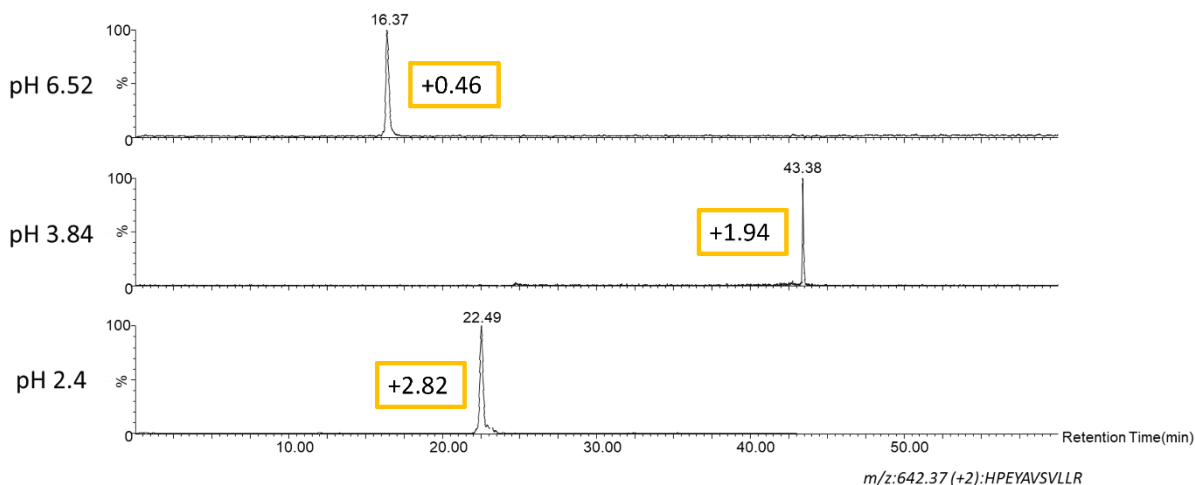


Fig.63 Electropherogram of a peptide with the sequence (HPEYAVSVLLR) at different pH of the background electrolytes with the average charges in solution provided.

It is important to highlight that several peptides deviate from the aforementioned example and exhibit a more atypical behavior. Due to factors described above, migration times of peptides appear to follow a consistent trend (convolution of the intrinsic electrophoretic mobility and EOF). However, in some cases, two peaks can be observed for acidic conditions (in this case pH 2.40) and evolve into a single-peak situation at pH 6.52 (Fig.64). This change could be attributed to the collapse of structures induced by a reduction in charges within each structure. The Coulomb repulsions within the structures play a pivotal role in maintaining their stability, and a decrease in these repulsions may lead to structural collapses. It is noteworthy that the presence of counter ions in the solution should mitigate Coulomb repulsion within the structures.

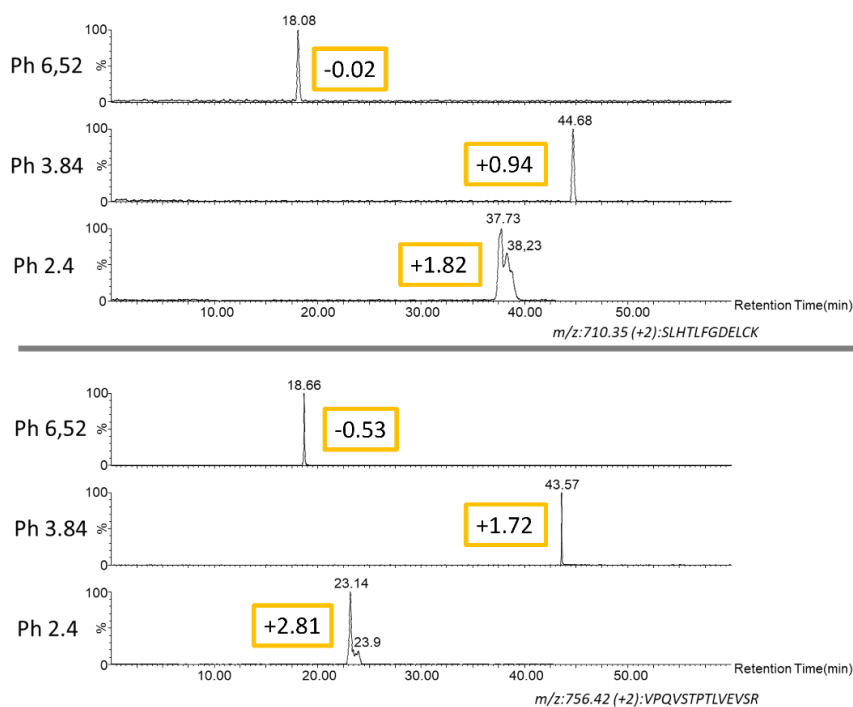


Fig.64 Electropherograms of two peptides with the sequences (SLHTLFGDELCK) and (VPQVSTPTLVEVSR) at different pH of the background electrolytes with their average charges in solution are highlighted in the yellow boxes.

Contrary to the examples in (Fig.64), the reduction in the average charge of a peptide in solution can result in the emergence of a new electrophoretic peak (Fig.65). According to the data (Fig.64), the addition of positive charges by lowering the pH of the BGE resulted in 2 conformational population in solution. Conversely, (Fig.65) shows that the increase of the averaged positive charge at low pH induces an extension of the peptide's conformation in solution resulting in a single electrophoretic peak while higher pH values (i.e. lower averaged charge state) induced the apparition of additional conformations.

Note that the presence of secondary structures is favored in longer peptides while in the shortest some peptides should exhibit random coil-like structures. Indeed, an alpha loop implies 3.6 residues by turn while beta sheet typically implies 3 to 10 residues. See (Fig.38 and 39) concerning the peptides' lengths distribution generated in this work. The average peptide length is 8 residues (median is 7 residues) for no miscleavage for the trypsin digestion of BSA.

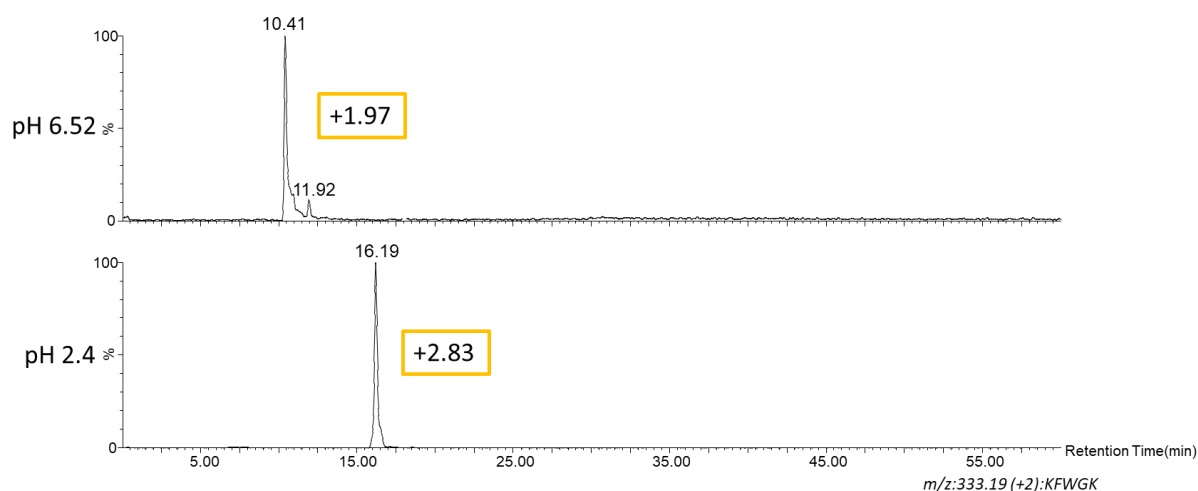


Fig.65 Electropherograms of a shorter peptide with the sequence (KFWGK) at pH 2.4 and pH 6.52 for the background electrolytes with their average charges in solution are highlighted in the yellow boxes.

The change in pH in CE does not appear to influence the equilibrium of conformations in IMS, which is not surprising since charges in the gaseous phase are positioned according to the proton affinities of the residues and not according to an acidity constant. However, it is important to note that these are only the examples observed, and it is possible that in other cases the positions of the charges in solution may influence the structure obtained in the gaseous phase (Fig.66).

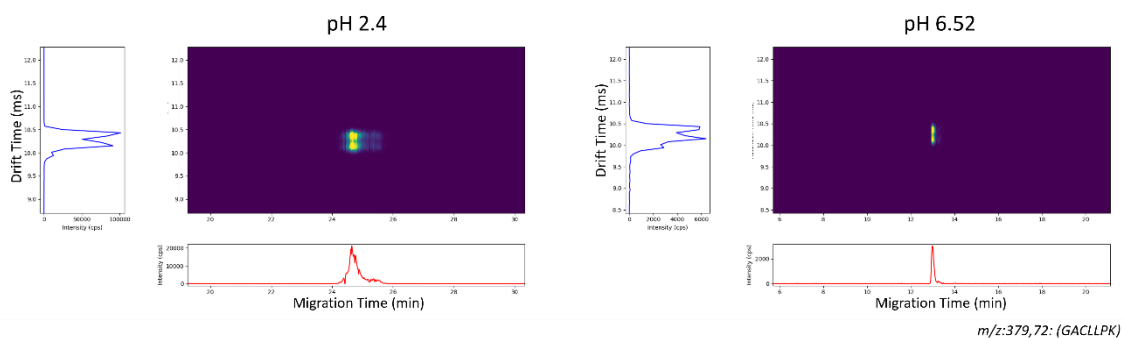


Fig.66 heatmap showing the conservation of the number of IMS peaks with pH evolution for the peptide GACLLPK

19. Conclusions

The understanding of the structures adopted by proteins and peptides is of paramount importance in the study of biological phenomena. Despite its crucial significance, the study of the different adopted conformations remains challenging, and a variety of characterization methods have been developed, each with its own strengths and limitations. Mass spectrometry coupled with capillary electrophoresis, ionic mobility, or a combination of both, has shown a very interesting potential to bring additional insight into this issue. However, despite its undeniable utility, the experiments conducted, and the results presented in this work show that the obtained results must always be compared between comparable results and taken with caution because the use of different instruments and different conditions can disturb the delicate balance that exists between the analyte, in our case peptides, and its environment.

Regarding the preservation or alteration of peptide conformations during the transition to the gas phase, a more extensive peptide library must be used to draw robust conclusions. This requires the introduction of dedicated home-made script and software to deal with the mass of generated information in the three dimensions of the CE-IM-MS coupling (migration times, arrival time distributions, and m/z), and even 4 dimensions if we include MS/MS for improved confidence level regarding the peptide identification. Indeed, all the data were manually processed (note for the reader: the current software processing the proteomic data generated by LC-MS does not focus on the multiple distributions of population, which are instead merged; the information of interest for this work is then lost). This is a quite time-consuming task which prevents the analysis of a larger peptide library such as the rabbit muscle phosphorylase B peptides generated by trypsin digestions.

Additionally, the use of computational chemistry to refine and support several hypotheses should be of precious help. Density Functional Theory would help for geometry optimization, energy calculation but above all the computation of theoretical proton affinity or gas phase basicity. Molecular Mechanics and Molecular Dynamics should help to assess the structure at higher temperatures and the dynamics of the conformational change. Amongst the hypotheses to be investigated concerned the origin of the origin of the electrophoretic peaks and ion mobility peaks observed for some peptides. About 80% of the detected peptides provided a single peak in the CE and IMS dimension, the others showed either several peaks in the CE and/or ion mobility dimension, using either the sheath liquid or the sheathless interface. We still must determine the balance and contribution between conformational changes and protonation site changes during the ion transfer into the gas phase. Amongst the most promising peptides to be further investigated, peptides containing proline(s) revealed several populations of conformation in the liquid phase and/or the gas phase. Additionally, a shorter peptide with several potential protonation site in the gas phase showed several arrival time distributions (ATD) peaks.

The determination of the effective temperature will also contribute to enhancing our comprehension of conformational changes or preservation during desolvation by the sheath liquid interface. This process might, in fact, thermalize or induce ion cooling during the droplet evaporation via electrospray ionization (ESI), despite the brief contact time between the organic solvent and the peptide at the Taylor cone's edge. Furthermore, this should help in assessing the increase in internal energy during the soft ion activation (or Collision-Induced Unfolding - CIU) conducted in this study. Several complementary experiments can be envisaged. The same type of experiment could be carried out, but this time in negative ESI mode using peptides with low "acid" isoelectric points to obtain a great and new variety of peptides. Other proteases such as pepsin or chymotrypsin should be used to digest proteins into peptides, as trypsin cleaves after lysines and arginines which can create a bias as all peptides have at least one positive end. The study of whole proteins rather than peptides could also be of interest in order to observe the influence of tertiary structures on the results, compared with

peptides which lack them. Finally, an important limitation is the resolution in IMS, and its increase could enable us to separate conformations with very similar CCS and potentially change cases with 2 peaks in CE and 1 in IMS into 2/2 cases.

20. Bibliography

- (1) Bodakuntla, S.; Jijumon, A. S.; Villablanca, C.; Gonzalez-Billault, C.; Janke, C. Microtubule-Associated Proteins: Structuring the Cytoskeleton. *Trends Cell Biol.* **2019**, *29* (10), 804–819. <https://doi.org/10.1016/j.tcb.2019.07.004>.
- (2) Kuivaniemi, H.; Tromp, G. Type III Collagen (COL3A1): Gene and Protein Structure, Tissue Distribution, and Associated Diseases. *Gene* **2019**, *707*, 151–171. <https://doi.org/10.1016/j.gene.2019.05.003>.
- (3) Adlakha, J.; Hong, Z.; Li, P.; Reinisch, K. M. Structural and Biochemical Insights into Lipid Transport by VPS13 Proteins. *J. Cell Biol.* **2022**, *221* (5), e202202030. <https://doi.org/10.1083/jcb.202202030>.
- (4) Hammes, G. G. Multiple Conformational Changes in Enzyme Catalysis. *Biochemistry* **2002**, *41* (26), 8221–8228. <https://doi.org/10.1021/bi0260839>.
- (5) Kim, J.; Dang, C. V. Multifaceted Roles of Glycolytic Enzymes. *Trends Biochem. Sci.* **2005**, *30* (3), 142–150. <https://doi.org/10.1016/j.tibs.2005.01.005>.
- (6) Zhang, Y.; Gladyshev, V. N. High Content of Proteins Containing 21st and 22nd Amino Acids, Selenocysteine and Pyrrolysine, in a Symbiotic Deltaproteobacterium of Gutless Worm *Olavius Algarvensis*. *Nucleic Acids Res.* **2007**, *35* (15), 4952–4963. <https://doi.org/10.1093/nar/gkm514>.
- (7) Santofimia-Castaño, P.; Rizzuti, B.; Xia, Y.; Abian, O.; Peng, L.; Velázquez-Campoy, A.; Neira, J. L.; Iovanna, J. Targeting Intrinsically Disordered Proteins Involved in Cancer. *Cell. Mol. Life Sci.* **2020**, *77* (9), 1695–1707. <https://doi.org/10.1007/s00018-019-03347-3>.
- (8) Cojocar, V.; Winn, P. J.; Wade, R. C. The Ins and Outs of Cytochrome P450s. *Biochim. Biophys. Acta BBA - Gen. Subj.* **2007**, *1770* (3), 390–401. <https://doi.org/10.1016/j.bbagen.2006.07.005>.
- (9) Scholtz, M.; Baldwin, R. L. THE MECHANISM OF A-HELIX FORMATION BY PEPTIDES.
- (10) Cuny, G. D.; Yu, P. B.; Laha, J. K.; Xing, X.; Liu, J.-F.; Lai, C. S.; Deng, D. Y.; Sachidanandan, C.; Bloch, K. D.; Peterson, R. T. Structure–Activity Relationship Study of Bone Morphogenetic Protein (BMP) Signaling Inhibitors. *Bioorg. Med. Chem. Lett.* **2008**, *18* (15), 4388–4392. <https://doi.org/10.1016/j.bmcl.2008.06.052>.
- (11) Belliotti, T. R.; Capiris, T.; Ekhato, I. V.; Kinsora, J. J.; Field, M. J.; Heffner, T. G.; Meltzer, L. T.; Schwarz, J. B.; Taylor, C. P.; Thorpe, A. J.; Vartanian, M. G.; Wise, L. D.; Zhi-Su, T.; Weber, M. L.; Wustrow, D. J. Structure–Activity Relationships of Pregabalin and Analogues That Target the $\alpha_2\text{-}\delta$ Protein. *J. Med. Chem.* **2005**, *48* (7), 2294–2307. <https://doi.org/10.1021/jm049762l>.
- (12) Xiong, Y. L. Protein Denaturation and Functionality Losses. In *Quality in Frozen Foods*; Erickson, M. C., Hung, Y.-C., Eds.; Springer US: Boston, MA, 1997; pp 111–140. https://doi.org/10.1007/978-1-4615-5975-7_8.
- (13) Hédoux, A.; Krenzlin, S.; Paccou, L.; Guinet, Y.; Flament, M.-P.; Siepmann, J. Influence of Urea and Guanidine Hydrochloride on Lysozyme Stability and Thermal Denaturation; a Correlation between Activity, Protein Dynamics and Conformational Changes. *Phys. Chem. Chem. Phys.* **2010**, *12* (40), 13189. <https://doi.org/10.1039/c0cp00602e>.
- (14) Longhi, S.; Cambillau, C. Structure-Activity of Cutinase, a Small Lipolytic Enzyme. *Biochim. Biophys. Acta BBA - Mol. Cell Biol. Lipids* **1999**, *1441* (2–3), 185–196. [https://doi.org/10.1016/S1388-1981\(99\)00159-6](https://doi.org/10.1016/S1388-1981(99)00159-6).
- (15) DeToma, A. S.; Salamekh, S.; Ramamoorthy, A.; Lim, M. H. Misfolded Proteins in Alzheimer’s Disease and Type II Diabetes. *Chem Soc Rev* **2012**, *41* (2), 608–621. <https://doi.org/10.1039/C1CS15112F>.

- (16) Vojcic, L.; Pitzler, C.; Körfer, G.; Jakob, F.; Ronny Martinez; Maurer, K.-H.; Schwaneberg, U. Advances in Protease Engineering for Laundry Detergents. *New Biotechnol.* **2015**, *32* (6), 629–634. <https://doi.org/10.1016/j.nbt.2014.12.010>.
- (17) Barth, A. Infrared Spectroscopy of Proteins. *Biochim. Biophys. Acta BBA - Bioenerg.* **2007**, *1767* (9), 1073–1101. <https://doi.org/10.1016/j.bbabi.2007.06.004>.
- (18) Kong, J.; Yu, S. Fourier Transform Infrared Spectroscopic Analysis of Protein Secondary Structures. *Acta Biochim. Biophys. Sin.* **2007**, *39* (8), 549–559. <https://doi.org/10.1111/j.1745-7270.2007.00320.x>.
- (19) *Near-Infrared Spectroscopy: Theory, Spectral Analysis, Instrumentation, and Applications*; Ozaki, Y., Huck, C., Tsuchikawa, S., Engelsen, S. B., Eds.; Springer Singapore: Singapore, 2021. <https://doi.org/10.1007/978-981-15-8648-4>.
- (20) Carissimi, G.; Baronio, C. M.; Montalbán, M. G.; Vllora, G.; Barth, A. On the Secondary Structure of Silk Fibroin Nanoparticles Obtained Using Ionic Liquids: An Infrared Spectroscopy Study. *Polymers* **2020**, *12* (6), 1294. <https://doi.org/10.3390/polym12061294>.
- (21) Greenfield, N. J. Using Circular Dichroism Spectra to Estimate Protein Secondary Structure. *Nat. Protoc.* **2006**, *1* (6), 2876–2890. <https://doi.org/10.1038/nprot.2006.202>.
- (22) Kelly, S. M.; Jess, T. J.; Price, N. C. How to Study Proteins by Circular Dichroism. *Biochim. Biophys. Acta BBA - Proteins Proteomics* **2005**, *1751* (2), 119–139. <https://doi.org/10.1016/j.bbapap.2005.06.005>.
- (23) Laur, P. The First Decades after the Discovery of CD and ORD by Aimé Cotton in 1895. In *Comprehensive Chiroptical Spectroscopy*; Berova, N., Polavarapu, P. L., Nakanishi, K., Woody, R. W., Eds.; John Wiley & Sons, Inc.: Hoboken, NJ, USA, 2012; pp 1–35. <https://doi.org/10.1002/9781118120392.ch1>.
- (24) Selling, G. W.; Hamaker, S. A. H.; Sessa, D. J. Effect of Solvent and Temperature on Secondary and Tertiary Structure of Zein by Circular Dichroism. *Cereal Chem. J.* **2007**, *84* (3), 265–270. <https://doi.org/10.1094/CCHEM-84-3-0265>.
- (25) Miles, A. J.; Wallace, B. A. Circular Dichroism Spectroscopy of Membrane Proteins. *Chem. Soc. Rev.* **2016**, *45* (18), 4859–4872. <https://doi.org/10.1039/C5CS00084J>.
- (26) Smyth, M. S. X Ray Crystallography. *Mol. Pathol.* **2000**, *53* (1), 8–14. <https://doi.org/10.1136/mp.53.1.8>.
- (27) Maveyraud, L.; Mourey, L. Protein X-Ray Crystallography and Drug Discovery. *Molecules* **2020**, *25* (5), 1030. <https://doi.org/10.3390/molecules25051030>.
- (28) McPherson, A.; Gavira, J. A. Introduction to Protein Crystallization. *Acta Crystallogr. Sect. F Struct. Biol. Commun.* **2014**, *70* (1), 2–20. <https://doi.org/10.1107/S2053230X13033141>.
- (29) Handing, K. B.; Niedzialkowska, E.; Shabalin, I. G.; Kuhn, M. L.; Zheng, H.; Minor, W. Characterizing Metal-Binding Sites in Proteins with X-Ray Crystallography. *Nat. Protoc.* **2018**, *13* (5), 1062–1090. <https://doi.org/10.1038/nprot.2018.018>.
- (30) Kay, L. E. NMR Studies of Protein Structure and Dynamics. *J. Magn. Reson.* **2011**, *213* (2), 477–491. <https://doi.org/10.1016/j.jmr.2011.09.009>.
- (31) Salzmann, M.; Wider, G.; Pervushin, K.; Senn, H.; Wüthrich, K. TROSY-Type Triple-Resonance Experiments for Sequential NMR Assignments of Large Proteins. *J. Am. Chem. Soc.* **1999**, *121* (4), 844–848. <https://doi.org/10.1021/ja9834226>.
- (32) Breeze, A. L. Isotope-Filtered NMR Methods for the Study of Biomolecular Structure and Interactions. *Prog. Nucl. Magn. Reson. Spectrosc.* **2000**, *36* (4), 323–372. [https://doi.org/10.1016/S0079-6565\(00\)00020-0](https://doi.org/10.1016/S0079-6565(00)00020-0).
- (33) Opella, S. J.; Marassi, F. M. Structure Determination of Membrane Proteins by NMR Spectroscopy. *Chem. Rev.* **2004**, *104* (8), 3587–3606. <https://doi.org/10.1021/cr0304121>.
- (34) Göbl, C.; Madl, T.; Simon, B.; Sattler, M. NMR Approaches for Structural Analysis of Multidomain Proteins and Complexes in Solution. *Prog. Nucl. Magn. Reson. Spectrosc.* **2014**, *80*, 26–63. <https://doi.org/10.1016/j.pnmrs.2014.05.003>.
- (35) Meissner, A.; Sørensen, O. W. Sequential HNCACB and CBCANH Protein NMR Pulse Sequences. *J. Magn. Reson.* **2001**, *151* (2), 328–331. <https://doi.org/10.1006/jmre.2001.2374>.
- (36) Rovnyak, D.; Frueh, D. P.; Sastry, M.; Sun, Z.-Y. J.; Stern, A. S.; Hoch, J. C.; Wagner, G. Accelerated Acquisition of High Resolution Triple-Resonance Spectra Using Non-Uniform

- Sampling and Maximum Entropy Reconstruction. *J. Magn. Reson.* **2004**, *170* (1), 15–21. <https://doi.org/10.1016/j.jmr.2004.05.016>.
- (37) Puthenveetil, R.; Vinogradova, O. Solution NMR: A Powerful Tool for Structural and Functional Studies of Membrane Proteins in Reconstituted Environments. *J. Biol. Chem.* **2019**, *294* (44), 15914–15931. <https://doi.org/10.1074/jbc.REV119.009178>.
- (38) Schuler, B. Single-Molecule FRET of Protein Structure and Dynamics - a Primer. *J. Nanobiotechnology* **2013**, *11* (Suppl 1), S2. <https://doi.org/10.1186/1477-3155-11-S1-S2>.
- (39) Piston, D. W.; Kremers, G.-J. Fluorescent Protein FRET: The Good, the Bad and the Ugly. *Trends Biochem. Sci.* **2007**, *32* (9), 407–414. <https://doi.org/10.1016/j.tibs.2007.08.003>.
- (40) Santini, S.; Bizzarri, A. R.; Cannistraro, S. Revisitation of FRET Methods to Measure Intraprotein Distances in Human Serum Albumin. *J. Lumin.* **2016**, *179*, 322–327. <https://doi.org/10.1016/j.jlumin.2016.07.029>.
- (41) Earl, L. A.; Falconieri, V.; Milne, J. L.; Subramaniam, S. Cryo-EM: Beyond the Microscope. *Curr. Opin. Struct. Biol.* **2017**, *46*, 71–78. <https://doi.org/10.1016/j.sbi.2017.06.002>.
- (42) Yip, K. M.; Fischer, N.; Paknia, E.; Chari, A.; Stark, H. Atomic-Resolution Protein Structure Determination by Cryo-EM. *Nature* **2020**, *587* (7832), 157–161. <https://doi.org/10.1038/s41586-020-2833-4>.
- (43) Tsai, M.-D.; Wu, W.-J.; Ho, M.-C. Enzymology and Dynamics by Cryogenic Electron Microscopy. *Annu. Rev. Biophys.* **2022**, *51* (1), 19–38. <https://doi.org/10.1146/annurev-biophys-100121-075228>.
- (44) Passmore, L. A.; Russo, C. J. Specimen Preparation for High-Resolution Cryo-EM. In *Methods in Enzymology*; Elsevier, 2016; Vol. 579, pp 51–86. <https://doi.org/10.1016/bs.mie.2016.04.011>.
- (45) Thonghin, N.; Kargas, V.; Clews, J.; Ford, R. C. Cryo-Electron Microscopy of Membrane Proteins. *Methods* **2018**, *147*, 176–186. <https://doi.org/10.1016/j.ymeth.2018.04.018>.
- (46) Muller, D. J. AFM: A Nanotool in Membrane Biology. *Biochemistry* **2008**, *47* (31), 7986–7998. <https://doi.org/10.1021/bi800753x>.
- (47) Müller, D. J.; Janovjak, H.; Lehto, T.; Kuerschner, L.; Anderson, K. Observing Structure, Function and Assembly of Single Proteins by AFM. *Prog. Biophys. Mol. Biol.* **2002**, *79* (1–3), 1–43. [https://doi.org/10.1016/S0079-6107\(02\)00009-3](https://doi.org/10.1016/S0079-6107(02)00009-3).
- (48) Ando, T. High-Speed AFM Imaging. *Curr. Opin. Struct. Biol.* **2014**, *28*, 63–68. <https://doi.org/10.1016/j.sbi.2014.07.011>.
- (49) Feist, A.; Bach, N.; Rubiano Da Silva, N.; Danz, T.; Möller, M.; Priebe, K. E.; Domröse, T.; Gatzmann, J. G.; Rost, S.; Schauss, J.; Strauch, S.; Bormann, R.; Sivilis, M.; Schäfer, S.; Ropers, C. Ultrafast Transmission Electron Microscopy Using a Laser-Driven Field Emitter: Femtosecond Resolution with a High Coherence Electron Beam. *Ultramicroscopy* **2017**, *176*, 63–73. <https://doi.org/10.1016/j.ultramic.2016.12.005>.
- (50) McAllister, C.; Karymov, M. A.; Kawano, Y.; Lushnikov, A. Y.; Mikheikin, A.; Uversky, V. N.; Lyubchenko, Y. L. Protein Interactions and Misfolding Analyzed by AFM Force Spectroscopy. *J. Mol. Biol.* **2005**, *354* (5), 1028–1042. <https://doi.org/10.1016/j.jmb.2005.10.012>.
- (51) Beseničar, M.; Maček, P.; Lakey, J. H.; Anderluh, G. Surface Plasmon Resonance in Protein–Membrane Interactions. *Chem. Phys. Lipids* **2006**, *141* (1), 169–178. <https://doi.org/10.1016/j.chemphyslip.2006.02.010>.
- (52) Drescher, D. G.; Selvakumar, D.; Drescher, M. J. Analysis of Protein Interactions by Surface Plasmon Resonance. In *Advances in Protein Chemistry and Structural Biology*; Elsevier, 2018; Vol. 110, pp 1–30. <https://doi.org/10.1016/bs.apcsb.2017.07.003>.
- (53) Omar, N. A. S.; Fen, Y. W.; Abdullah, J.; Chik, C. E. N. C. E.; Mahdi, M. A. Development of an Optical Sensor Based on Surface Plasmon Resonance Phenomenon for Diagnosis of Dengue Virus E-Protein. *Sens. Bio-Sens. Res.* **2018**, *20*, 16–21. <https://doi.org/10.1016/j.sbsr.2018.06.001>.
- (54) Floudas, C. A.; Fung, H. K.; McAllister, S. R.; Mönnigmann, M.; Rajgaria, R. Advances in Protein Structure Prediction and de Novo Protein Design: A Review. *Chem. Eng. Sci.* **2006**, *61* (3), 966–988. <https://doi.org/10.1016/j.ces.2005.04.009>.
- (55) Rao, V. S.; Srinivas, K.; Sujini, G. N.; Kumar, G. N. S. Protein-Protein Interaction Detection: Methods and Analysis. *Int. J. Proteomics* **2014**, *2014*, 1–12. <https://doi.org/10.1155/2014/147648>.

- (56) Webb, B.; Sali, A. Comparative Protein Structure Modeling Using MODELLER. *Curr. Protoc. Bioinforma.* **2016**, *54* (1). <https://doi.org/10.1002/cpbi.3>.
- (57) Pearce, R.; Zhang, Y. Toward the Solution of the Protein Structure Prediction Problem. *J. Biol. Chem.* **2021**, *297* (1), 100870. <https://doi.org/10.1016/j.jbc.2021.100870>.
- (58) Standing, K. Peptide and Protein de Novo Sequencing by Mass Spectrometry. *Curr. Opin. Struct. Biol.* **2003**, *13* (5), 595–601. <https://doi.org/10.1016/j.sbi.2003.09.005>.
- (59) Coon, J. J.; Syka, J. E. P.; Shabanowitz, J.; Hunt, D. F. Tandem Mass Spectrometry for Peptide and Protein Sequence Analysis. *BioTechniques* **2005**, *38* (4), 519–523. <https://doi.org/10.2144/05384TE01>.
- (60) Morsa, D.; Baiwir, D.; La Rocca, R.; Zimmerman, T. A.; Hanozin, E.; Grifnée, E.; Longuespée, R.; Meuwis, M.-A.; Smargiasso, N.; Pauw, E. D.; Mazzucchelli, G. Multi-Enzymatic Limited Digestion: The Next-Generation Sequencing for Proteomics? *J. Proteome Res.* **2019**, *18* (6), 2501–2513. <https://doi.org/10.1021/acs.jproteome.9b00044>.
- (61) Duong, V.-A.; Park, J.-M.; Lee, H. Review of Three-Dimensional Liquid Chromatography Platforms for Bottom-Up Proteomics. *Int. J. Mol. Sci.* **2020**, *21* (4), 1524. <https://doi.org/10.3390/ijms21041524>.
- (62) Ali, I.; Aboul-Enein, H. Y.; Singh, P.; Singh, R.; Sharma, B. Separation of Biological Proteins by Liquid Chromatography. *Saudi Pharm. J.* **2010**, *18* (2), 59–73. <https://doi.org/10.1016/j.jsps.2010.02.001>.
- (63) Hao, X.; Fu, L.; Shao, L.; Chen, Q.; Dorus, B.; Cao, X.; Fang, F. Quantification of Major Milk Proteins Using Ultra-Performance Liquid Chromatography Tandem Triple Quadrupole Mass Spectrometry and Its Application in Milk Authenticity Analysis. *Food Control* **2022**, *131*, 108455. <https://doi.org/10.1016/j.foodcont.2021.108455>.
- (64) Konermann, L.; Pan, J.; Liu, Y.-H. Hydrogen Exchange Mass Spectrometry for Studying Protein Structure and Dynamics. *Chem Soc Rev* **2011**, *40* (3), 1224–1234. <https://doi.org/10.1039/C0CS00113A>.
- (65) Oganessian, I.; Lento, C.; Wilson, D. J. Contemporary Hydrogen Deuterium Exchange Mass Spectrometry. *Methods* **2018**, *144*, 27–42. <https://doi.org/10.1016/j.ymeth.2018.04.023>.
- (66) Holding, A. N. XL-MS: Protein Cross-Linking Coupled with Mass Spectrometry. *Methods* **2015**, *89*, 54–63. <https://doi.org/10.1016/j.ymeth.2015.06.010>.
- (67) Back, J. W.; De Jong, L.; Muijsers, A. O.; De Koster, C. G. Chemical Cross-Linking and Mass Spectrometry for Protein Structural Modeling. *J. Mol. Biol.* **2003**, *331* (2), 303–313. [https://doi.org/10.1016/S0022-2836\(03\)00721-6](https://doi.org/10.1016/S0022-2836(03)00721-6).
- (68) Ferguson, P. L.; Pan, J.; Wilson, D. J.; Dempsey, B.; Lajoie, G.; Shilton, B.; Konermann, L. Hydrogen/Deuterium Scrambling during Quadrupole Time-of-Flight MS/MS Analysis of a Zinc-Binding Protein Domain. *Anal. Chem.* **2007**, *79* (1), 153–160. <https://doi.org/10.1021/ac061261f>.
- (69) Tamara, S.; den Boer, M. A.; Heck, A. J. R. High-Resolution Native Mass Spectrometry. *Chem. Rev.* **2022**, *122* (8), 7269–7326. <https://doi.org/10.1021/acs.chemrev.1c00212>.
- (70) Voeten, R. L. C.; Ventouri, I. K.; Haselberg, R.; Somsen, G. W. Capillary Electrophoresis: Trends and Recent Advances. *Anal. Chem.* **2018**, *90* (3), 1464–1481. <https://doi.org/10.1021/acs.analchem.8b00015>.
- (71) Zhu, Z.; Lu, J. J.; Liu, S. Protein Separation by Capillary Gel Electrophoresis: A Review. *Anal. Chim. Acta* **2012**, *709*, 21–31. <https://doi.org/10.1016/j.aca.2011.10.022>.
- (72) Rogacs, A.; Marshall, L. A.; Santiago, J. G. Purification of Nucleic Acids Using Isotachopheresis. *J. Chromatogr. A* **2014**, *1335*, 105–120. <https://doi.org/10.1016/j.chroma.2013.12.027>.
- (73) Terabe, S. Capillary Separation: Micellar Electrokinetic Chromatography. *Annu. Rev. Anal. Chem.* **2009**, *2* (1), 99–120. <https://doi.org/10.1146/annurev.anchem.1.031207.113005>.
- (74) Dovichi, N. J. DNA Sequencing by Capillary Electrophoresis. *Electrophoresis* **1997**, *18* (12–13), 2393–2399. <https://doi.org/10.1002/elps.1150181229>.
- (75) Yan, H.; Jiang, E.; Zhu, H.; Hu, L.; Liu, J.; Qu, L. The Novel 22 Bp Insertion Mutation in a Promoter Region of the *PITX2* Gene Is Associated with Litter Size and Growth Traits in Goats. *Arch. Anim. Breed.* **2018**, *61* (3), 329–336. <https://doi.org/10.5194/aab-61-329-2018>.

- (76) De Luna-Valdez, L. A.; Villaseñor-Salmerón, C. I.; Cordoba, E.; Vera-Estrella, R.; León-Mejía, P.; Guevara-García, A. A. Functional Analysis of the Chloroplast GrpE (CGE) Proteins from *Arabidopsis Thaliana*. *Plant Physiol. Biochem.* **2019**, *139*, 293–306. <https://doi.org/10.1016/j.plaphy.2019.03.027>.
- (77) Berezovski, M. V.; Mironov, G. G. Utility of Kinetic Capillary Electrophoresis-Mass Spectrometry to Study Protein Dynamics and Affinity Interactions. *Expert Rev. Proteomics* **2012**, *9* (5), 477–479. <https://doi.org/10.1586/epr.12.45>.
- (78) Krylov, S. N. Nonequilibrium Capillary Electrophoresis of Equilibrium Mixtures (NECEEM): A Novel Method for Biomolecular Screening. *SLAS Discov.* **2006**, *11* (2), 115–122. <https://doi.org/10.1177/1087057105284339>.
- (79) Krylov, S. N.; Berezovski, M. Non-Equilibrium Capillary Electrophoresis of Equilibrium Mixtures—Appreciation of Kinetics in Capillary Electrophoresis. *The Analyst* **2003**, *128* (6), 571–575. <https://doi.org/10.1039/B212913B>.
- (80) Belov, A. M.; Viner, R.; Santos, M. R.; Horn, D. M.; Bern, M.; Karger, B. L.; Ivanov, A. R. Analysis of Proteins, Protein Complexes, and Organellar Proteomes Using Sheathless Capillary Zone Electrophoresis - Native Mass Spectrometry. *J. Am. Soc. Mass Spectrom.* **2017**, *28* (12), 2614–2634. <https://doi.org/10.1007/s13361-017-1781-1>.
- (81) Zhang, W.; Wu, H.; Zhang, R.; Fang, X.; Xu, W. Structure and Effective Charge Characterization of Proteins by a Mobility Capillary Electrophoresis Based Method. *Chem. Sci.* **2019**, *10* (33), 7779–7787. <https://doi.org/10.1039/C9SC02039J>.
- (82) Borsdorf, H.; Eiceman, G. A. Ion Mobility Spectrometry: Principles and Applications. *Appl. Spectrosc. Rev.* **2006**, *41* (4), 323–375. <https://doi.org/10.1080/05704920600663469>.
- (83) Creaser, C. S.; Griffiths, J. R.; Bramwell, C. J.; Noreen, S.; Hill, C. A.; Thomas, C. L. P. Ion Mobility Spectrometry: A Review. Part 1. Structural Analysis by Mobility Measurement. *The Analyst* **2004**, *129* (11), 984. <https://doi.org/10.1039/b404531a>.
- (84) Hill, H. H.; Simpson, G. Capabilities and Limitations of Ion Mobility Spectrometry for Field Screening Applications. *Field Anal. Chem. Technol.* **1997**, *1* (3), 119–134. [https://doi.org/10.1002/\(SICI\)1520-6521\(1997\)1:3<119::AID-FACT2>3.0.CO;2-S](https://doi.org/10.1002/(SICI)1520-6521(1997)1:3<119::AID-FACT2>3.0.CO;2-S).
- (85) Gabelica, V.; Shvartsburg, A. A.; Afonso, C.; Barran, P.; Benesch, J. L. P.; Bleiholder, C.; Bowers, M. T.; Bilbao, A.; Bush, M. F.; Campbell, J. L.; Campuzano, I. D. G.; Causon, T.; Clowers, B. H.; Creaser, C. S.; De Pauw, E.; Far, J.; Fernandez-Lima, F.; Fjeldsted, J. C.; Giles, K.; Groessl, M.; Hogan, C. J.; Hann, S.; Kim, H. I.; Kurulugama, R. T.; May, J. C.; McLean, J. A.; Pagel, K.; Richardson, K.; Ridgeway, M. E.; Rosu, F.; Sobott, F.; Thalassinos, K.; Valentine, S. J.; Wytenbach, T. Recommendations for Reporting Ion Mobility Mass Spectrometry Measurements. *Mass Spectrom. Rev.* **2019**, *38* (3), 291–320. <https://doi.org/10.1002/mas.21585>.
- (86) Christofi, E.; Barran, P. Ion Mobility Mass Spectrometry (IM-MS) for Structural Biology: Insights Gained by Measuring Mass, Charge, and Collision Cross Section. *Chem. Rev.* **2023**, *123* (6), 2902–2949. <https://doi.org/10.1021/acs.chemrev.2c00600>.
- (87) Dixit, S. M.; Polasky, D. A.; Ruotolo, B. T. Collision Induced Unfolding of Isolated Proteins in the Gas Phase: Past, Present, and Future. *Curr. Opin. Chem. Biol.* **2018**, *42*, 93–100. <https://doi.org/10.1016/j.cbpa.2017.11.010>.
- (88) Mitchell Wells, J.; McLuckey, S. A. Collision-Induced Dissociation (CID) of Peptides and Proteins. In *Methods in Enzymology*; Elsevier, 2005; Vol. 402, pp 148–185. [https://doi.org/10.1016/S0076-6879\(05\)02005-7](https://doi.org/10.1016/S0076-6879(05)02005-7).
- (89) Syka, J. E. P.; Coon, J. J.; Schroeder, M. J.; Shabanowitz, J.; Hunt, D. F. Peptide and Protein Sequence Analysis by Electron Transfer Dissociation Mass Spectrometry. *Proc. Natl. Acad. Sci.* **2004**, *101* (26), 9528–9533. <https://doi.org/10.1073/pnas.0402700101>.
- (90) Zubarev, R. A. Electron-Capture Dissociation Tandem Mass Spectrometry. *Curr. Opin. Biotechnol.* **2004**, *15* (1), 12–16. <https://doi.org/10.1016/j.copbio.2003.12.002>.
- (91) Cannon, J. R.; Cammarata, M. B.; Robotham, S. A.; Cotham, V. C.; Shaw, J. B.; Fellers, R. T.; Early, B. P.; Thomas, P. M.; Kelleher, N. L.; Brodbelt, J. S. Ultraviolet Photodissociation for Characterization of Whole Proteins on a Chromatographic Time Scale. *Anal. Chem.* **2014**, *86* (4), 2185–2192. <https://doi.org/10.1021/ac403859a>.
- (92) Phetsanthad, A.; Li, G.; Jeon, C. K.; Ruotolo, B. T.; Li, L. Comparing Selected-Ion Collision Induced Unfolding with All Ion Unfolding Methods for Comprehensive Protein Conformational

- Characterization. *J. Am. Soc. Mass Spectrom.* **2022**, *33* (6), 944–951. <https://doi.org/10.1021/jasms.2c00004>.
- (93) McCabe, J. W.; Hebert, M. J.; Shirzadeh, M.; Mallis, C. S.; Denton, J. K.; Walker, T. E.; Russell, D. H. THE IMS PARADOX: A PERSPECTIVE ON STRUCTURAL ION MOBILITY-MASS SPECTROMETRY. *Mass Spectrom. Rev.* **2021**, *40* (3), 280–305. <https://doi.org/10.1002/mas.21642>.
- (94) Harms, M. J.; Castañeda, C. A.; Schlessman, J. L.; Sue, G. R.; Isom, D. G.; Cannon, B. R.; García-Moreno E., B. The pKa Values of Acidic and Basic Residues Buried at the Same Internal Location in a Protein Are Governed by Different Factors. *J. Mol. Biol.* **2009**, *389* (1), 34–47. <https://doi.org/10.1016/j.jmb.2009.03.039>.
- (95) Grimsley, G. R.; Scholtz, J. M.; Pace, C. N. A Summary of the Measured pK Values of the Ionizable Groups in Folded Proteins. *Protein Sci.* **2009**, *18* (1), 247–251. <https://doi.org/10.1002/pro.19>.
- (96) Bleiholder, C.; Suhai, S.; Paizs, B. Revising the Proton Affinity Scale of the Naturally Occurring α -Amino Acids. *J. Am. Soc. Mass Spectrom.* **2006**, *17* (9), 1275–1281. <https://doi.org/10.1016/j.jasms.2006.05.010>.
- (97) Kune, C.; Delvaux, C.; Haler, J. R. N.; Quinton, L.; Eppe, G.; De Pauw, E.; Far, J. A Mechanistic Study of Protonated Aniline to Protonated Phenol Substitution Considering Tautomerization by Ion Mobility Mass Spectrometry and Tandem Mass Spectrometry. *J. Am. Soc. Mass Spectrom.* **2019**, *30* (11), 2238–2249. <https://doi.org/10.1007/s13361-019-02321-4>.
- (98) McCann, A.; Kune, C.; Massonnet, P.; Far, J.; Ongena, M.; Eppe, G.; Quinton, L.; De Pauw, E. Cyclic Peptide Protomer Detection in the Gas Phase: Impact on CCS Measurement and Fragmentation Patterns. *J. Am. Soc. Mass Spectrom.* **2022**, *33* (5), 851–858. <https://doi.org/10.1021/jasms.2c00035>.
- (99) Paizs, Béla.; Suhai, S. Towards Understanding the Tandem Mass Spectra of Protonated Oligopeptides. 1: Mechanism of Amide Bond Cleavage. *J. Am. Soc. Mass Spectrom.* **2004**, *15* (1), 103–113. <https://doi.org/10.1016/j.jasms.2003.09.010>.
- (100) Bythell, B. J.; Somogyi, Á.; Paizs, B. What Is the Structure of b_2 Ions Generated from Doubly Protonated Tryptic Peptides? *J. Am. Soc. Mass Spectrom.* **2009**, *20* (4), 618–624. <https://doi.org/10.1016/j.jasms.2008.11.021>.
- (101) Hong, S.; Bush, M. F. Collision-Induced Unfolding Is Sensitive to the Polarity of Proteins and Protein Complexes. *J. Am. Soc. Mass Spectrom.* **2019**, *30* (11), 2430–2437. <https://doi.org/10.1007/s13361-019-02326-z>.
- (102) Donor, M. T.; Mroz, A. M.; Prell, J. S. Experimental and Theoretical Investigation of Overall Energy Deposition in Surface-Induced Unfolding of Protein Ions. *Chem. Sci.* **2019**, *10* (14), 4097–4106. <https://doi.org/10.1039/C9SC00644C>.
- (103) Fabris, D.; Kelly, M.; Murphy, C.; Wu, Z.; Fenselau, C. High-Energy Collision-Induced Dissociation of Multiply Charged Polypeptides Produced by Electrospray. *J. Am. Soc. Mass Spectrom.* **1993**, *4* (8), 652–661. [https://doi.org/10.1016/1044-0305\(93\)85030-2](https://doi.org/10.1016/1044-0305(93)85030-2).
- (104) Collette, C.; Drahos, L.; Pauw, E. D.; Vékey, K. Comparison of the Internal Energy Distributions of Ions Produced by Different Electrospray Sources. *Rapid Commun. Mass Spectrom.* **1998**, *12* (22), 1673–1678. [https://doi.org/10.1002/\(SICI\)1097-0231\(19981130\)12:22<1673::AID-RCM385>3.0.CO;2-A](https://doi.org/10.1002/(SICI)1097-0231(19981130)12:22<1673::AID-RCM385>3.0.CO;2-A).
- (105) Herskovits, T. T.; Gadegbeku, B.; Jailliet, H. On the Structural Stability and Solvent Denaturation of Proteins. *J. Biol. Chem.* **1970**, *245* (10), 2588–2598. [https://doi.org/10.1016/S0021-9258\(18\)63111-4](https://doi.org/10.1016/S0021-9258(18)63111-4).
- (106) González-Ruiz, V.; Codesido, S.; Far, J.; Rudaz, S.; Schappler, J. Evaluation of a New Low Sheath-Flow Interface for CE-MS: CE and CEC. *ELECTROPHORESIS* **2016**, *37* (7–8), 936–946. <https://doi.org/10.1002/elps.201500523>.
- (107) Kim, H.-H.; Kim, J.-H.; Ogata, A. Time-Resolved High-Speed Camera Observation of Electrospray. *J. Aerosol Sci.* **2011**, *42* (4), 249–263. <https://doi.org/10.1016/j.jaerosci.2011.01.007>.